DIPLOMARBEIT
Master´s Thesis

Uniaxial compression tests on sandstone prisms with circular openings

ausgeführt zum Zwecke der Erlangung des akademischen Grades
einer Diplom-Ingenieurin unter der Leitung von

a.o. Univ. Prof. Diplo. -Ing. Dr. techn. Rainer Poisel

und

Univ. Ass. Dipl. -Ing. Dr. techn. Alexander Preh

E220

Institut für Geotechnik, Forschungsbereich für Ingenieurgeologie

eingereicht an der Technischen Universität Wien
Fakultät für Bauingenieurwesen

von

Sofía Núñez Arranz

Matr. Nr.: 0827488

Avda. de la Albufera
Nº76 1ºA CP 28038
Madrid Spain

Wien, Januar 2011

Acknowledgements

First, I would like to express my deep gratitude towards Univ. Prof. Dipl. -Ing. Dr. tech. Rainer Poisel and Dipl. -Ing. Dr. tech. Alexander Preh, who gave me an opportunity to participate in this project. Their guidance and their excellent supervision made this work possible.

I would also like to thank Ao. Univ. Prof. Mag. Dr. Andreas Rohatsch for his patience and his explanations during tests. Of course I would not forget the technical staff, Christoph Hauser and Dipl. –Ing. Victor Navas-Basantes for their patience with all my questions and their invaluable help.

I would like to thank my family for being by my side in good and bad times during this hard road. I can never be grateful enough for their patience during my exams, their support when things did not going well as well as when they shared my joys and for the extra effort that they have been required to complete my studies in Vienna. Thank you for believing in me and encouraging me to continue and never give up.

Another of my supports for overcoming these years have been my school friends, who helped me take breaths of fresch air, not to think only in studies and supported me when I need them.

To my university colleagues, which have become more than friends, with whom I shared so many moments. We have suffered together exams, lectures, library, disappointments, joys... thanks to them I have lived unforgettable moments between the four walls of the university and not everything has been studies, but also growth, getting to know ourselves better and meeting wonderful people on the journey.

I also want to thank everyone who supported me, especially these last two years. Knowing that being away from home is difficult and have encouraged me to continue and make my stay shorter. Both friends which have visited me because they knew that I missed them, like the people I've met in Vienna. Incredible people, very different and I am glad to have met them, with whom I shared so much and have been like my family in Vienna.

1. ABSTRACT

The application of equal and unequal external stresses to large rectangular blocks with pre-drilled circular holes has been investigated by several researchers and has been also used to model boreholes or tunnels. The fracturing occurs on the two opposite sides of the hole and the resulting failure grew in the minimum field stress direction, orthogonal to the borehole axis. Similar failures are also common around tunnels and galleries in highly stressed rock.

Fracture and breaking stress around the opening in blocks of sandstone with pre-drilled circular holes were investigated through several tests series. First the compressive strength of the material was obtained by means of uniaxial compression test of cylindrical specimens of sandstone. 6 test bodies of sandstone were tested with 100mm height and 50 mm diameter.

24 tests in specimens of St. Margarethen´s sandstone were tested under uniaxial compression stress, 19 of them with dimensions 200x200x50 mm and a circular 25 mm diameter cavity and 5 of them with dimensions 300x300x100 mm and 36 mm diameter cavity. Experiments were performed using different loading conditions. The first aim was to find out the optimal way to load the sample by “trial and error” means .Some specimens were placed in direct contact with the loading platen and some specimens had an interface (an aluminium plate) between the loading platen and the specimen.

Finally 29 cylindrical specimens, of 5 different sizes, were tested under uniaxial compressive loading. The dimensions of the cylindrical specimens varied from the biggest with 100 mm diameter and 200 mm length of, to the smallest specimen with 19 mm diameter and 40 mm length. For all the specimens an interface (aluminium plate) was used. The results of the test performed for this thesis did not show size effect in contrast to the results of previous experiments with the same material, which were performed in 2003 at the Vienna University of Technology.

Theoretically the apparent strength of the rock adjacent to the unsupported cavity is two to three times the uniaxial compressive strength. Throughout the tests fracture phenomena at the edge of the hole was observed at a point close to the maximum force. Thus these results contradict the theory. Observation of other experiments and of the results of the tests can explain this discrepancy between the obtained and expected results.

2. INTRODUCTION

The ancient art of tunneling has evolved throughout history with occasional impressive development periods, for example during the roman era and during the industrial revolution. As projects become more and more ambitious and new problems appear over the last century considerable improvements have been made in the investigation, design and construction of tunnels.

Investigation of unsupported opening has been carried out for centuries by means of experience based on observations, development of theoretical or analytical models and physical models of prototypes. The advent of high-speed computers and rapid developments in computing techniques over the past decades provide potentially powerful tools to help the geotechnical engineer respond to this challenge. The application of analytical methods, as well as numerical methods, has dominated the research in this area over the last decade and many important contributions have been made.

2.1. Analytical methods

Continuum mechanics and the theory of elasticity were established during the second half of the 18^{th} century and several analytical elastic solutions were obtained. Classical solutions for holes in elastic medium were design by Lame, Kirsch and Inglis.

The French mathematician and engineer Lame (1852) worked in various areas, mainly in engineering mathematics. He studied the stress distribution around a cylindrical or spherical cavity in an elastic continuum under the same pressure from all sides. This theory was extended by Kirsch 46 years later.

Kirsch (1898) developed the mathematical formulations in the case of biaxial loading. Kirsch's solution was applicable for stress distribution around a circular hole in an elastic plate under anisotropic in-situ stresses. Later Inglis (1913) extended the Kirsch result to considerations of an elliptical cavity in an elastic continuum.

Figure 2.1 shows formulations of Lame, Kirsch and Inglis. The expressions for the elastic stress distribution show that the stresses vary proportionally to the square of the dimensionless ratio a/r, where a is radius of the cavity and r the radial distance. In the case of a cylindrical tunnel the stress concentrations in the medium decrease with the ratio $(a/r)^2$ and $(a/r)^3$ in the case of a spherical cavity. The deformations are proportional to the ratio σ/E, where σ is the applied stress and E the elastic modulus of the medium.

a) Lame

Cylinder

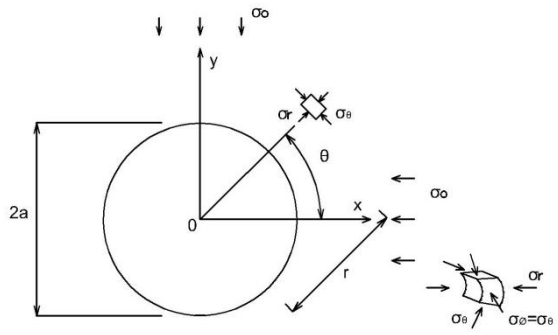

$$\sigma_r = \sigma_0 \left(1 - \frac{a^2}{r^2}\right)$$

$$\sigma_\theta = \sigma_0 \left(1 + \frac{a^2}{r^2}\right)$$

$$u_r = \sigma_0 \frac{1+\vartheta}{E} \frac{a^2}{r}$$

Sphere

$$\sigma_r = \sigma_0 \left(1 - \frac{a^3}{r^3}\right)$$

$$\sigma_\theta = \sigma_0 \left(1 + \frac{1}{3}\frac{a^3}{r^3}\right)$$

$$u_r = \sigma_0 \frac{1+\vartheta}{2E} \frac{a^3}{r^2}$$

b) Kirsch

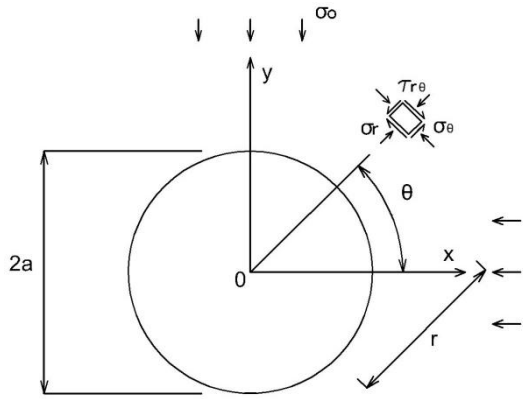

$$\sigma_r = \frac{\sigma_1+\sigma_3}{2}\left(1 - \frac{a^2}{r^2}\right) - \frac{\sigma_1-\sigma_3}{2}\left(1 - \frac{4a^2}{r^2} - \frac{3a^4}{r^4}\right)\cos 2\theta$$

$$\sigma_\theta = \frac{\sigma_1+\sigma_3}{2}\left(1 + \frac{a^2}{r^2}\right) + \frac{\sigma_1-\sigma_3}{2}\left(1 + \frac{3a^4}{r^4}\right)\cos 2\theta$$

$$\tau_{r\theta} = \frac{\sigma_1-\sigma_3}{2}\left(1 + \frac{2a^2}{r^2} - \frac{3a^4}{r^4}\right)\sin 2\theta$$

c) Inglis

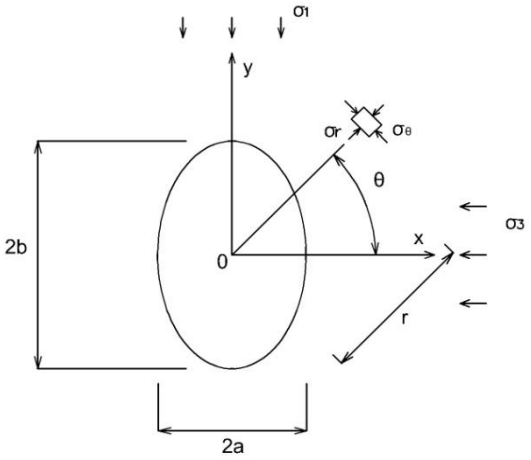

$$\sigma_\theta^{wall} = (\sigma_1 + \sigma_3) - \frac{[(a-b)(\sigma_1+\sigma_3) + (a+b)(\sigma_1-\sigma_3)]}{a^2 \sin^2\theta + b^2 \cos^2\theta}$$

$$\times \left(a \sin^2\theta - b \cos^2\theta\right)$$

Note: when

$$\frac{b}{a} = \frac{\sigma_1}{\sigma_3}$$

Then

$$\sigma_\theta^{wall} = (\sigma_1 + \sigma_3) \quad \text{(Constant)}$$

Fig. 2.1: Elastic stress distribution. From: Carranza-Torres (1998).

Elastic analysis attempts to optimize the profile of excavations in rock. Various studies and tests have been carried out to find out which form is most suitable. Isaacson (1958) discussed the stability of the elliptical opening. The most stable shape was considered an elliptical opening in which the major:minor axis ratio was the same as the major:minor stress ratio, since the tangential stress was constant around the tunnel wall.

Later works of Carranza-Torres (1998) about the stress distribution behind the periphery of elliptical cavity reveals that the region of high stress is not constant. As seen in Figure 2.2, the cavities have various large plastic zones dependant on the orientation of their axis. A reduction of the inelastic region occurs when the ellipse rotates by 90º to the original orientation.

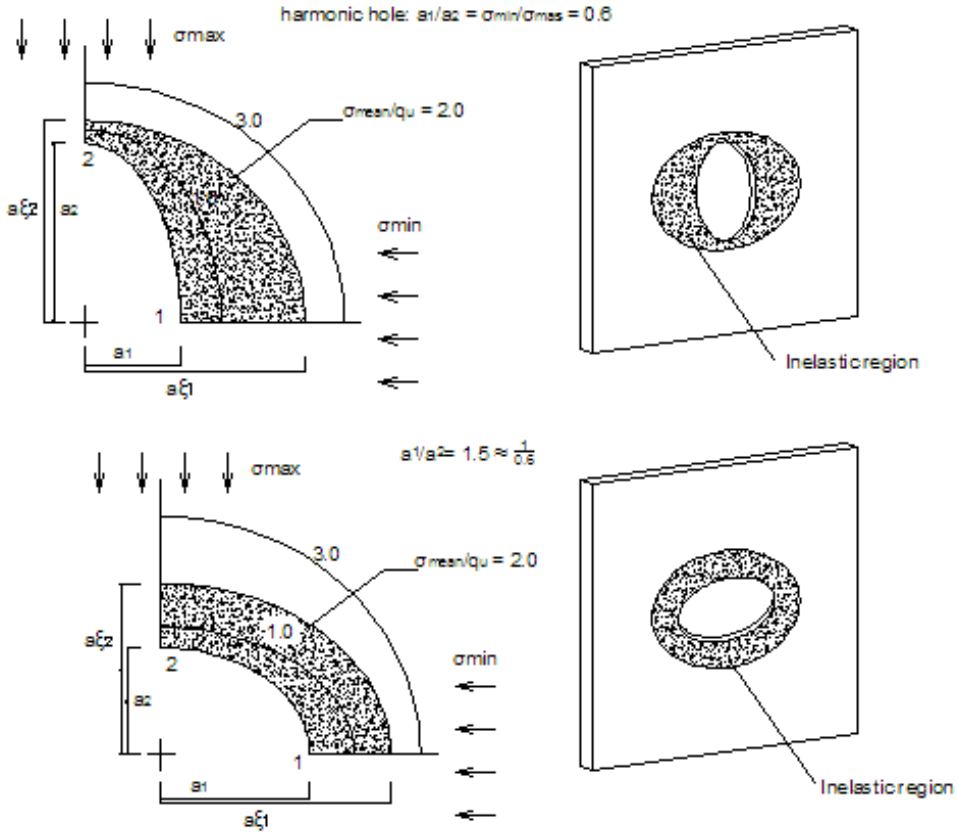

Fig. 2.2: Inelastic region in elliptical opening. From: Carranza-Torres (1998).

Fairhurst and Carranza-Torres (2002) investigated elliptical cavities in anisotropic stress fields by means of the use of a mathematical model. Figure 2.2 shows the analysis of the elastic stress distribution behind the tunnel periphery in an elliptical opening in two different orientations, the original orientation and after a rotation of the ellipse by 90º. In the first case the longest axis was aligned to the direction of the greatest in-situ stress and in the second case the shorter axis is aligned in the direction

of the greater in-situ stress. The analysis of the elastic stress distribution can provide a reasonable indication of where inelastic deformation is likely to develop in the event that failure does occur. The elliptical cavity with the longer axis aligned at right angles to the largest in-situ stress is more stable than the elliptical cavity with the shorter axis aligned in the direction of the largest in-situ stress.

The elasto-plastic analysis for a circular cavity under isotropic in situ stress was described by Kastner (1962). He reached the conclusion that the structural stability of a cavity with the cross-sectional shape of an ellipse is not better than the stability of a circular cavity.

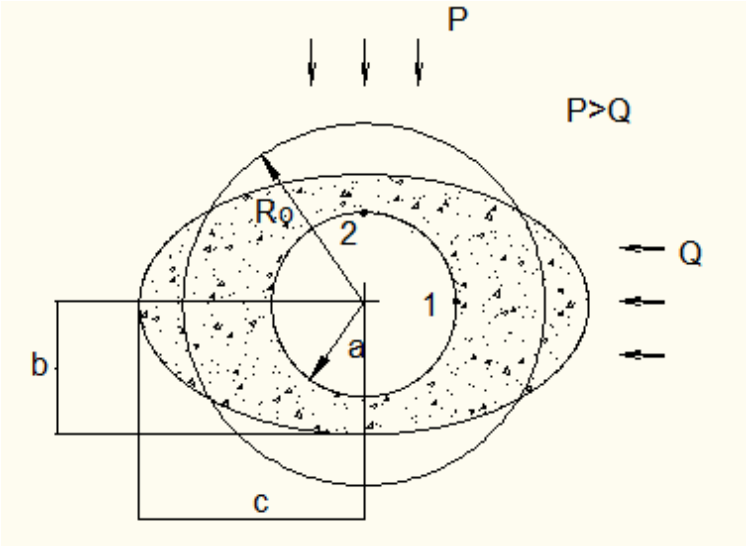

Fig. 2.3: Inelastic zone around tunnel.

The elasto-plastic extension of the Kirsch solution was developed by Detournay (1983), who established a semi-analytical method around the circular cavities under anisotropic in-situ stress conditions to obtain the stress and displacement around the circular cavity. The failure zones, that figure 2.3 shows, have the shape of an ellipse. The major extension of the plastic zone is normal to the direction of the maximum far-field stress.

Figure 2.3 shows the elliptical form of the inelastic region obtained. The radius Ro is equal to the average of the minor and major semi-axes of the ellipse $\left(\frac{b+c}{2}\right)$. The maximum displacement is located on the wall along the axis parallel to the maximum stress, initially at point 2, but changes to point 1, the point normal to the maximum stress direction as the radius Ro increases.

2.2. Numerical Methods

In the last years there have been many advances in computer technology with a rapid growth in algorithmic methodology. Numerical methods advance with the technology and tools have been developed for analysis and design of engineering systems. Numerical methods provide tools for analysis and design of engineering systems with complex factors that was not possible or very complex using conventional methods. Over the years a large number of numerical methods appeared. The codes can be divided into:

- Continuum mechanics codes: e.g. FLAC, ABAQUS, PENTAGON.
- Discontinuum mechanics codes: e.g. EDEM, UDEC, 3DEC, PFC.

Depending on the number of discontinuities with respect to the size of the problem that needs to be solved continuum or discontinuum methods are chosen. For rocks continuum methods are appropriate can be used. For rocks continuum or a discontinuum model can be used. When a large number of discontinuities are present in the medium a discontinuum model is a better choice but with few discontinuities a continuum model can be used.

The most used methods are: Continuum, Finite Difference Method (FDM), Finite Element Method (FEM) and Boundary Element Method (BEM); Discontinuum, Distinct Element Method (DEM), Discontinuous Deformation Analysis (DDA), and Bonded Particle Model (BPM). The following is a list of the codes most referenced in the literature:

- FDM:
  - ✓ FLAC and FLAC3D (ITASCA Consulting Group, Inc.)
- FEM:
  - ✓ ABAQUS (Hibbit, Karlson and Sorensen, Inc.)
  - ✓ PENTAGON-2D and -3D (Emerald Soft)
- Boundary Element Method:
  - ✓ BEFE (Computer Software and Services (CSS))
  - ✓ EXAMINE2D and EXAMINE3D (Rockscience)
- Distinct Element Method:
  - ✓ UDEC
  - ✓ 3DEC (ITASCA Consulting Group, Inc.)
- Bonded Particle Method
  - ✓ PFC2D and PFC3D (ITASCA Consulting Group, Inc.)

The numerical models need all the details of the problem that it analyzes. The geometry of the problem (depth, extent...), boundary conditions, material behaviour (elastic, plastic, visco-elastic) and construction process need to be determined. In many cases this properties are not fully known. The goal is to create a model so the approximate sufficiently the performance of the design.

Finite element method (FEM)

This numerical method is the most employed for rock mechanics and rock engineering. One of the reasons is that it can be used for problem solving and it does not require detailed programming experience.

The continuum problem is analyzed in terms of sets of nodal displacement and force for the problem domain. The displacements at any point within the element can be expressed in terms of nodal displacements, through appropriately chosen interpolation functions. Derivation of these displacements describes strain in the element. The stiffness of the medium to this induced strain determines stress in the element. Total stress within an element can be found out by superimposition of initial and induced stresses.

If the problem is non-linear, the time required in preparing input data increases enormously. This is a disadvantage of this method. With this method it is possible to analyze in two and three dimensions (figure 2.4) and for static or dynamic analysis.

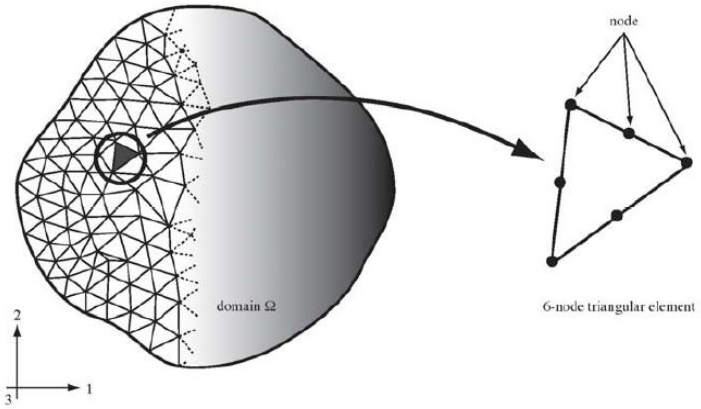

Fig. 2.4: Finite Element Discretization in 2D. From: BOBETobet (2010).

Finite difference method (FDM)

This numerical method is one of the oldest numerical techniques and was used before the arrival of computers. The Finite Difference Method (FDM) is based on the premise that governing differential equations can

be adequately represented by finite differences. The Method used a grid superimposed to the domain. Figure 2.5 shows a grid in 2D. The grid divided the domain into a connected series of points called nodes. These nodes are used for obtaining the solution. The method relies on the approximation of the field equations by finite difference formulas.

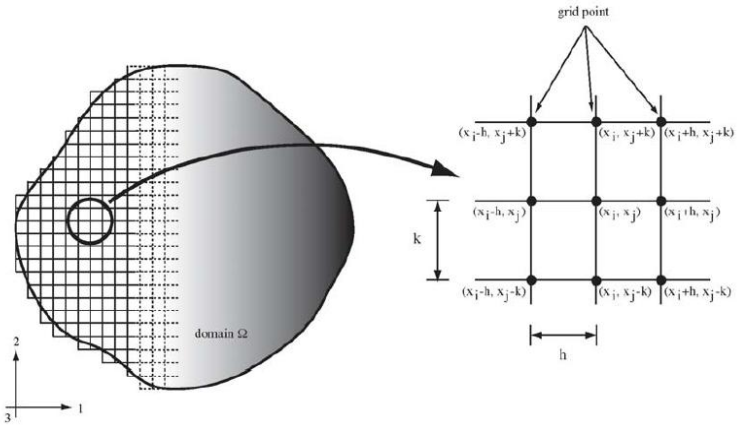

Fig. 2.5: Finite Difference Grid in 2D. From: Bobet (2010).

The solution is obtained on a stepwise process with small loading increments until the final state is reached. In each loading step the displacements at the node are obtained, then stresses are updated and a loading increment is added for the next step. The new loading increment starts with the updated stress field from the previous step.

FDM is difficult to use for irregular shaped domain or problems with singularities, i.e. complex boundary conditions and material heterogeneity. It is particularly suitable for large, non-linear problems which may involve collapse or progressive failure. This method can be used to solve dynamic problems, where displacements are function of position and time.

Boundary element method (BEM)

The Boundary Element Method discretized only the boundaries of the continuum. This method is particularly useful when the volume to boundary surface ratio is large, because the amount of input data required for describing a problem is greatly reduced and the influence of infinite rock mass is considered in the rock mass. BEM is most effective with linear elastic behaviour, with small boundary to volume ratios and with displacement or stresses applied to the boundaries.

In the BEM, the solution is approximate at the boundaries while equilibrium and compatibility are exactly satisfied in the interior of the medium. The technique consists of transforming the differential

equations, which apply to the entire medium, to integral equations which only consider boundary values. Line elements at the boundary represent in case of two-dimensional situations, figure 2.6, while for three-dimensional problems the method used surface elements.

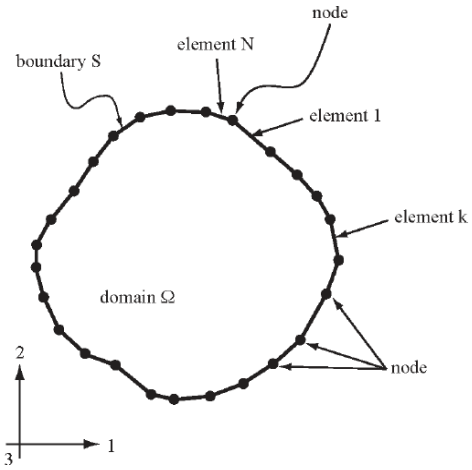

Fig. 2.6: Discretization with Boundary elements in 2D. From: Bobet (2010).

There are two approaches to solve the problem, direct and indirect BEM. Direct BEM solves the unknown parameters directly and stresses and displacements at any point in the continuum can be obtained directly from the solution. Indirect BEM solved the unknown parameters in terms of typically stresses or displacement. The stresses and displacement at any point in the medium are expressed in terms of these typically stresses or displacement.

Some applications of BEM include stress analysis of underground excavations, dynamic problems, back analysis of in situ stress and elastic properties and borehole tests for permeability measurements.

Distinct element method (DEM)

The distinct element method is relatively new and was introduced as a model to simulate large movements in blocky rock masses. This method has been applied to spherical and polyhedral blocks for both soils and rocks. There are applications in particle flow research studies of granular material and crack development in rock and concrete.

This method treats domain as a discontinuum. DEM is capable of analyzing multiple interacting deformable continuous, discontinuous or fracturing bodies and it can be used for static and for dynamic calculations. The DEM has a very versatile and extensively validated applicability: Rock dynamics, slopes and fracture, underground

excavation, rock reinforcement, borehole stability, acoustic emission in rock etcetera.

In DEM the medium is divided by discontinuities which delimit through their intersections a finite number of blocks, figure 2.7, which are interconnected through the discontinuities. Dynamic equilibrium equation is solved for each body subjected to boundary interaction forces. The force acting at the boundaries are originated by the interaction of the elements, this generated force can be made to obey various interacting laws depending upon the physical nature of simulation. As a result of the relative movements between the two elements that share the discontinuity we have two forces, a normal and a shear force. The normal force is proportional to the relative movement of the two blocks across the contact and along the normal direction. The shear force is proportional to the relative movement along the direction of the contact.

.

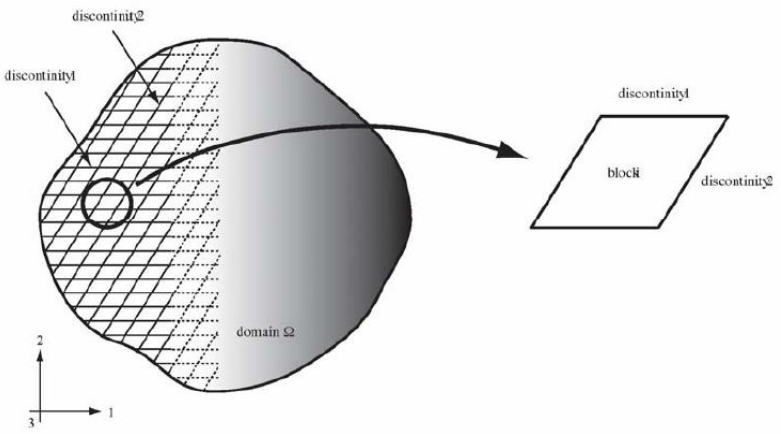

Fig. 2.7: Distinct Element Method. From: Bobet (2010).

Bonded particle method (BPM)

The Bonded Particle Method was created for discontinuous mediums modeled as discs in two dimensions or spheres in three dimensions. BPM codes provide valuable new insights to problems in rock mechanics where continuum mechanics has been of limited utility.

The base is that the material can be approximated by an agglomerate of cemented grains (figure 2.8). These grains or particles are assumed rigid with spherical or circular shape with a non-uniform distribution. The particles interact with each other. The BPM codes assume that forces and deformations are transmitted through the solid via particle to particle interface contact. The relative displacement between particles or the particle contacts produced deformation. Tensile and shear cracks between particles occur when the tensile or shear strength of the contact

is reached. The forces arise from the weight of the particle and from the contact forces between particles. The method requires very small time steps to obtain the solution.

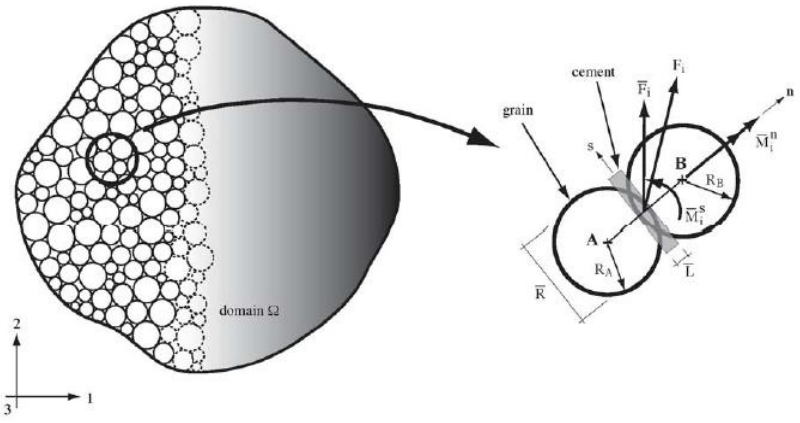

Fig. 2.8: Bonded Particle method Discretization. From: Bobet (2010).

Some applications of this model are: slope stability, damage to rock mass during tunnel excavation and tunnel support, blasting and dynamic analysis, the strength of soils and rock materials and the behaviour of granular materials and powders.

Analytical as well as numerical methods assume that failure of the tunnel wall starts when uniaxial compressive strength is reached. Thus uniaxial compression tests on sandstone prisms with circular openings have been performed in order to investigate whether this condition is met.

3. Uniaxial compression test

The compression test determines the behavior of materials under a compressive load. It is one of the most important laboratory rock mechanics tests and is a simple and versatile method that it can be used in almost all kinds of material. The test specimen is placed in the testing machine between two loading platens and then the uniaxial load is applied. The specimens are loaded axially up to failure or any other prescribed level. During the test the specimen is compressed, and the deformation versus the applied load is recorded.

The most common method to study mechanical properties of rock is by axial compression of circular cylinders, the length of which is twice the diameter in order to generate an area of uniaxial stress in the mid region of the sample. Figure 3.1 shows an example of a Stress-Strain Curve. The compression test is used to determine the compressive strength, which is calculated by dividing the failure load by the original cross sectional area of the specimen $\sigma = \frac{F}{A}$.

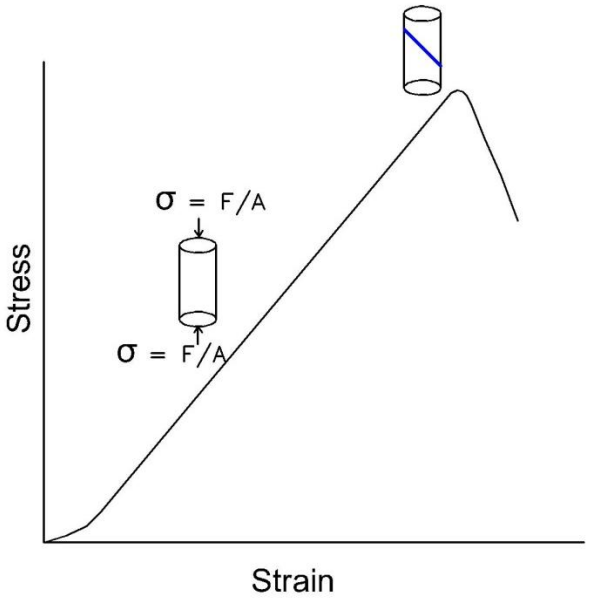

Fig. 3.1: Stress-Strain curve during a compression test.

Size effect

The influence of size upon rock strength has been discussed in geotechnical literature. Studies on size effects in materials like concrete or rock gained interest in the last decades and experimental results showed that the specimen size has an influence on strength and ductility. Therefore, the experimentally determined strength is not a material property. The available theoretical size effect models describe the variation of strength with size

based on different physical assumptions and show different behaviour with increasing size.

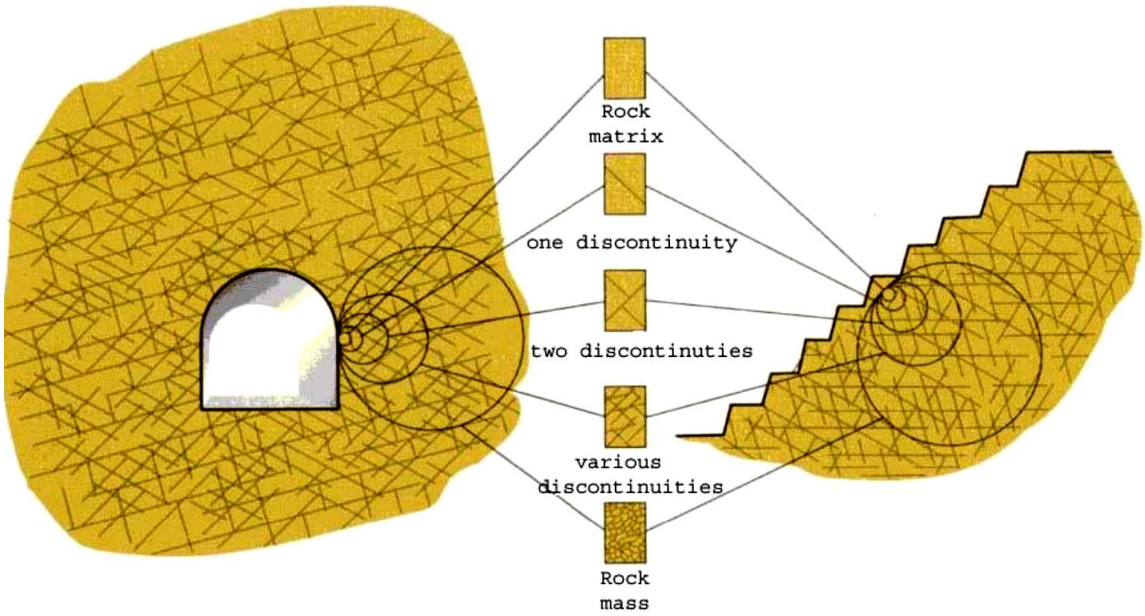

Fig. 3.2: Simplified representation of the influence of scale on the type of rock mass behaviour model which should be used in designing underground excavations or rock slopes. From: Hoek (1983).

Hoek showed with figure 3.2 the transition from an isotropic intact rock specimen, through a highly anisotropic rock mass in which failure is controlled by one or two discontinuities, to an isotropic heavily jointed rock mass. At one end, we have the intact rock (homogenous, isotropic, solid, and continuous with no obvious structural defects) which really exists only at the hand-specimen scale. At the other end the rock mass that is heterogeneous and anisotropic carrying all the characteristic defects of the rock mass at the field scale. This idealized diagram shows the transition from intact to a heavily jointed rock mass with increasing sample size.

Theoretical models indicate that the strength change is not linear with size. When multiplying all the specimen dimensions by a scale factor the length changes linearly with the size factor, the cross section changes by the order of two with the size factor and the volume by the order of three. In practice this means that the testing frame has to be adapted to the length of each specimen type and that the maximum load changes, disregarding the size effect, by the order of two with the size factor from one size to the other. The experimental investigations on the size effect are a difficult task, because one has to deal with different sizes of geometrically equal specimen. The phenomena is observed on large size ranges, the larger the size range the more pronounced the effect of size on strength. All geometric dimensions of the specimens have to be scaled by the same factor and all the test bodies should have the same load and boundary conditions. The larger the factor

from the smallest to the biggest specimen the more pronounced the effect of size on strength.

The Institute for Structural concrete and the Institute for Steel Structures at the Vienna University of Technology carried out an extensive experimental investigation for sandstone under compression, (Burtscher et al., 2003). The purpose of these investigations was the determination of the influence of size on the nominal strength. This investigation is important, not only because it has the highest number of specimens, but also because the material is the same as the one used in this master thesis and has the same origin and therefore the same characteristics. The material was sandstone from the quarry in St. Margarethen (more information in section 5.1).

The experiments were carried on specimens of six different sizes in a scale range of 1:32, where the smallest was appointed as XS (20x20x40 mm) and the biggest as XXL (640x640x1280 mm). All specimens were geometrically similar, were provide with notches and were tested under centric and eccentric loading. The specimen dimensions, the notch and the eccentricity were all scaled with the same factor.

The strength is clearly decreasing with increasing strength, thus a size effect was present. The mean strength decreases from the XS to the XXL from 36.6 to 19.4, which corresponds to a strength decrease of 47%. The mean strengths of the sizes XS and L are 36.6 and 24.6 N/mm^2, a strength decrease of 33%. Specimens of the same size showed different grain structure on the specimen surface and also different strength. The fine grained structure always showed higher strength values than the coarse grain structure. These results are in contrast to the results of the test performed for this thesis (see chapter 5).

4. PREVIOUS EXPERIMENTS

Observations in practice and in laboratory tests have been performed on several occasions. Researchers have applied isotropic as well as anisotropic external stresses to rectangular blocks with predrilled circular holes and laboratory studies have also been performed, using model openings such as hollow cylinders.

100 years ago at Vienna University of Technology, Leon & Willheim (1910) performed tests in rock plates with a circular hole similar to tunnels and they investigated the fracture process at the edge of a cavity in a rock mass under uniaxial loading.

The tests showed the breakage failure of the cavity wall and of the entire sample occurred more or less at the same time. Probably the rock plate was too small in relation to the size of the cavity; the failure phenomena in the cavity wall affected the entire specimen. Figure 4.1 shows a marble specimen with a circular cavity after the test.

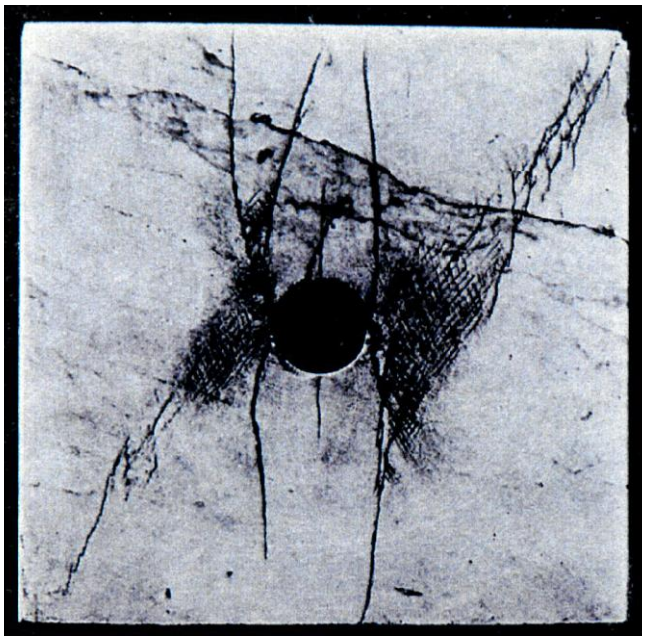

Fig. 4.1: Marble specimen with model tunnel. From: Leon & Willheim (1910).

Kaiser, Guenot & Morgenstern (1985) used a specific test on special coal to investigate the behaviour of openings in a jointed rock mass during the failure process. Two different modes of behaviour were observed during the test if overstressing of the rock mass near the opening occurs: yielding and rupture. Yield is defined as the beginning of inelastic behaviour and is associated with initiation and stable propagation of cracks. On the other hand rupture occurs during yielding if a mode of instability is reached locally, ultimate collapse in the wall of the tunnel. Rupture was initiated at stress

levels between 2.2-3.3 times the unconfined compressive strength of the test material, because yielding and rupture constitute two separate phases of the failure process of underground openings but during a uniaxial test yield and rupture points are almost identical.

Ewy & Cook (1990) investigated fracture and failure, elastic (before failure) and inelastic (during failure) deformation behaviour around underground openings by means of experiments on thick-walled hollow cylinders. The samples were subjected to axisymmetric pressures on the inner and outer diameters, and were constrained to near zero axial deformation (plane strain). They obtained that the theoretical tangential stress on the hole wall was 2-3 times higher than the uniaxial compressive strengths of the material. Failure occurs on the two opposite sides of the hole subject to the highest compressive stress concentration, then cracks grow in the direction of the minimum field stress orthogonal to the hole axis. The fracture mechanism around the cavity was initiation and growth of small cracks oriented parallel to the tangential stress. These cracks coalesce from macroscopic splitting fractures subparallel to the wall of the opening. The final stress state, strain rate, stress path and test boundary conditions have an influence in the size of the failed zones.

Wang et al. (2009) studied the behaviour of the excavation damaged/disturbed Zone (EDZ) around highly-stressed underground openings by means of numerical modelling and experimental tests. The tests were carried out on prismatic specimens of granite under uniaxial compression. Figure 4.2 shows the results of their experiments and numerical modelling.

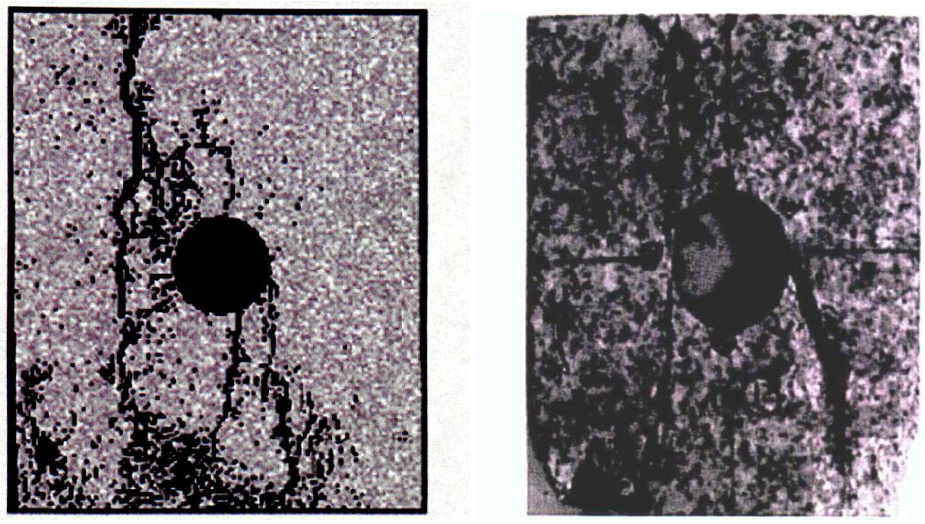

Fig.4.2: Results around a circular opening in an inhomogeneous rock sample. a) Numerical result. b) Experimental result. From: Wang et al. (2009).

Progressive failures in these tests are characterized by initiation, propagation and coalescence of microcracks. Figure 4.3 shows different damage levels; A crack closure, B crack initiation stress, C crucial energy release stress and D is peak strength. The crack initiation stress was observed about 45-60 % of the peak strength and the critical energy release stress was about 75-80% of the peak strength.

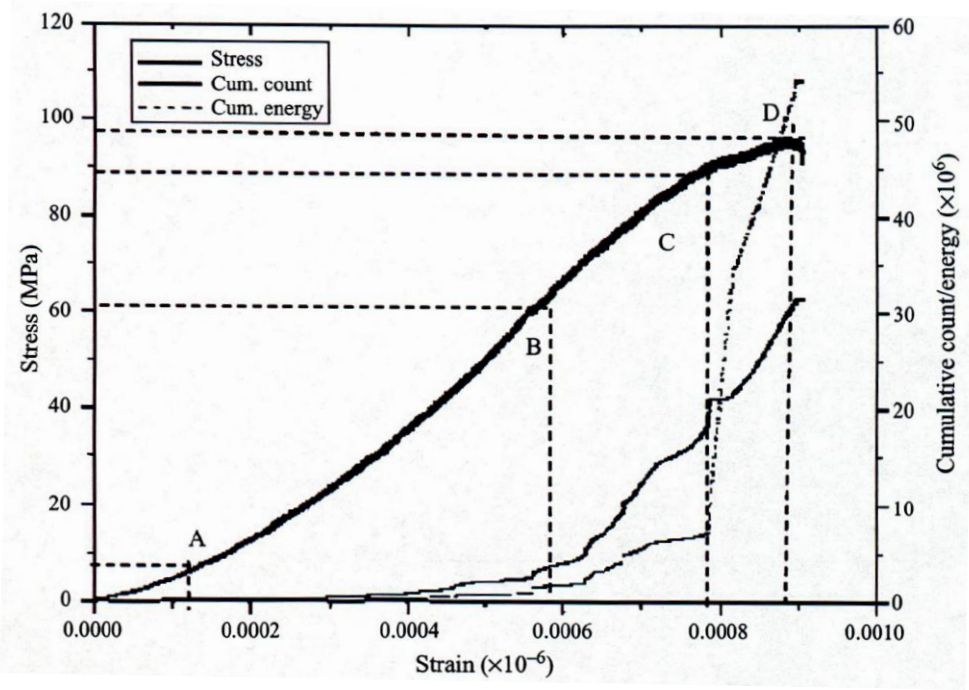

Fig. 4.3: Stress-strain curve and Acoustic Emission distribution in the sample. From: Wang et al. (2009).

5. EXPERIMENTS

5.1. The material

St. Margarethen´s Sandstone was the material used in these tests. In St. Margarethen area, which belongs to Burgenland province (fig 5.1), Austria, there were numerous quarries where sandstone was exploited. This area is close to "Römersteinbruch" (Roman quarry). Römersteinbruch is one of the oldest and largest quarries in Europe and one of the main features of the area. The sandstone from St. Margarethen is one of the most important natural stones from Leithakalk-Formation in eastern Austria. This sandstone is a porous limestone and was created by deposition of debris and skeletal remains mainly of coralline algae and foraminifers in a warm and shallow subtropical lagoon about 15 million years ago.

Fig. 5.1: Localization of quarry.

Since very early ages (dates back to the roman period) the famous Römersteinbruch sandstone was used for sculptures and masonry. At the moment only one of the quarries is still in use for the production of building blocks, facade claddings, pavements and several other applications indoor and outdoor. The rock was often used due to its easy extractability and good workability (fig. 5.2). This specific sandstone material can be seen in the following monuments: St. Stephen`s cathedral, the Dominican and the Franciscan church, the Musikverein, the Albertina, the Imperial Palace, Opera, Karlskirche church, Castle Schönbrunn, Rathaus and other places.

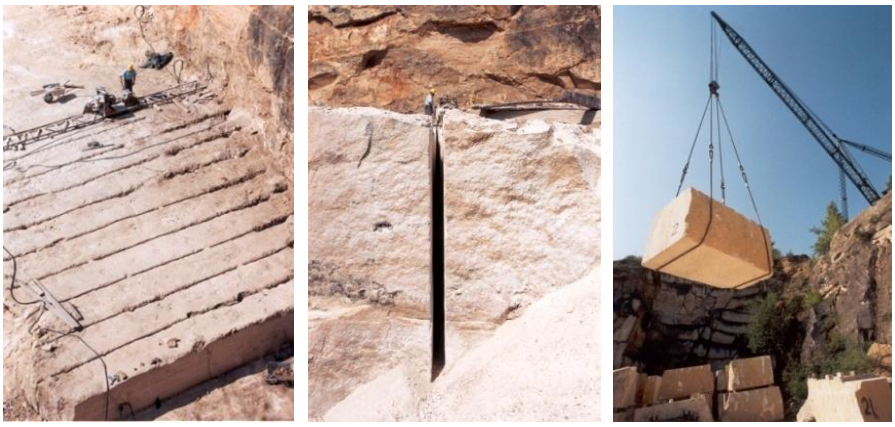

Fig. 5.2: Extracting technology in the quarry of St. Margarethen with a stonecutting machine. From: Gustav Hummel.

The colour of this sandstone ranges from light grey to a light yellowish brown, the grain size distribution from fine- to coarse grained.

- ✓ Bulk Density (ÖNORM EN 1936): 1,97 - 2,26 g/cm^3
- ✓ Effective Porosity (ÖNORM EN 1936): 16 - 25 R.%
- ✓ Water adsorption (ÖNORM EN 13755): 7,6 - 12,2 M.%
- ✓ Uniaxial compressive strength(ÖNORM EN 1926): 20 – 45 N/mm^2
- ✓ Bending tensile strength (ÖNORM EN 12372): 7 - 10 N/mm^2

5.2. Specimen dimensions and geometry

The laboratory had several blocks with dimensions 200x200x200 mm and a circular cavity with a diameter of 25 mm. Test bodies had dimensions 200x200x50 mm, so it was necessary to cut the blocks. The blocks were cut in the geotechnics institute laboratory with a power saw and specimens with the appropriate dimensions were obtained. A total of six blocks were cut to obtain 18 samples with the necessary dimensions.

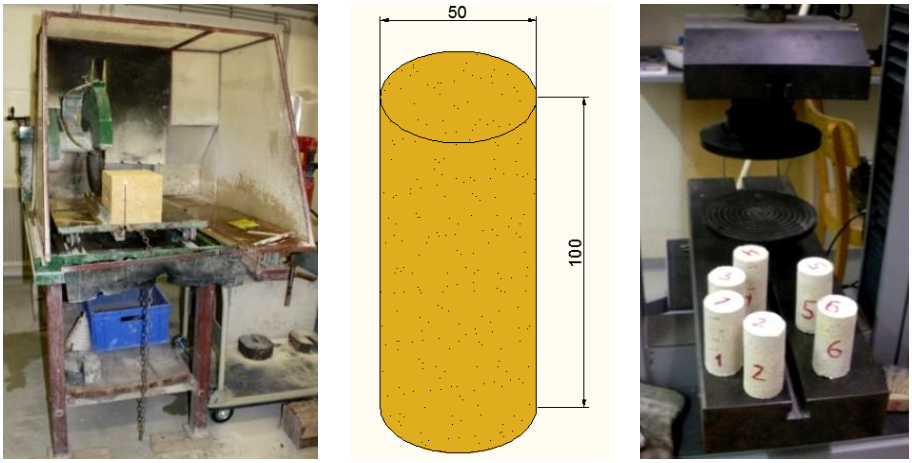

Fig.5.3: a) Power saw with specimen. b) Dimensions of cylinder specimens. c) Cylinder specimens.

Furthermore 6 cylindrical samples were cut with 50 mm diameter and 100 mm height (figure 5.3). These samples were used to obtain compressive strength by means of the uniaxial compressive test. All of them were wiped with a cloth and then the cylinders and rectangular samples were put in a drying furnace with a temperature of 70 degrees Celsius during 48 hours until the samples were totally dry.

5 new blocks were ordered at the quarry with a size of 300x300x100 mm for more tests. Once in the laboratory, the blocks were bored to obtain a drillhole with 36 mm diameter. Figures 5.4 and 5.5 show the dimensions of the test bodies and, as can be observed, the difference in size among the specimens is considerable.

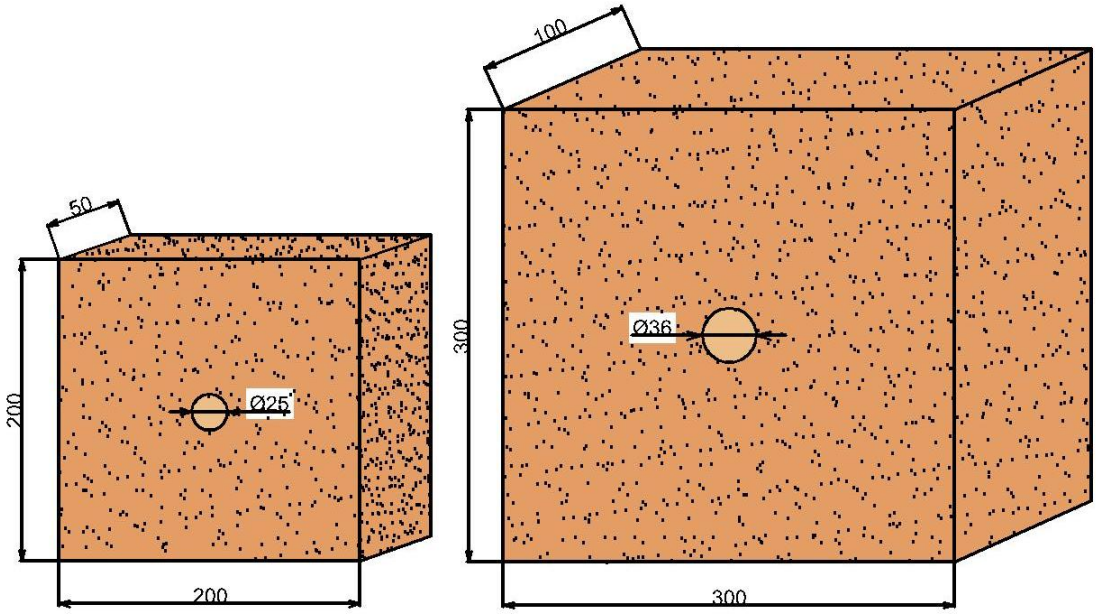

Fig.5.4: Dimensions (mm) of prisms rock with circular cavity.

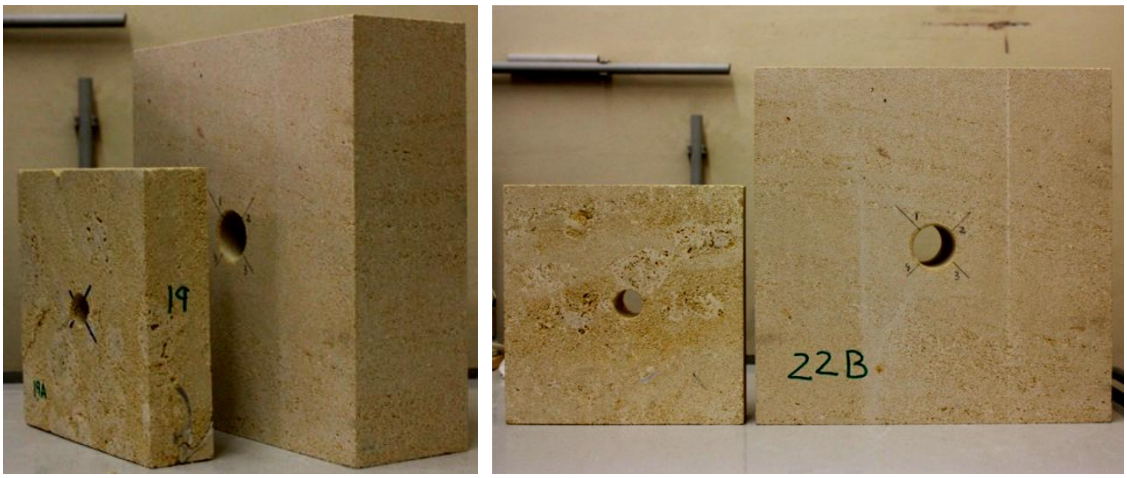

Fig. 5.5: Prismatic samples with drillholes.

5.3. Uniaxial compression test

6 test bodies of sandstone were tested: cylinders with 100 mm height and 50 mm diameter. Three of them were tested with a loading velocity of 1 N/s, (specimens with the numbers 1, 2 and 3). The rest of them were tested with a 10 times higher velocity, 10 N/s, the test bodies with the numbers 4, 5 and 6. Figure 5.6 shows an example of the compression test and one specimen after testing.

Fig.5.6. a) Compression test. b) Specimen after testing.

The cross section surface of the sample was 1963.50 mm^2 and the necessary load to failure varied from 29.630 N to 39.925 N. The results are shown in table 5.1. The results show that the loading velocity was not an important factor. The average value of compressive strength was 18.3 N/mm^2.

Sample	Force	Compressive Strength
-	N	N/mm^2
1	32.850	16.7
2	39.520	20.1
3	36.740	18.7
4	29.630	15.1
5	37.230	19.0
6	39.925	20.6

Table 5.1: Compression test results.

Following diagrams, fig. 5.7, show the test results comparing the load with the displacement and marking the maximum force, reached in each test. Load is expressed in kN and displacement in mm.

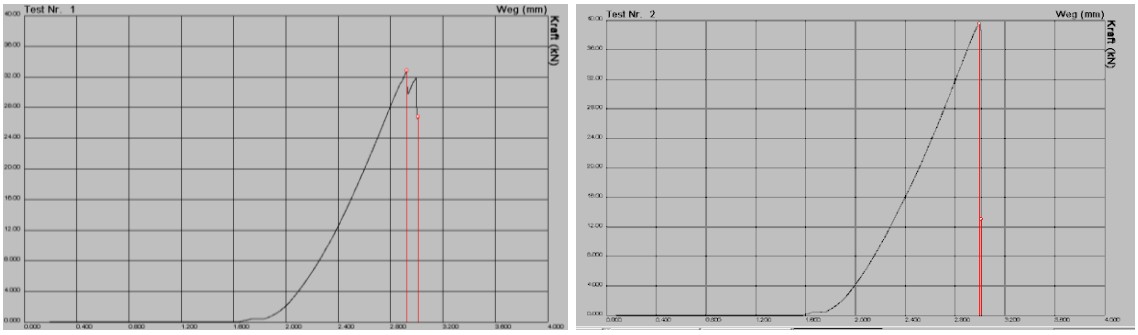

a) Specimen 1. b) Specimen 2.

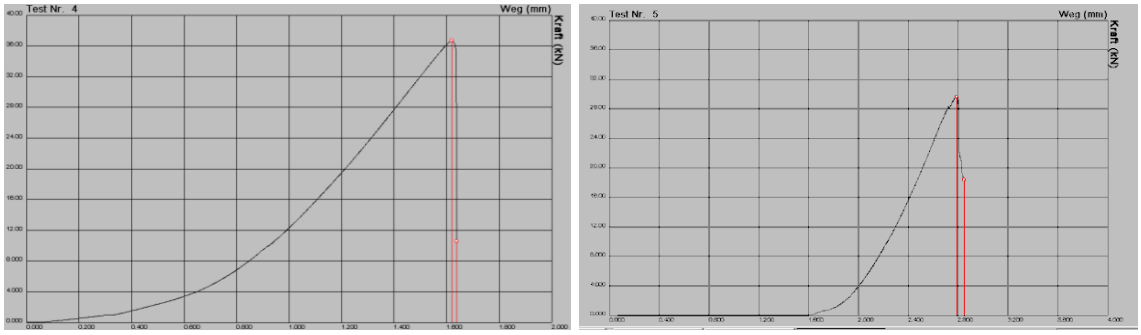

c) Specimen 3. d) Specimen 4.

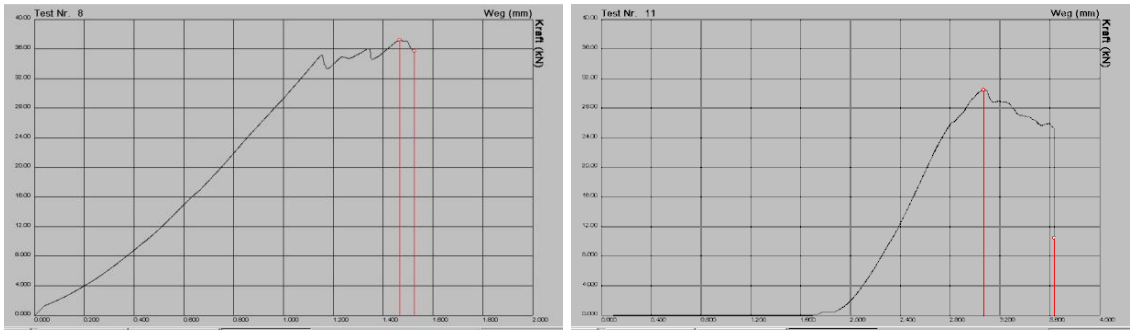

e) Specimen 5. f) Specimen 6.

Fig.5.7: Load displacement curve of uniaxial compression test. Red lines mark the maximum force and the end of the test.

5.4. Short introduction to results

An overview of the results can be found in table 5.3. The first column shows the test number and in the next column the number of the test specimen. Test numbers match with the number of the specimen. In the following four columns maximum force reached during the test, duration of experiment, displacement and compressive strength of the test specimen are presented.

The first aim of the tests was to find out the optimal loading conditions by means of “trial and error”. As a result of this search some experiments were not valid. 3 loading methods were tested until the optimal loading conditions for the specimen were found. Table 5.2 shows an example of each loading processes. The number of stages and values of each stage of the loading process varied according to the test specimen.

Specimens 1 to 8 were tested under the same loading conditions. The loading process of the sample was divided in phases. Each phase finishes when the load reached a fixed value (e.g. 140 kN, 145 kN…) and then the new phase starts with the new loading rate. The first phase of the experiment was the same for all tests; this phase was carried out at 2 mm/min rate up to 5kN. The next phase used a loading increase rate $\Delta F/\Delta t$ 2000 N/min up to 140 kN. The third phase was carried out at 10^{-4} N/min rate up to 145 kN. The next phase used a loading increase rate 100 N/min up to 160 kN. The last phase was carried out at 10^{-4} N/min up to 165 kN. It was possible to estimate the compressive strength of the test specimens as well as the loading conditions.

Specimen test	Test parameters					
-	-		kN	-	-	-
From 1 to 8	F0		5	V0	2	mm/min
	V1-V2		140	V1	2000	N/min
	V2-V3		145	V2	10^{-4}	N/min
	V3-V4		160	V3	100	N/min
	V4-V5		165	V4	10^{-4}	N/min
-	-	kN	-	kN/s	-	m
9	E1	200	V1	1	T1	60
	E2	205	V2	10	T2	120
	E3	210	V3	10	T3	60
-	-		kN	-	-	-
From 10 to 24	F0		5	V0	2	mm/min
	V1-V2		100	V1	0.8	kN/min
	V2-V3		300	V2	0.004	mm/min

Table 5.2: Example of loading conditions

A new way to load the sample was tested in specimen 9. In this case the loading rate, with unit of measurement kN/s, is constant till the load reaches a fixed value (e.g. 200 kN, 205 kN ...). Once the value of load is reached, this force is maintained for a time called T_i measured in minutes. Once this period ends the load increases and is maintained according to the parameters of the next phase and so on. Table 5.2 shows an example where the test was carried out at 1kN/s rate from 0 to 200 kN and when the load reaches 200 kN this force is maintained 60 minutes. Once this period ends, the next phase starts.

A third method was used for specimens 10 to 24. The first phase was the same that for the first method, a loading rate of 2 mm/min up to 5kN. For specimens 10 to 19, the second phase was up to 100 kN (100 kN was used because fracture in the previous test occurred after the load reaches this value), with a loading rate of 0.8 kN/min. This phase used a rapid loading rate because the rupture always started after 100 kN and in this phase it is only necessary to increase the load with a rapid loading rate the decreasing the duration of the test. For the next phase a loading rate of 0.004 mm/min as used, a slow rate, because in this phase initiation and propagation of the cracks occurs. Specimens 20 to 24 a rapid loading was also used rate up to 800 or 1000 kN, and in the next phase a slow loading rate between 0.001 mm/min and 0.004 mm/min was used.

Throughout the tests six different cases were observed:

- ✓ Case A: Specimens do not have cracks or breakages. These tests are not valid, because they were used to find the loading condition by means of “trial and error”.
- ✓ Case B: Rupture is caused by testing difficulties. When the cracks started, the loading rate was too fast. The press didn´t stop when the maximum force was reached and the destruction of the entire specimen happened. These cases cannot be taken into account for the comparison of the results.
- ✓ Case C: The rupture of the body and the drillhole occur simultaneously.
- ✓ Case D: First the rupture in the body of the specimen occurs, on the right side, on the left side, on the back side or on the front side of the specimen. Afterwards the crack in the sidewalls of the drillhole became visible.

- ✓ Case E: First the rupture on both sidewalls of the drillhole occurs. Later, soon after reaching the point of maximum force, the first cracks on the body of the specimen became visible. The cracks start on the two opposite sides of the opening and grow parallel to the applied load. There are more cracks on the right side and on the left side of the specimen.
- ✓ Case F: Tensile fracture. The fracture appears along the tunnel, on the roof and on the floor, and propagates away from the cavity parallel to the applied loading.

Tests 1 to 19 were performed on specimens with dimensions 200x200x50 mm and a circular 25 mm drillhole. The displacement values varied between 0.31 mm and 0.92 mm. The compressive strength reached values between 10.3 and 22.9 N/mm^2 and the test duration varied from one hour for the shortest to about ten hours for the longest.

Specimens 20 to 24 measured 300x300x100 mm with a circular 36 mm drillhole. The displacement values varied between 0.89 mm and 1.06 mm. The compressive strength had values between 36.7 N/mm^2 and 45.1 N/mm^2. The test duration varied from an hour and a half in the shortest one up to about nine hours the longest test.

Test	Body Nr.	Force max.	Time		Way	Compressive Strength	Break type
-	-	kN	h	m	mm	N/mm^2	-
1	1	141.6	2	45	-	-	A
2	1	165.0	4	28	-	-	B
3	3	204.2	2	51	0.43	20.4	C
4	4	202.3	2	3	0.92	20.2	C
5	5	184.0	2	4	0.66	18.4	C
6	6	60.5	0	34	0.54	06.2	F
7	7	102.6	0	57	0.75	10.3	F
8	8	51.4	1	45	-	-	A
		102.6	3	58	-	-	A
8a	8	130.5	9	50	-	-	A
8b	8	144.6	8	32	-	-	A
8c	8	161.6	7	45	-	-	A
8d	8	170.0	1	5	-	-	B
9	9	160.0	5	20	-	-	A
9a	9	175.0	9	28	-	-	A
9b	9	180.0	7	11	-	-	A
9c	9	185.0	7	12	-	-	A
9d	9	190.0	4	12	-	-	A
9e	9	200.0	3	20	-	-	A
9f	9	200.0	0	7	-	-	B
10	10	163.7	3	49	0.44	16.4	D
11	11	154.3	6	15	0.31	15.4	D
12	12	200.7	4	43	0.47	20.1	D
13	13	106.6	4	6	0.50	10.7	D
14	14	138.0	4	28	0.45	13.8	D
15+A	15	125.9	4	18	0.53	12.6	D
16+A	16	123.0	4	19	0.47	12.3	D
17+A	17	154.6	4	29	0.44	15.5	D
18+A	18	103.1	3	3	0.33	10.3	D
19+A	19	229.9	4	21	0.45	22.9	D
20+A	20	1309.7	6	45	1.06	43.7	E
21+A	21	973.1	9	54	-	-	A
21a+A	21	1128.5	5	54	0.89	37.6	E
22+A	22	1353.2	1	24	0.89	45.1	E
23+A	23	1101.1	4	41	0.96	36.7	E
24+A	24	1332.5	8	56	0.97	44.4	E

Table 5.3: Summary of tests results.

5.5. Description of individual specimens from 1 to 9

5.5.1. Introduction

As mentioned above, these first nine tests were conducted in specimens of sandstone with dimensions 200x200x50 mm and a 25 mm drillhole. Table 5.4 shows a summary of the test results and the parameters of each test. In order to get the correct results and to find the loading conditions, in this first test series some changes were made in the parameters ("trial and error") and some tests were not valid (test number 1, 2, 8 and 9). These tests are not included in the table 5.4.

Test	Body Nr.	Force max.	Time		Way	Compressive Strength	Break type	Test parameters			
-	-	kN	h	m	mm	N/mm^2	-		kN		N/min
3	3	204.2	2	51	0.43	20.4	C	F0	5	V0	2 mm/min
								V1-V2	170	V1	830
								V2-V3	171	V2	10^{-6}
4	4	202.3	2	3	0.92	20.2	C	F0	5	V0	2 mm/min
								V1-V2	150	V1	1600
								V2-V3	151	V2	10^{-6}
5	5	184	2	4	0.66	18.4	C	F0	5	V0	2 mm/min
								V1-V2	150	V1	1600
								V2-V3	151	V2	10^{-6}
6	6	60.5	0	34	0.54	6.1	F	F0	5	V0	2 mm/min
								V1-V2	140	V1	1600
								V2-V3	141	V2	10^{-6}
										V3	10 mm/min
7	7	102.6	0	57	0.75	10.3	F	F0	5	V0	2 mm/min
								V1-V2	50	V1	1600
								V2-V3	51	V2	10^{-6}

Table 5.4: Summary of the results and parameters of each test of the first test series from 1 to 9.

Certain factors must take into account when results are studied:

- ✓ In test case number 6, the rupture was interesting but it is not related to our purpose. The fractures appear along the tunnel, on the roof and on the floor, and propagate away from the cavity parallel to the applied loading direction.
- ✓ Specimen number 7 had a thickness of four centimeters, while the rest had a thickness of five centimeters. This is due to the fact that a total of five blocks were cut to obtain 18 samples with the necessary measures, leaving six samples with approximate dimensions

200x200x40 could not be used, one was used to obtain the loading conditions. The difference in centimeters is due to the loss of material produced by cutting the block.

- ✓ For the comparison of results only specimens number 3, 4 and 5 were taken into account. The mean of the compressive strength in these tests was 19.7 N/mm^2 and the mean of the displacement 0.67 mm.

5.5.2. Description of test 4

Specimen 4 is an example of case C, the rupture of the body and the drillhole occur simultaneously. Once the load reached 150 kN, after two hours and three minutes, in a few seconds the load increased up to 202.3 kN, the maximum force, because the loading rate in this step was 10 mm/min and specimen and drillhole broke simultaneously. Figure 5.8 shows the load displacement curve for the specimen, a change in the drawing is visible when the abrupt increase occurs in the last phase. The compressive strength value was 20.2 N/mm^2 and the displacement was 0.92 mm.

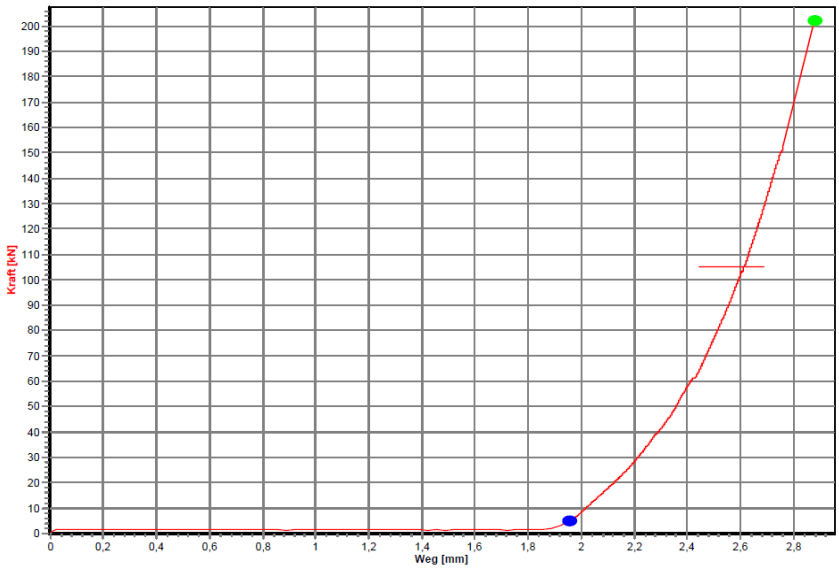

Fig. 5.8: Load displacement curve for specimen 4. The blue dot represents the point where the displacement of the test starts and the green dot represents the maximum force and the point where the displacement of the test finishes.

The final states of the piece, on the front side and on the back side of the specimen and on both sidewalls of the drillhole, are showed in figure 5.9 and for those cracks that cannot be clearly observed in the pictures, a sketch was added with the final state of the specimen in figure 5.10.

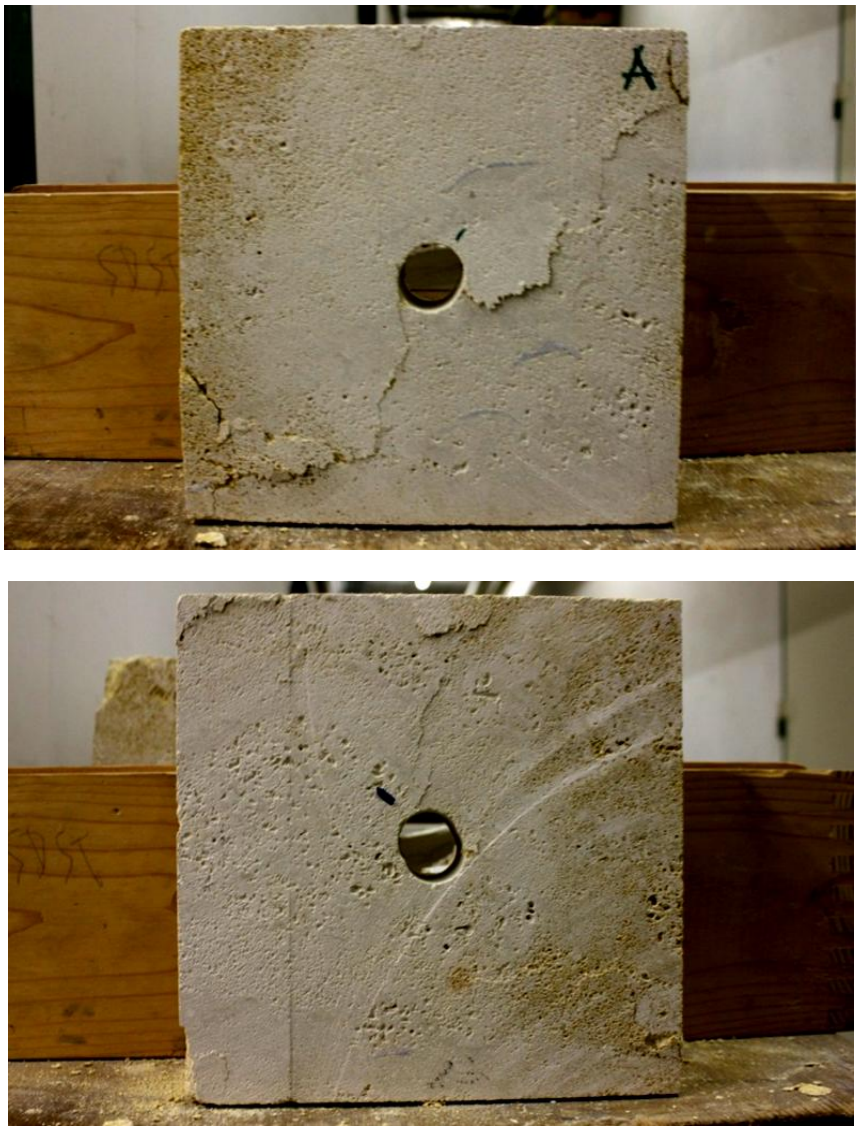

Fig. 5.9: Specimen 4 after testing. a) Side A. b) Side B. c) Drillhole of the specimen. The drillhole was photographed from side A.

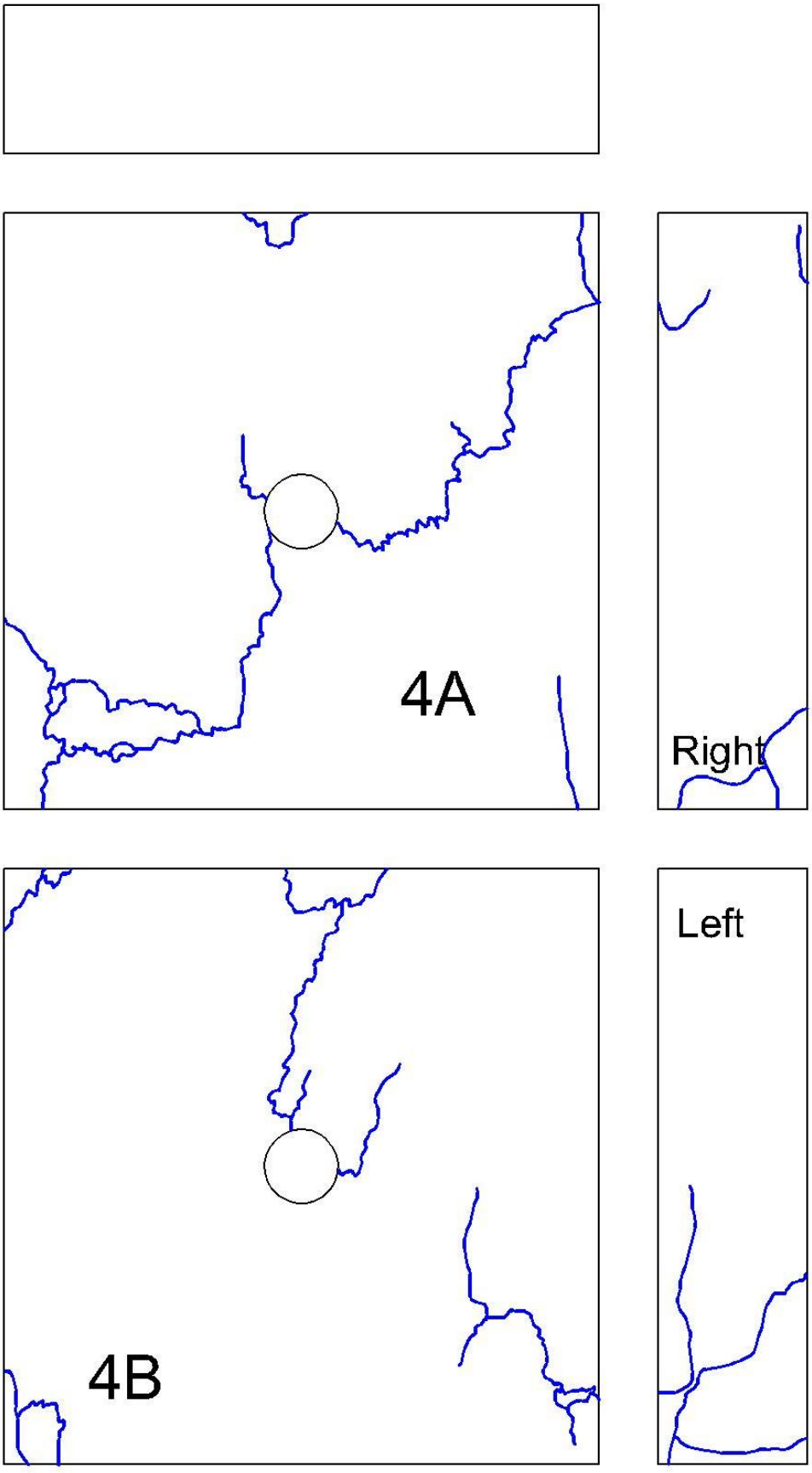

Fig. 5.10: Sketch of final state of specimen 4.

5.6. Description of individual specimens from 10 to 14

5.6.1. Introduction

The second series of experiments comprise from test number ten to fourteen. In this case all the tests were performed with the same parameters. Table 5.5 shows the results and parameter of tests.

Test	Body Nr.	Force max.	Time		Way	Compressive Strength	Break type					
-	-	kN	h	m	mm	N/mm²	-		kN			
10	10	163.7	3	49	0.44	16.4	D	V0	5	V0	2	mm/min
								V1-V2	100	V1	0.8	kN/min
								V2-V3	300	V2	0.004	mm/min
11	11	154.3	6	15	0.31	15.4	D	V0	5	V0	2	mm/min
								V1-V2	100	V1	0.8	kN/min
								V2-V3	300	V2	0.004	mm/min
12	12	200.7	4	43	0.47	20.1	D	V0	5	V0	2	mm/min
								V1-V2	100	V1	0.8	kN/min
								V2-V3	300	V2	0.004	mm/min
13	13	106.6	4	6	0.50	10.7	D	V0	5	V0	2	mm/min
								V1-V2	100	V1	0.8	kN/min
								V2-V3	300	V2	0.004	mm/min
14	14	138.0	4	28	0.45	13.8	D	V0	5	V0	2	mm/min
								V1-V2	100	V1	0.8	kN/min
								V2-V3	300	V2	0.004	mm/min

Table 5.5: Summary of the results and parameters of each test of the second test series from 10 to 14.

In this series of tests all the experiments were valid and they showed a new break type, type D. Values of the compressive strength varied between 13.8 N/mm^2 and 20.1 N/mm^2 and the average compressive strength value was 15.3 N/mm^2. In this series the average displacement was 0.43 mm, with values ranging between 0.31 mm and 0.50 mm. Duration of these tests varied from four hours to six hours.

First the rupture in the body of the specimen occurs, on the right side, on the left side, on the back side or on the front side of the specimen. Afterwards the crack on the sidewalls of the drillhole became visible.

5.6.2. Description of test 12

Specimen 12 is an example of case D. First the rupture in the body of the specimen occurs, on the right side, on the left side, on the back side or on the front side of the specimen and then rupture on the sidewalls of the drillhole became visible. Until the end of the trial, more cracks appeared in the body of the specimen. In figure 5.11 the load is plotted versus displacement.

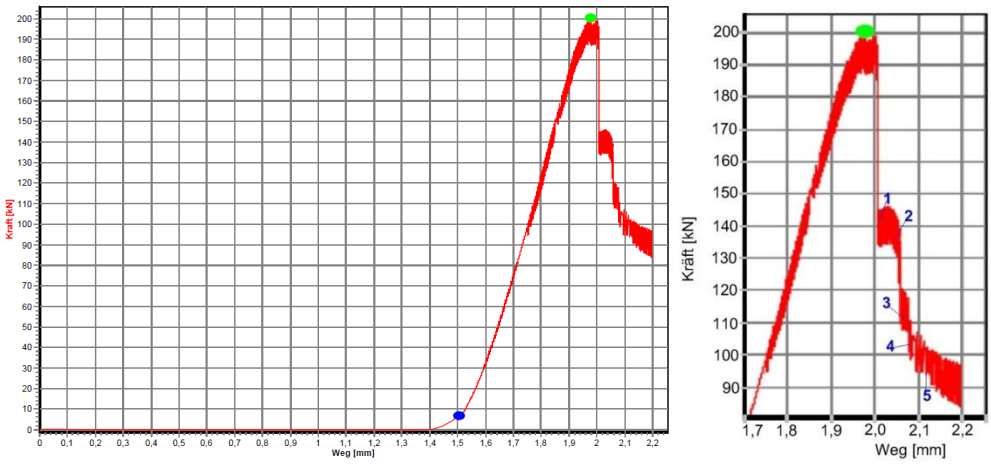

Fig. 5.11: a) Load displacement curve for specimen 12. The blue dot represents the point where the displacement of the test starts and the green dot represents the maximum force and the point where the displacement of the test finishes. b) Area of interest in the load displacement curve for specimen 12.

In this test there were five points where cracks could be seen in the body of the specimen and in the drillhole. These moments were marked with numbers in diagram. Soon after reaching the point of maximum force, green point in diagram, the force fell to 136 kN. At this moment first cracks became visible, one on the left side of the surface B, and rest of them on the right side of the specimen, figure 5.12. In the curve, figure 5.11, this moment is marked with number 1.

A short time after, where the load was more or less the same, a decrease of the force started and when the force arrived to 134 kN, point number 2 of the curve, a fracture appeared in the drillhole, on the right sidewall. In addition, the existing fracture on side B grew until it joined the drillhole. Another crack appeared around the opening, figures 5.13 and 5.14 show cracks of point 2.

The crack on the left sidewall of the drillhole could be observed when the force decreased to 112 kN, point 3 of the curve. The crack on the right side of the specimen grew to the top of the specimen, figures 5.15 and 5.16 show cracks of point 3.

The next crack, point number 4 of the curve, appeared on side A after another fall in the force to 107 kN. The crack crossed the piece from one side of the hole to the right side of the specimen, figures 5.17 and 5.18.

In point 5, the force reduced to 94 kN and a new crack became visible on the left side of the surface A. Crack grew from the left side of the hole to the top of the specimen and in the parallel direction of applied load, figure 5.19.

Figure 5.20 shows some sketches of the initiation and propagation of cracks. New cracks are marked with red lines and previous cracks are marked with blue lines.

The final state of the piece and of the drillhole can be seen in figure 5.21. For those cracks couldn´t be seen clearly in the pictures, a sketch was added with the final state of the specimen figure 5.22.

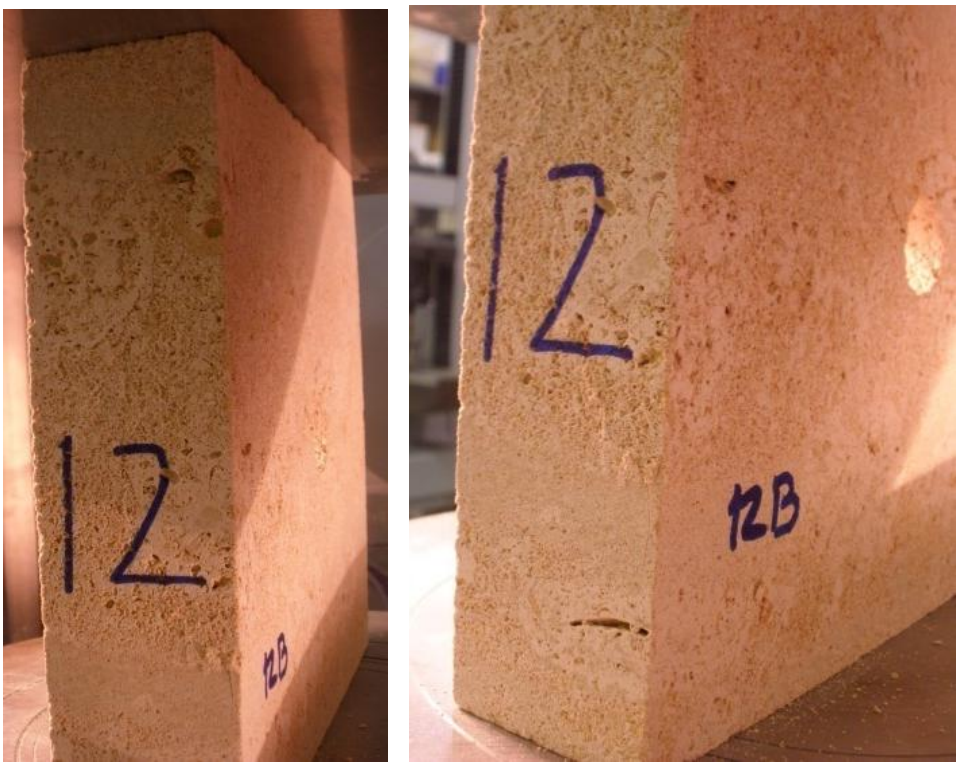

Fig. 5.12: Cracks in specimen 12 for point 1 of the figure 5.11. a) Cracks on right the side A of the specimen. b) Cracks on the side B of the specimen.

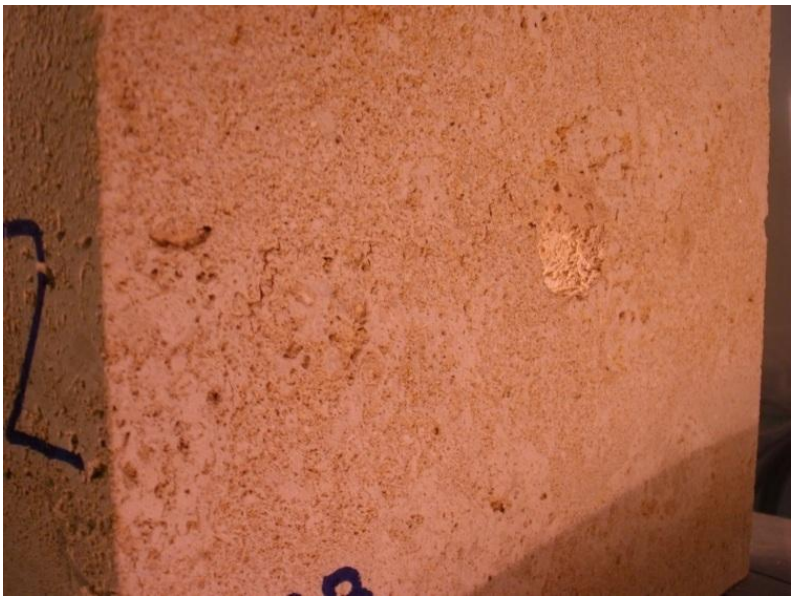

Fig. 5.13: Cracks in specimen 12 for point 2 of the figure 5.11. Cracks on the side B of the specimen.

Fig. 5.14: Cracks in specimen 12 for point 2 of the figure 5.11. Rupture on the right wall of the drillhole. Picture was taken from side A of the specimen.

Fig. 5.15: Cracks in specimen 12 for point 3 of the figure 5.11. Rupture on the left wall of the drillhole.

Fig.5.16: Cracks in specimen 12 for point 3 of the figure 5.11. Cracks on the right side of the specimen.

Fig.5.17: Cracks in specimen 12 for point 4 of the figure 5.11. Cracks on the side A of the specimen.

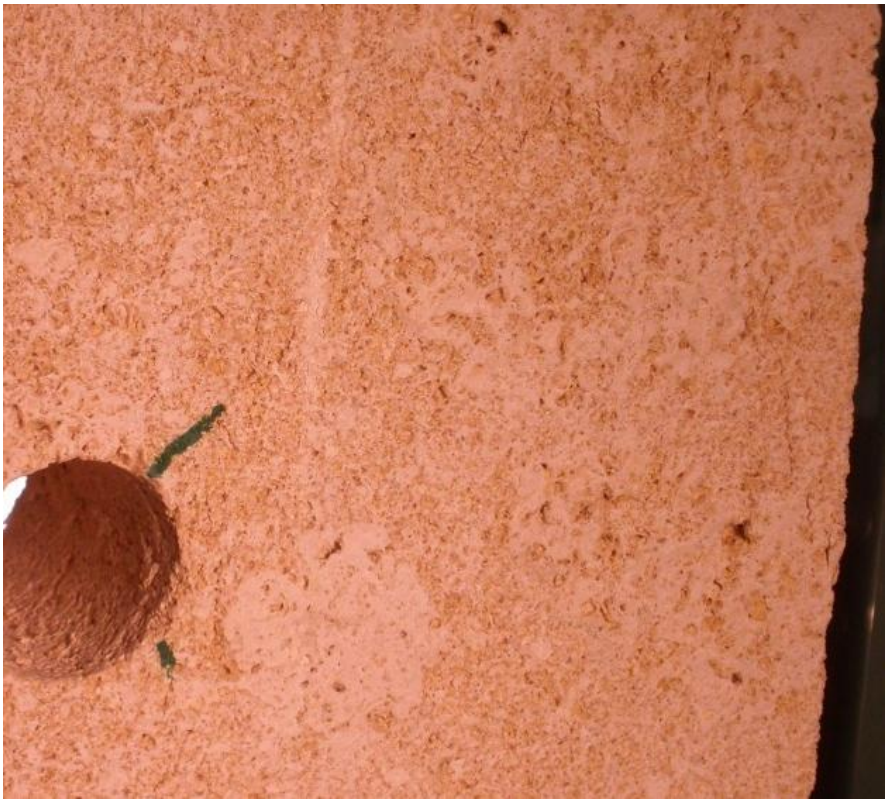

Fig.5.18: Cracks in specimen 12 for point 4 of the figure 5.11. Cracks on the side A of the specimen.

Fig. 5.19: Cracks in specimen 12 for point 5 of the figure 5.11. Cracks on the side A of the specimen.

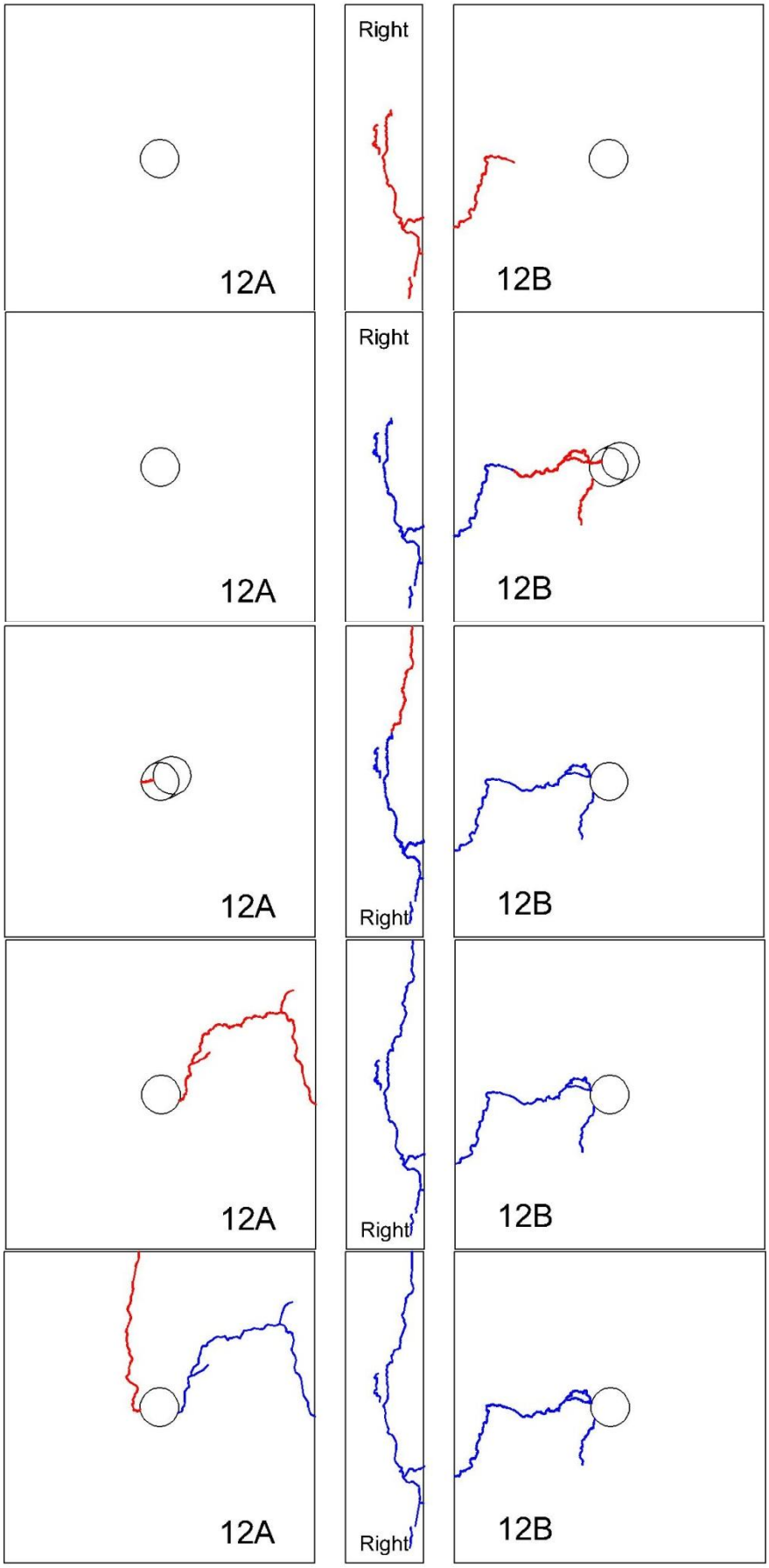

Fig. 5.20: Sketch of specimen 12 for points 1, 2, 3, 4 and 5 of the figure 5.11.

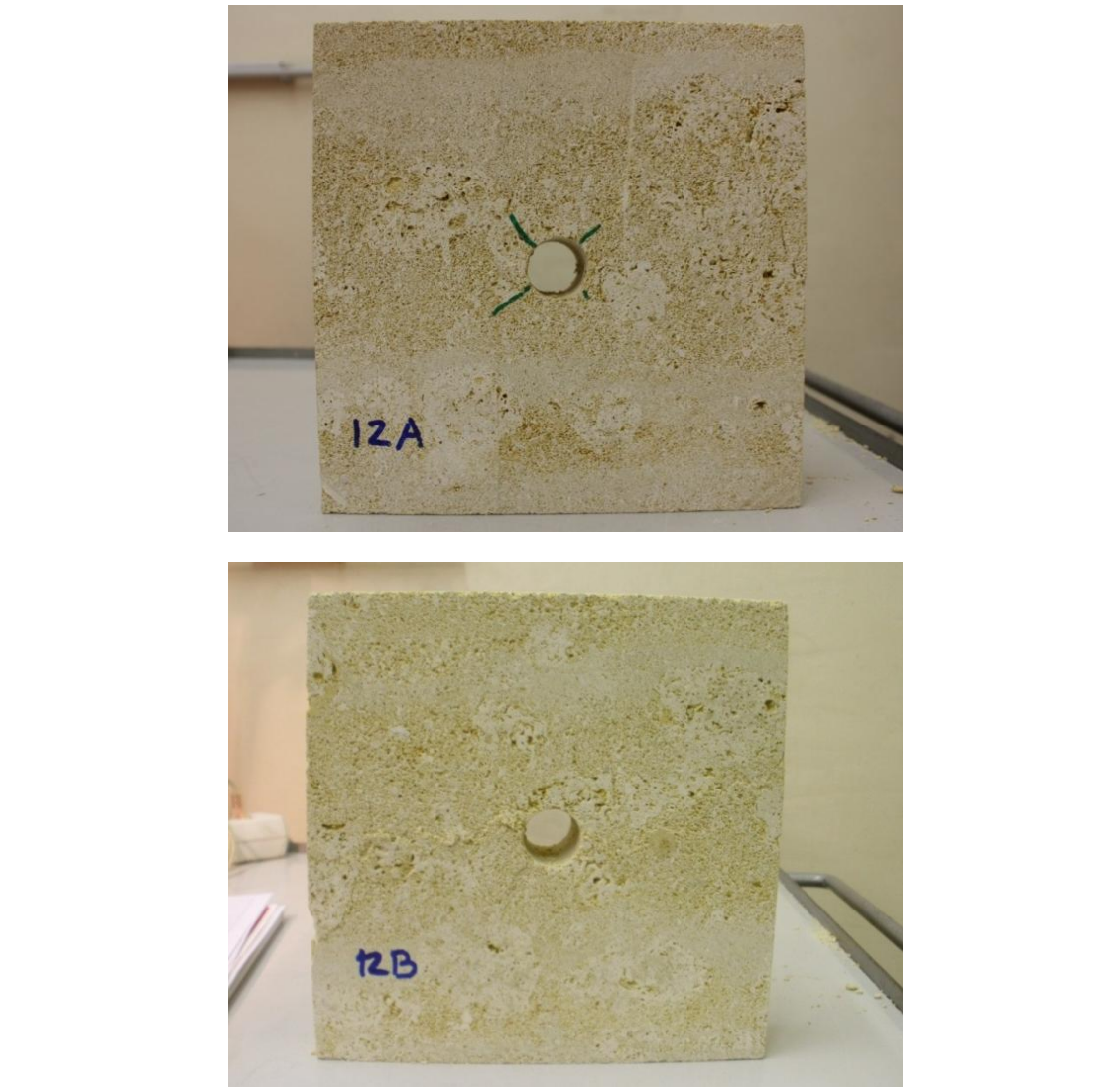

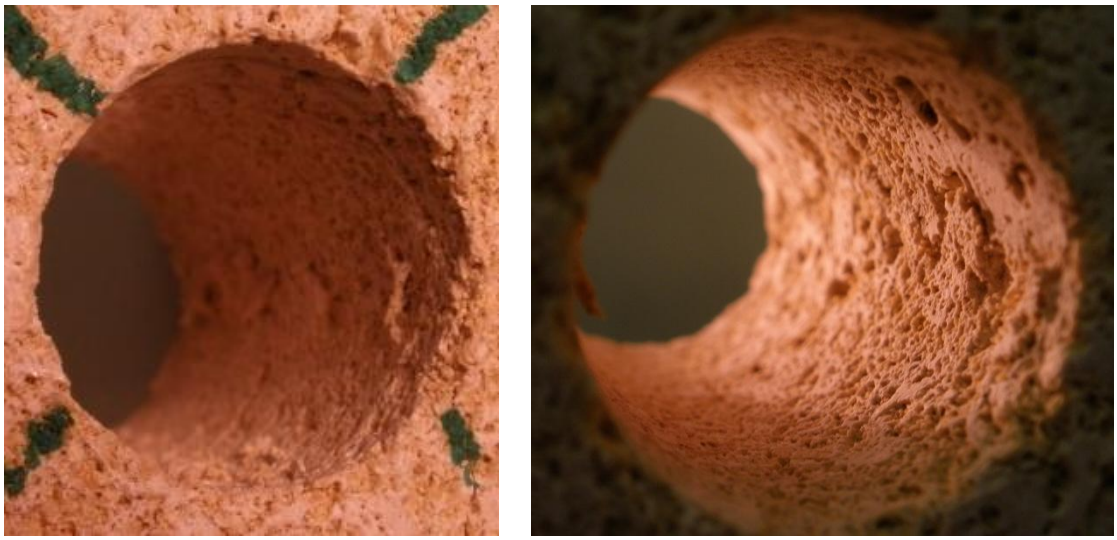

Fig.5.21: Specimen 12 after testing. a) Side A. b) Side B. c) Drillhole of the specimen (Left) The drillhole was photographed from side A. (Right) The drillhole was photographed from side B.

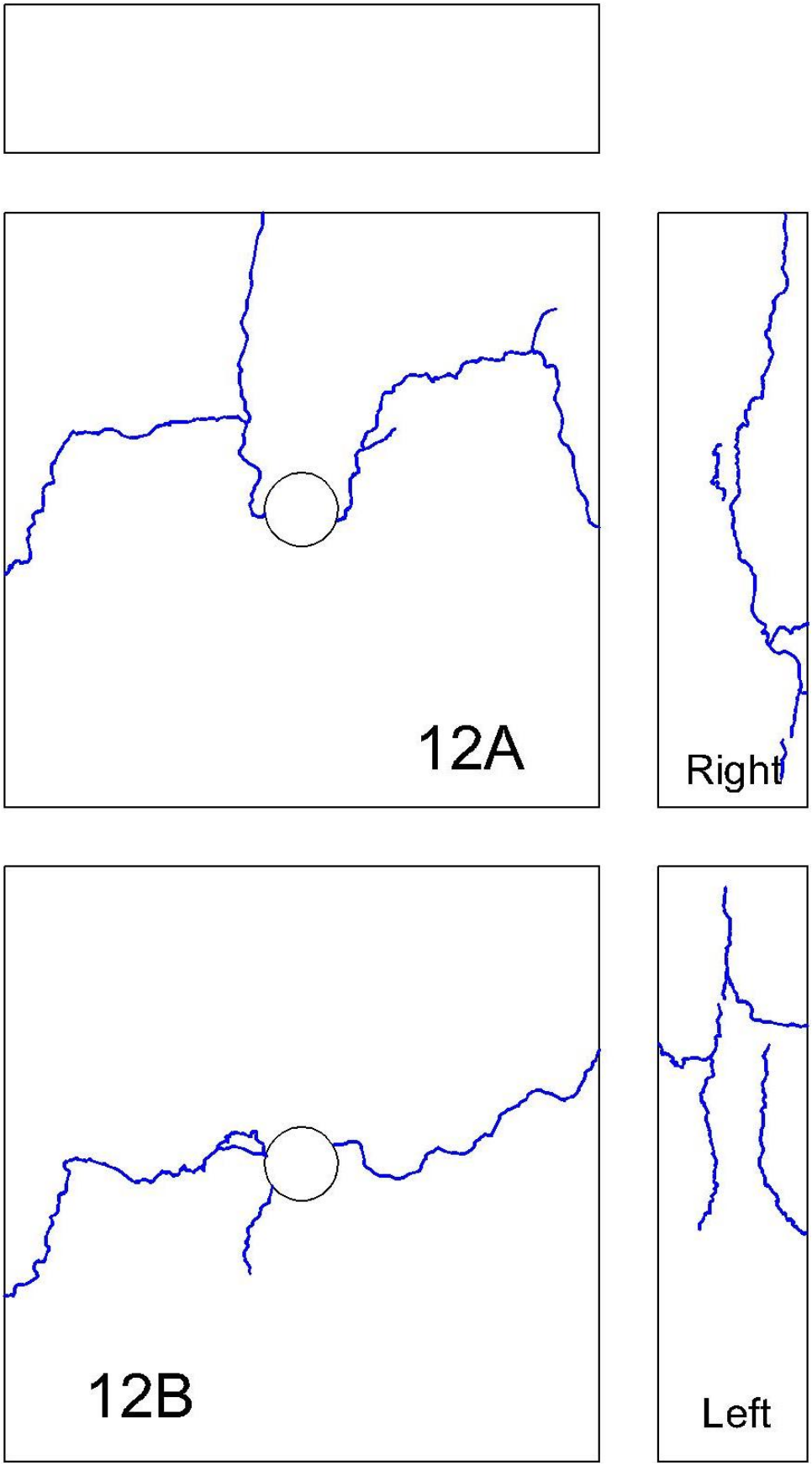

Fig. 5.22: Sketch of final state of specimen 12.

5.7. Description of individual specimens from 15 to 19

5.7.1. Introduction

The third series of experiments comprise specimens fifteen to nineteen. These are the last tests with specimens of dimensions 200x200x200 mm and a circular cavity with 25 mm diameter. In this series of tests, there a new element was added, an aluminum plate with dimensions 200x50x3 mm. This plate was used as interface between the loading platen and the specimen. It was added after consulting previous experiments in different papers, where an interface was used between the specimen and the loading platen. The most important aspect of the interface was to transfer the load uniformly into the specimen. If the loading surface of the specimen was bumpy or weaker regions where present, it was difficult to establish proper interface conditions.

Test	Body Nr.	Force max.	Time		Way	Compressive Strength	Break type					
-	-	kN	h	m	mm	N/mm^2	-		kN			
15+A	15	125.9	4	18	0.53	12.6	D	V0	5	V0	2	mm/min
								V1-V2	100	V1	0.8	kN/min
								V2-V3	500	V2	0.004	mm/min
16+A	16	123	4	19	0.47	12.3	D	V0	5	V0	2	mm/min
								V1-V2	100	V1	0.8	kN/min
								V2-V3	500	V2	0.004	mm/min
17+A	17	154.6	4	29	0.44	15.5	D	V0	5	V0	2	mm/min
								V1-V2	100	V1	0.8	kN/min
								V2-V3	500	V2	0.004	mm/min
18+A	18	103.1	3	3	0.33	10.3	D	V0	5	V0	2	mm/min
								V1-V2	100	V1	0.8	kN/min
								V2-V3	500	V2	0.004	mm/min
19+A	19	229.9	4	21	0.45	22.9	D	V0	5	V0	2	mm/min
								V1-V2	100	V1	0.8	kN/min
								V2-V3	500	V2	0.004	mm/min

Table 5.6: Summary of the results and parameters of each test of the third test series from 15 to 19.

In this series of tests all the experiments were valid and they showed the same breaking type. Table 5.6 shows the results and parameters of tests. As in the previous series, first the rupture on the body of the specimen happened and afterwards breaking of the sidewalls of the drillhole appeared.

The values of the compressive strength varied between 10.3 N/mm^2 and 22.9 N/mm^2 and the average value of compressive strength was 14.7 N/mm^2. In this series the average of displacement was 0.44 mm, with values ranging between 0.33 mm and 0.53 mm. The duration of these tests were about four hours.

5.7.2. Description of test 19

This test reached the greatest compressive strength in this series, 22.9 N/mm^2 with a displacement of 0.45 mm and the total duration of the experiment was four hours and a half. First, the rupture of the test specimen happened, on the left side and on the back side of the specimen. Later it was on both sidewalls of the drillhole, first on the left wall and later on the right wall, and until the end of the experiment, more cracks appeared on the body of the specimen.

Figures 5.34 and 5.35 show some sketches of the initiation and propagation of the cracks during testing. Rupture of the drillhole on both sidewalls can be observed in figure 5.36. Photographs from side A and other from side B were chosen. The final state of the piece on the front and on the back side after, experiment is showed in figure 5.36 and a sketch was added with the final state of the specimen in figure 5.37.

In this test there were nine points in the diagram where cracks could be seen in the body of the specimen or in the drillhole. Soon after reaching the point of maximum force, the force fell to 203 kN and the first cracks became visible, point 1 in figure 5.23, one on the left side of the specimen and another one on the lower left corner on side B (figure 5.24).

The force decreased again to 163 kN, point number 2 of the curve, a fracture appeared on the left sidewall of the drillhole (figure 5.25). In point number 3 of the curve a new crack appeared on the left of surface A, figure 5.26 shows the new crack. When the force reached 160 kN a new crack appeared on the top of side B, see figure 5.27. In the next point, point 5 of the curve, after the force fell to 148 kN the existing crack on side B enlarged (figure 5.28).

The force decreased to 140 kN and the rupture on the right sidewall of the drillhole became visible, see figure 5.29. In the next point, 7, when the force fell to 129 kN a crack crossed the specimen on side A from the left side of the drillhole to the left side of the specimen, figures 5.30 and 5.31 show cracks of point 7. At 115 kN, the existing fracture on side B grew and a new crack appeared, which grew in the parallel direction of applied load (see figure 5.32).

The last crack appeared on side A, point number 9 of the curve, when the force decreased to 109 kN. Crack crossed the specimen from the right side of the drillhole to the right side of the specimen, figure 5.33.

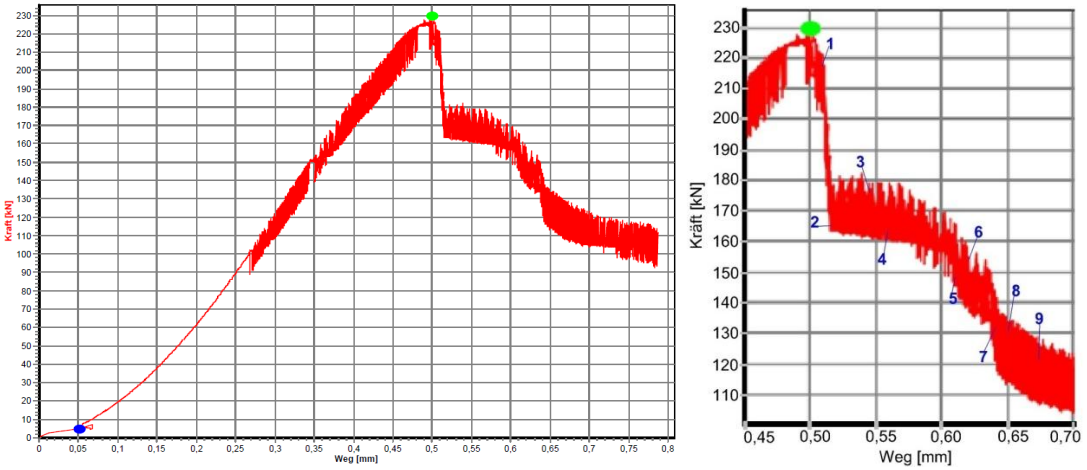

Fig. 5.23: a) Load displacement curve for specimen 19. The blue dot represents the point where the displacement of the test starts and the green dot represents the maximum force and the point where the displacement of the test finishes. b) Area of interest in the load displacement curve for specimen 19.

Fig. 5.24: Cracks in specimen 19 for point 1 of the figure 5.23. a) Cracks on right side of the specimen. b) Cracks on the side B of the specimen.

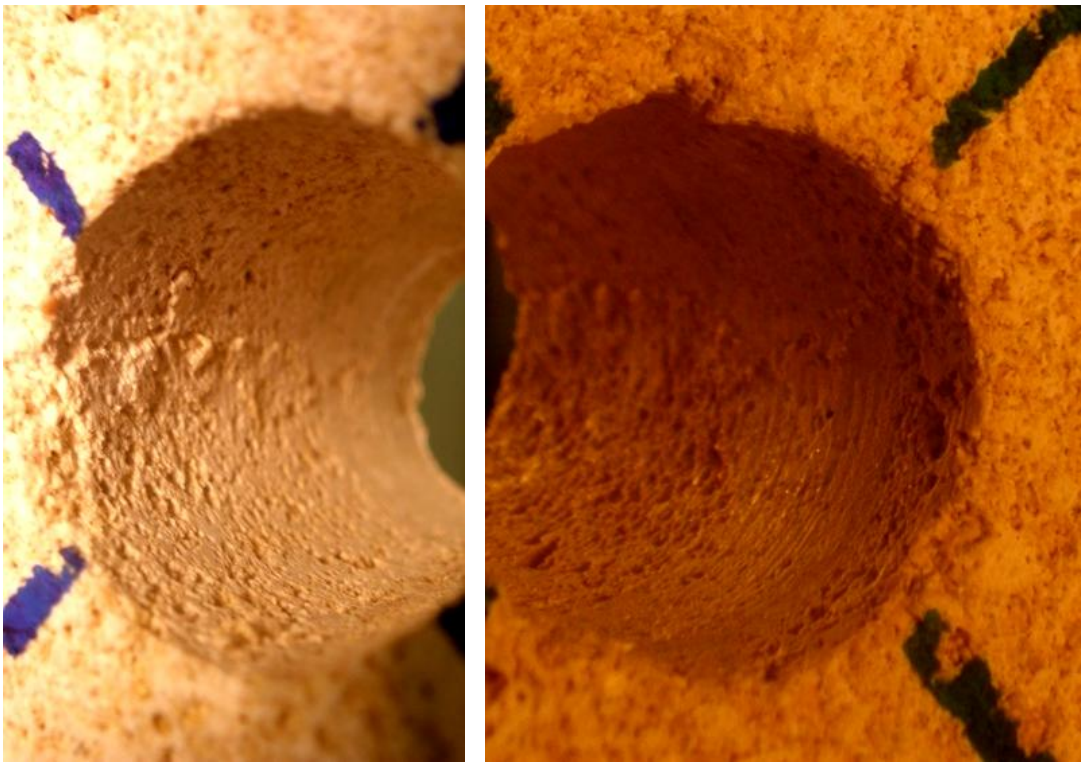

Fig. 5.25: Cracks in specimen 19 for point 2 of the figure 5.23. Rupture on the left wall of the drillhole. a) Picture was taken from side A of the specimen. b) Picture was taken from side B of the specimen.

Fig. 5.26: Cracks in specimen 19 for point 3 of the figure 5.23. Cracks on the side A of the specimen.

Fig. 5.27: Cracks in specimen 19 for point 4 of the figure 5.23. Cracks on the side B of the specimen.

Fig. 5.28: Cracks in specimen 19 for point 5 of the figure 5.23. Cracks on the side B of the specimen.

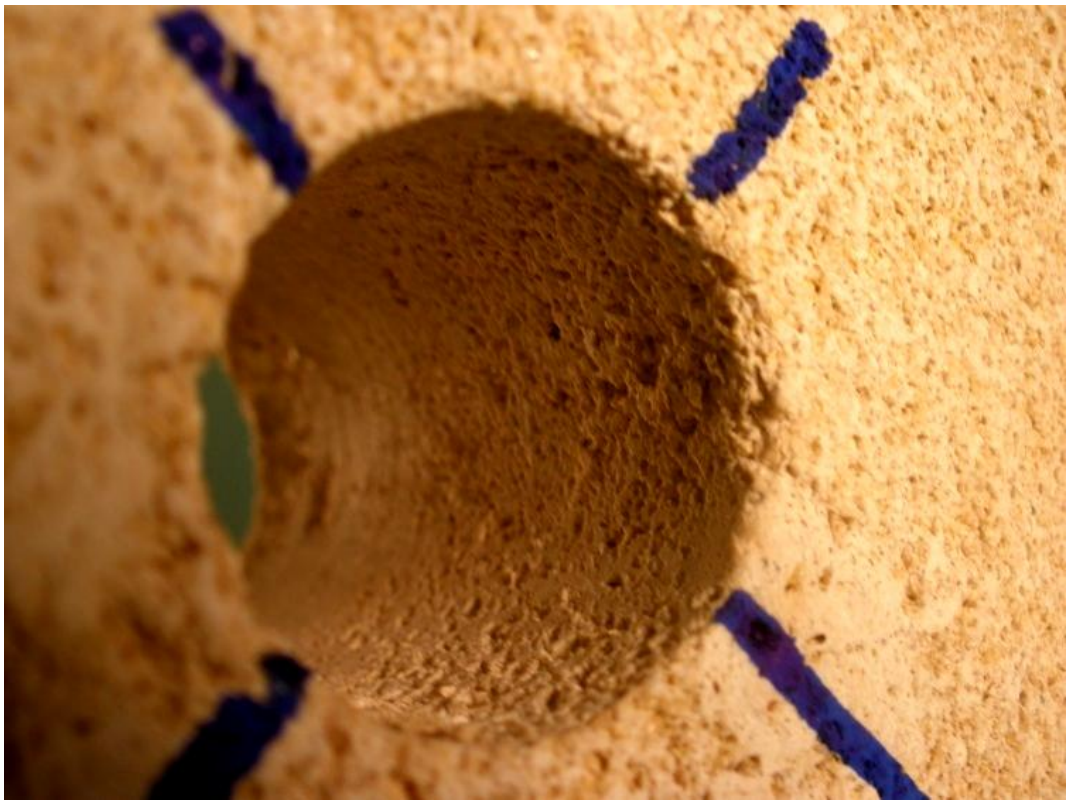

Fig. 5.29: Cracks in specimen 19 for point 6 of the figure 5.23. Rupture on the right wall of the drillhole. Picture was taken from side A of the specimen.

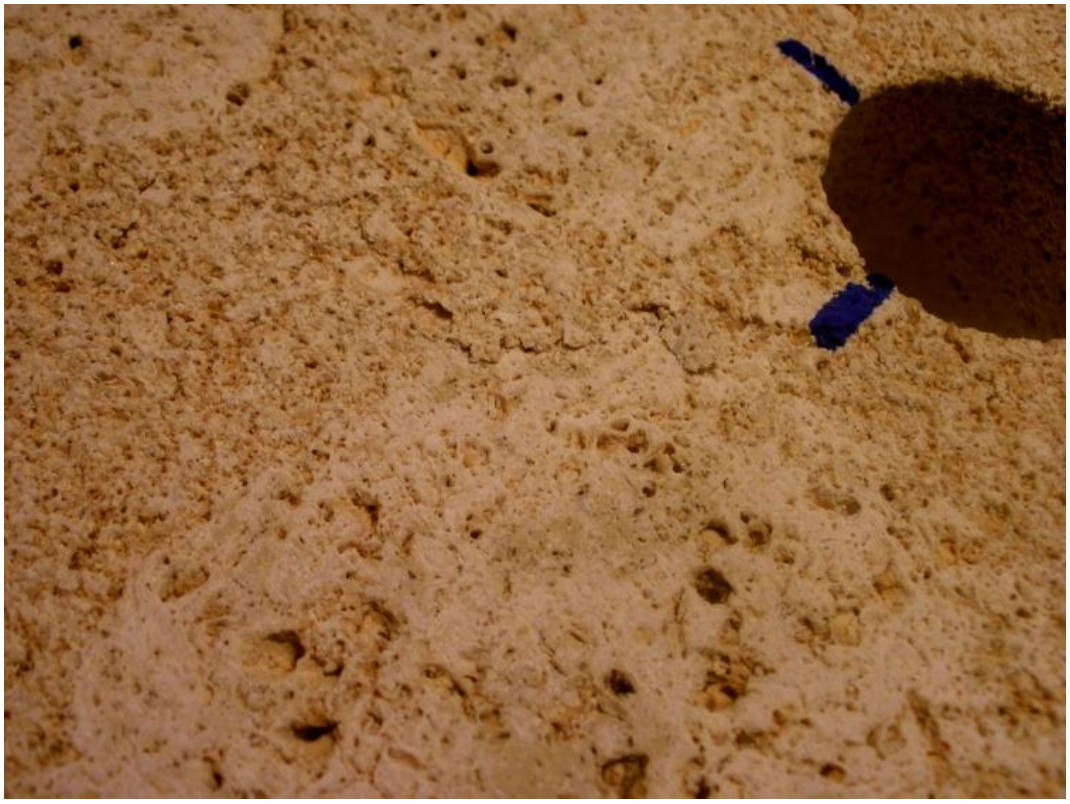

Fig. 5.30: Cracks in specimen 19 for point 7 of the figure 5.23. Cracks on the side A of the specimen.

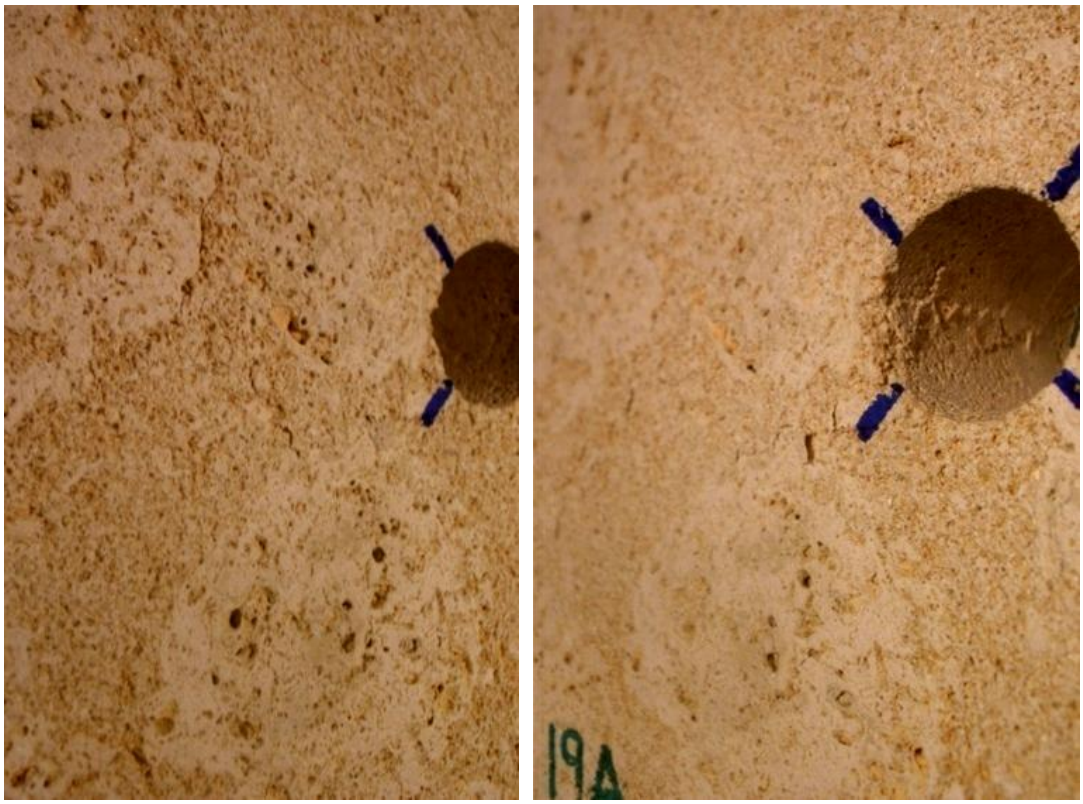

Fig. 5.31: Cracks in specimen 19 for point 7 of the figure 5.23. Cracks on the side A of the specimen.

Fig. 5.32: Cracks in specimen 19 for point 8 of the figure 5.23. Cracks on the side B of the specimen.

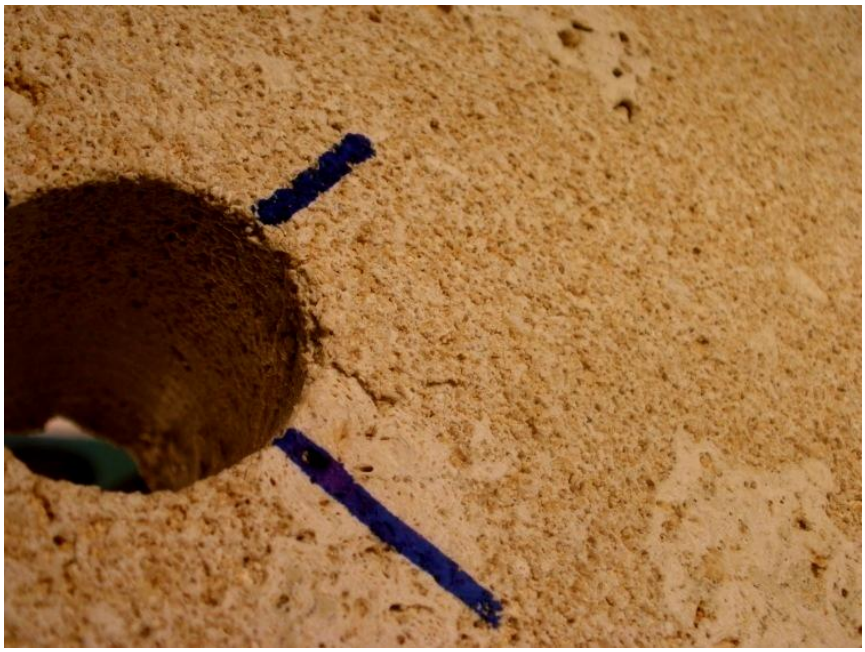

Fig. 5.33: Cracks in specimen 19 for point 9 of the figure 5.23. Cracks on the side A of the specimen.

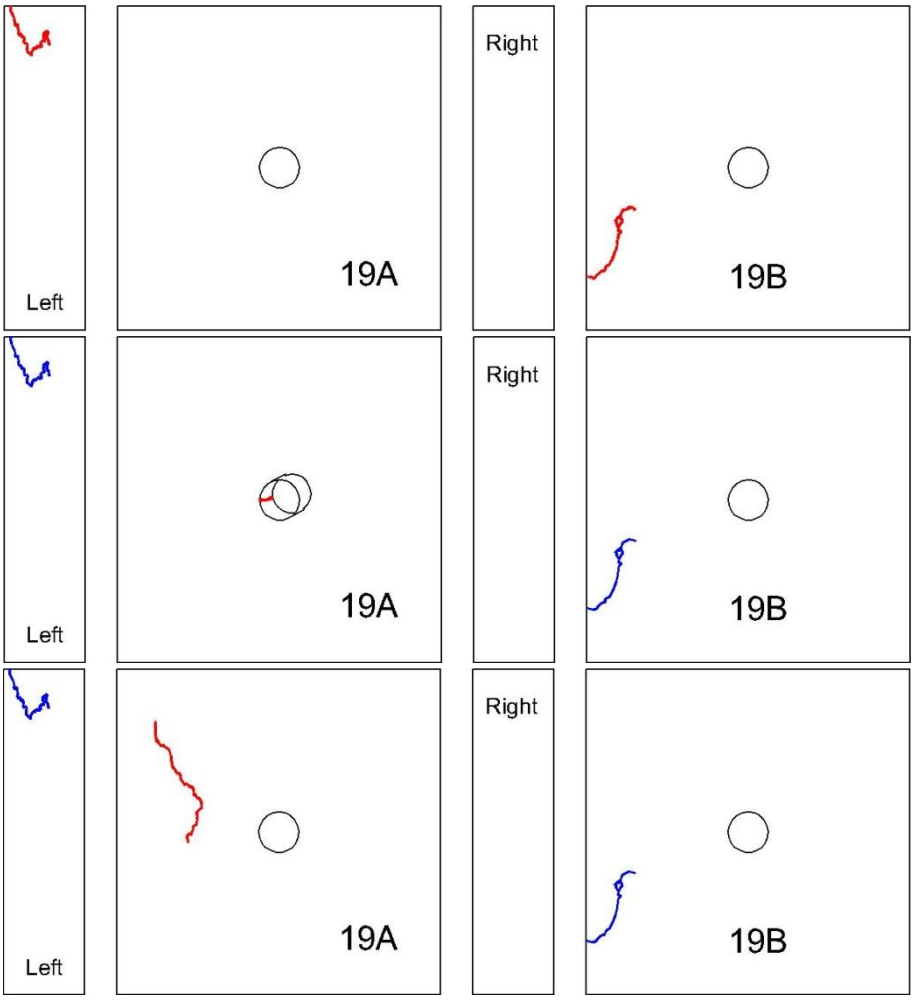

Fig. 5.34: Sketch of specimen 19 for points 1, 2 and 3 of the figure 5.23.

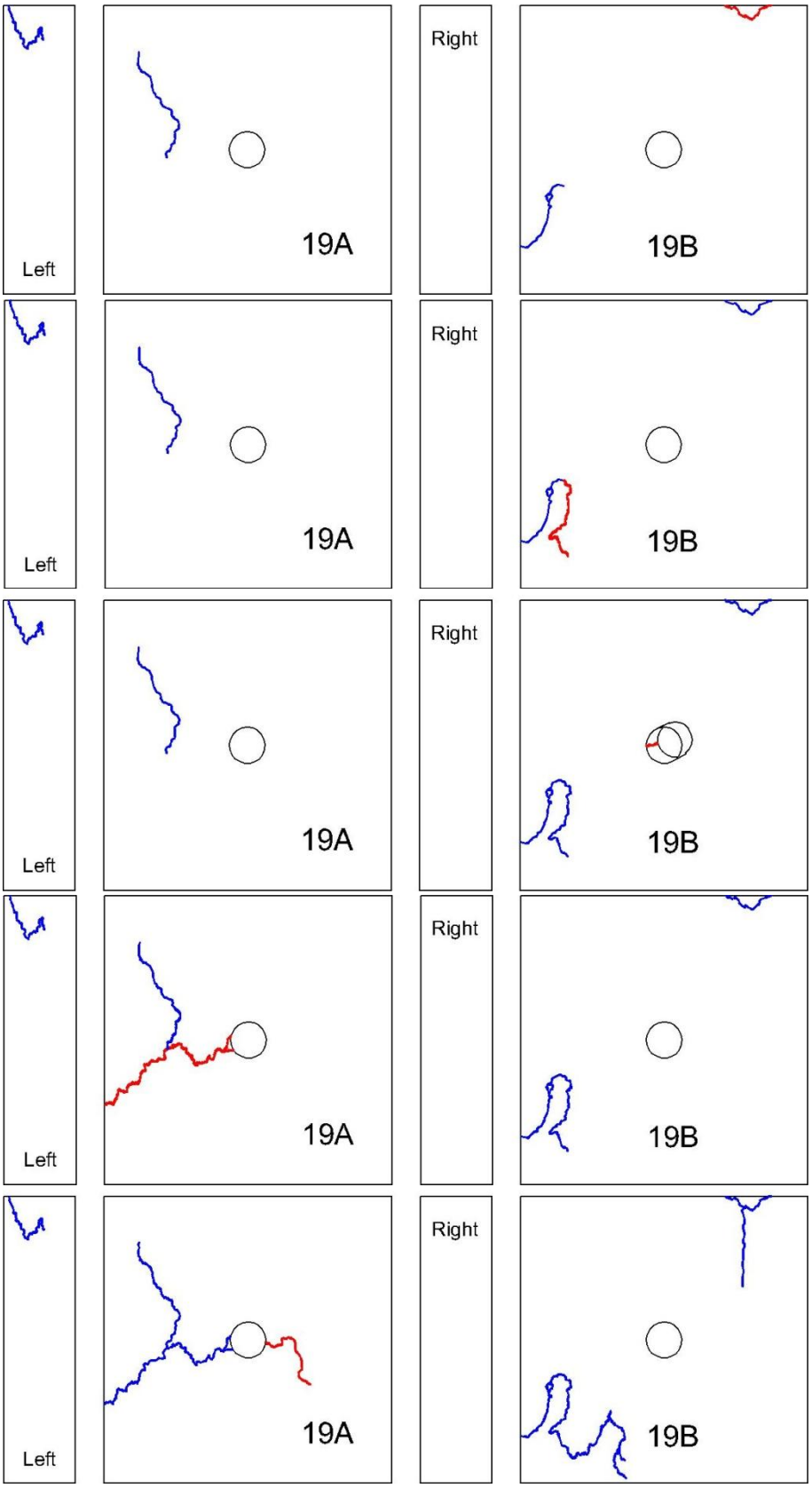

Fig. 5.35: Sketch of specimen 19 for points 4, 5, 6, 7 and 8 of the figure 5.23.

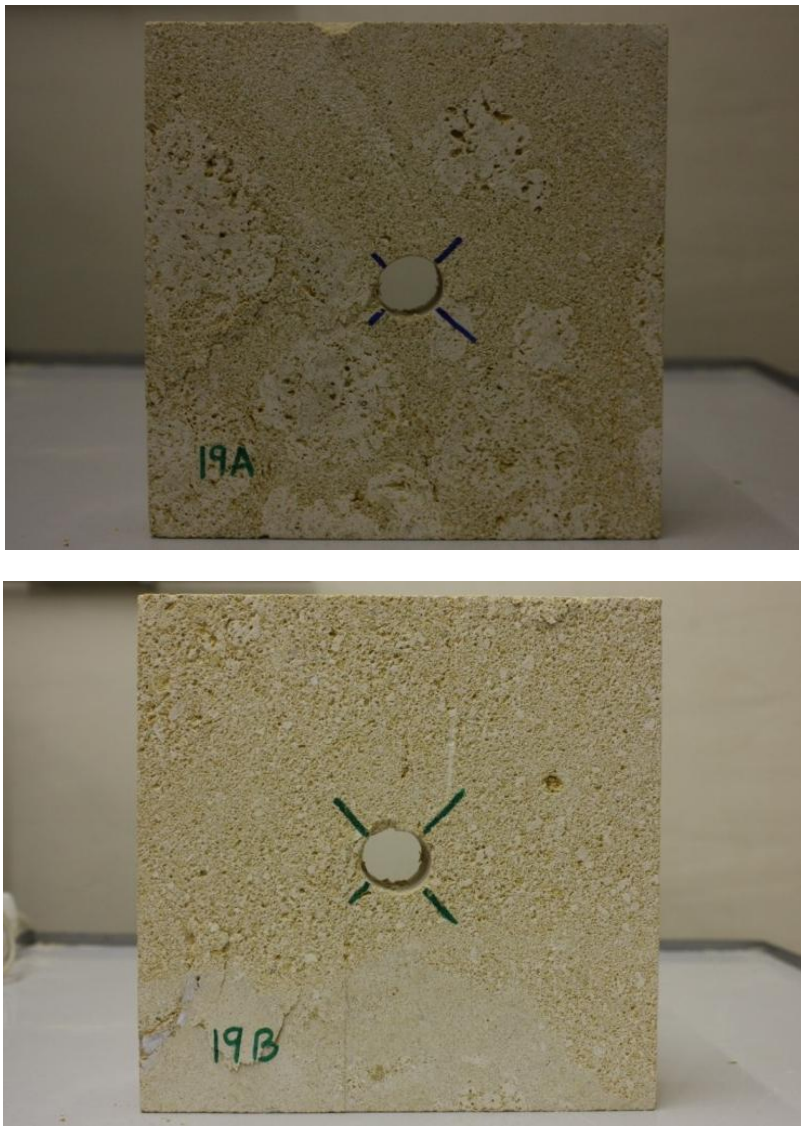

Fig. 5.36: Specimen 19 after testing. a) Side A. b) Side B. c) Drillhole of the specimen. (Left) The drillhole was photographed from side A. (Right) The drillhole was photographed from side B.

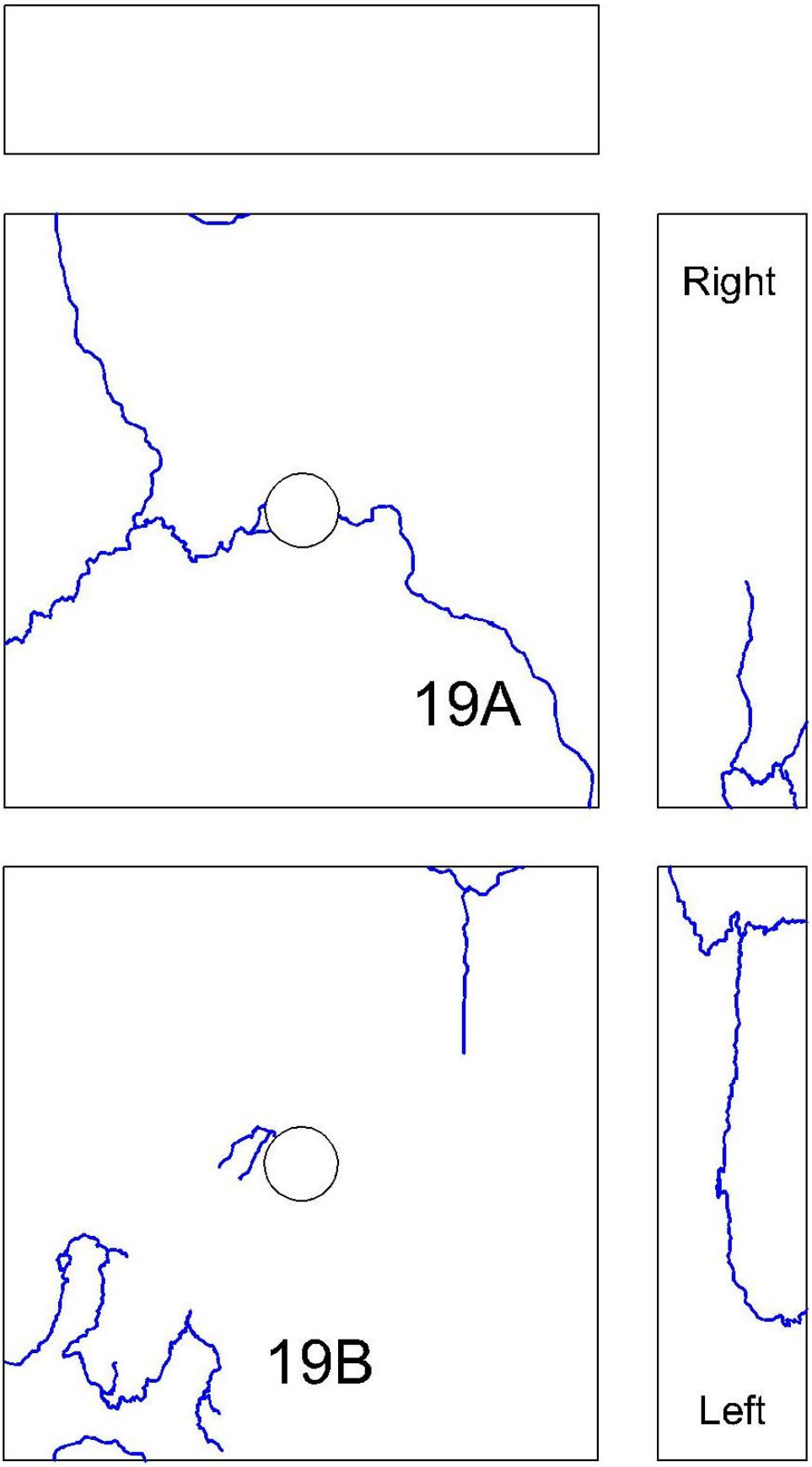

Fig. 5.37: Sketch of final state of specimen 19.

5.8. Description of individual specimens from 20 to 24

5.8.1. Introduction

The fourth series of experiments comprise from test number twenty to twenty-four. These tests were carried out in specimens with dimensions 300x300x100 mm and a circular drillhole with a diameter of 36 mm. In this series of tests an aluminum plate with dimensions 300x100x20 mm was used. This plate was used as interface between the loading platen and the specimen as in the previous series of tests.

In this series of tests all experiments showed a new breaking type. In all tests, at the beginning the rupture on both walls of the drillhole occurred. Later, soon after reaching the point of maximum force, the first cracks on the body of the specimen became visible. The cracks start on the two opposite sides of the opening and grow parallel to the applied load. More cracks appeared on the right side and on the left side of the specimen. Table 5.7 shows the results and parameters of tests.

Test	Body Nr.	Force max.	Time		Way	Compressive Strength	Break type					
-	-	kN	h	m	mm	N/mm²	-		kN			
20+A	20	1309.7	6	45	1.06	43.7	E	V0	5	V0	2	mm/min
								V1-V2	6.34	V1	0.8	kN/min
								V2-V3	2800	V2	0.004	mm/min
21a+A	21	1128.5	5	54	0.89	37.6	E	V0	5	V0	2	mm/min
								V1-V2	800	V1	10	kN/min
								V2-V3	2800	V2	0.002	mm/min
22+A	22	1353.2	11	24	0.89	45.1	E	V0	5	V0	2	mm/min
								V1-V2	800	V1	10	kN/min
								V2-V3	2800	V2	0.001	mm/min
23+A	23	1101.1	4	41	0.96	36.7	E	V0	5	V0	2	mm/min
								V1-V2	1000	V1	10	kN/min
								V2-V3	2800	V2	0.001	mm/min
24+A	24	1332.5	8	56	0.97	44.4	E	V0	5	V0	2	mm/min
								V1-V2	800	V1	10	kN/min
								V2-V3	2800	V2	0.001	mm/min

Table 5.7: Summary of the results and parameters of each test of the fourth test series from 20 to 24.

The values of the compressive strength varied between 36.7 N/mm^2 and 45.1 N/mm^2 and the average value of compressive strength was 41.5 N/mm^2. In this series the mean displacement was 0.95 mm, with values ranging between 0.89 mm and 1.06 mm. The duration of these tests varied between six hours and eleven hours.

5.8.2. Description of test 22

This test reached the greatest compressive strength in this series, 45.1 N/mm^2 with a displacement of 0.89 mm and the total duration of the experiment was 11 hours and a half, the longest in this series too.

At 1187 kN, point 1 of the curve (figure 5.38), the first crack in the drillhole became visible. The right tunnel wall was still intact, but the failure occurred on the left tunnel wall of the circular drillhole. In figure 5.39 one can easily see the cracks on the left sidewall of the opening and that the right wall was still intact.

Soon after reaching the point of maximum force, 1353.2 kN, the force fell and in point 2 of the curve, 1283.3 kN, the rupture on the right sidewall of the drillhole happened. In this point cracks on the two opposite sides of the opening became visible too, on side A. On side B a new crack appeared on the left side of the opening, figures 5.40, 5.41 and 5.42 show cracks of point 2. The force fell to 1258 kN, point 3 of the curve, and on side B a new crack appeared on the right side of the hole, which grew parallel to the applied load (figure 5.43).

The force decrease to 902 kN, point 4 of the curve, and the existing cracks on side A grew parallel to the applied load towards the top and bottom of the specimen, figures 5.44 and 5.45 show cracks of point 4. After this point the force increase and when the force reached 1046 kN the last crack became visible on side A, see figure 5.46.

The specimen was photographed after testing, see figure 5.48. For those which cracks couldn´t be clearly seen in the pictures, a sketch was added with the final state of the specimen in figure 5.49. The initiation and propagation of the cracks can be seen by means of sketches in figure 5.47.

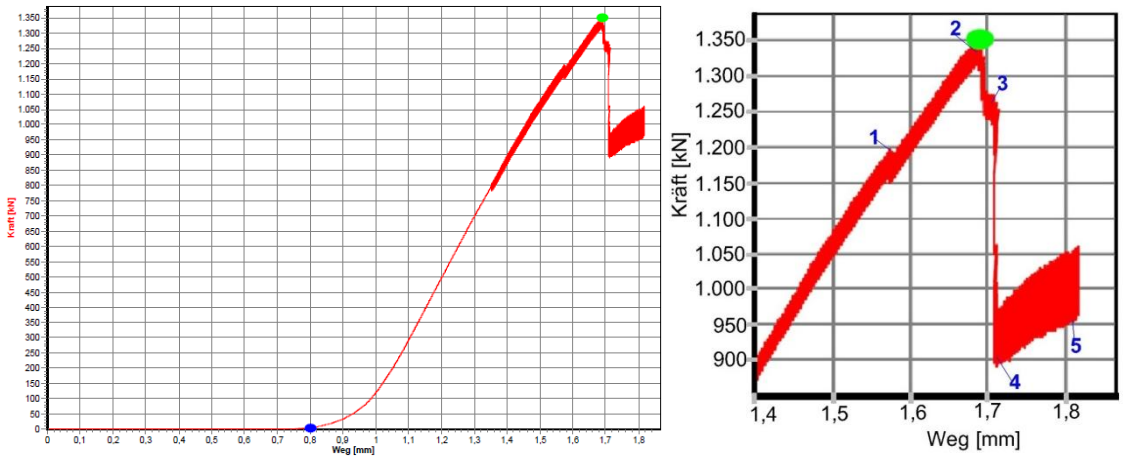

Fig. 5.38: a) Load displacement curve for specimen 22. The blue dot represents the point where the displacement of the test starts and the green dot represents the maximum force and the point where the displacement of the test finishes. b) Area of interest in the load displacement curve for specimen 22.

Fig. 5.39: Cracks in specimen 22 for point 1 of the figure 5.38. a) No rupture on the left wall of the drillhole. b) Rupture on the right wall of the drillhole. Picture was taken from side B of the specimen.

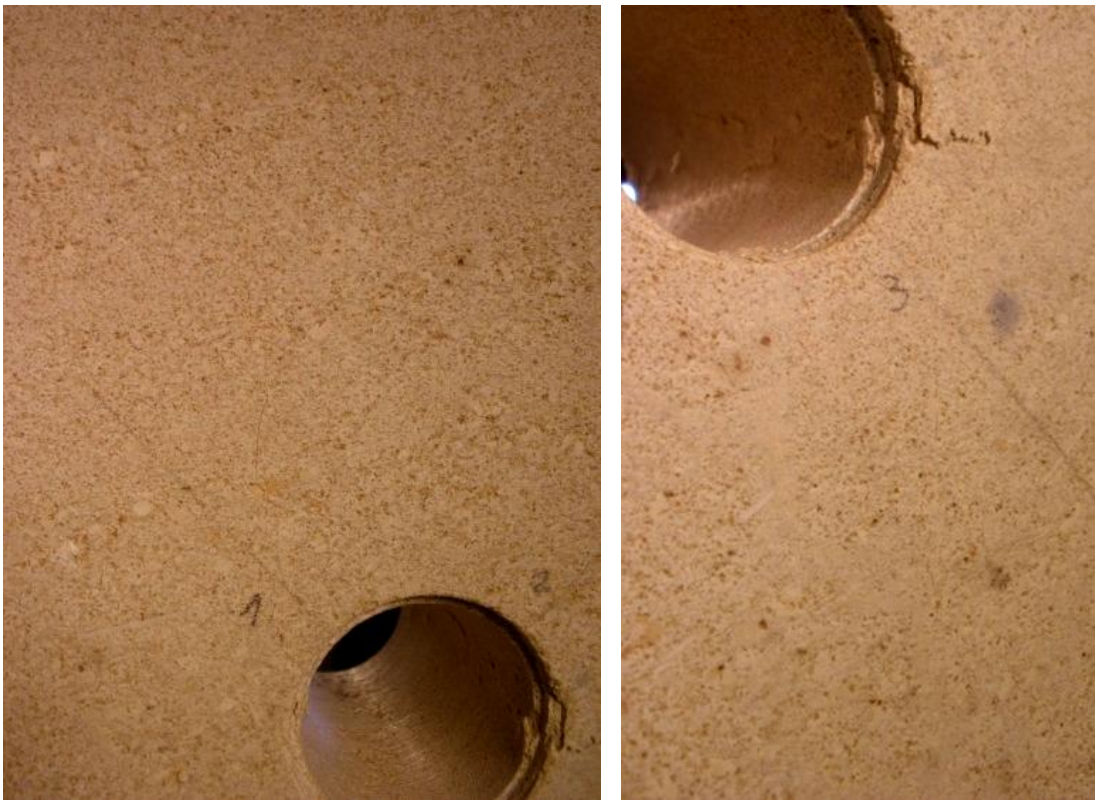

Fig. 5.40: Cracks in specimen 22 for point 2 of the figure 5.38. Cracks on the side A of the specimen.

Fig. 5.41: Cracks in specimen 22 for point 2 of the figure 5.38. Rupture on the right wall of the drillhole. Picture was taken from side A of the specimen.

Fig. 5.42: Cracks in specimen 22 for point 2 of the figure 5.38. Cracks on the side B of the specimen.

Fig. 5.43: Cracks in specimen 22 for point 3 of the figure 5.38. Cracks on the side B of the specimen.

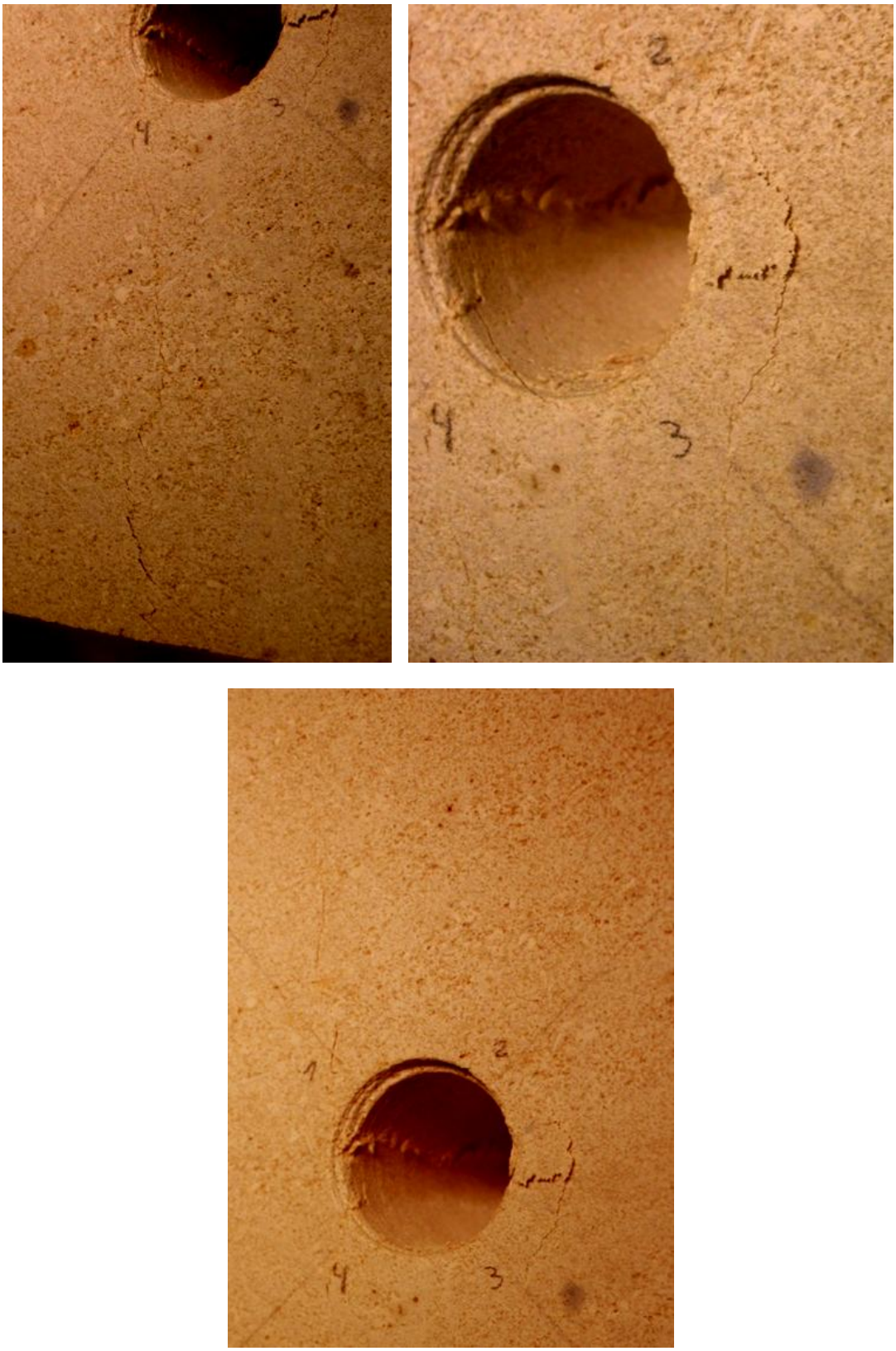

Fig. 5.44: Cracks in specimen 22 for point 4 of the figure 5.38. Cracks on the side A of the specimen.

Fig. 5.45: Cracks in specimen 22 for point 4 of the figure 5.38. Cracks on the side A of the specimen.

Fig. 5.46: Cracks in specimen 22 for point 5 of the figure 5.38. Cracks on the side A of the specimen.

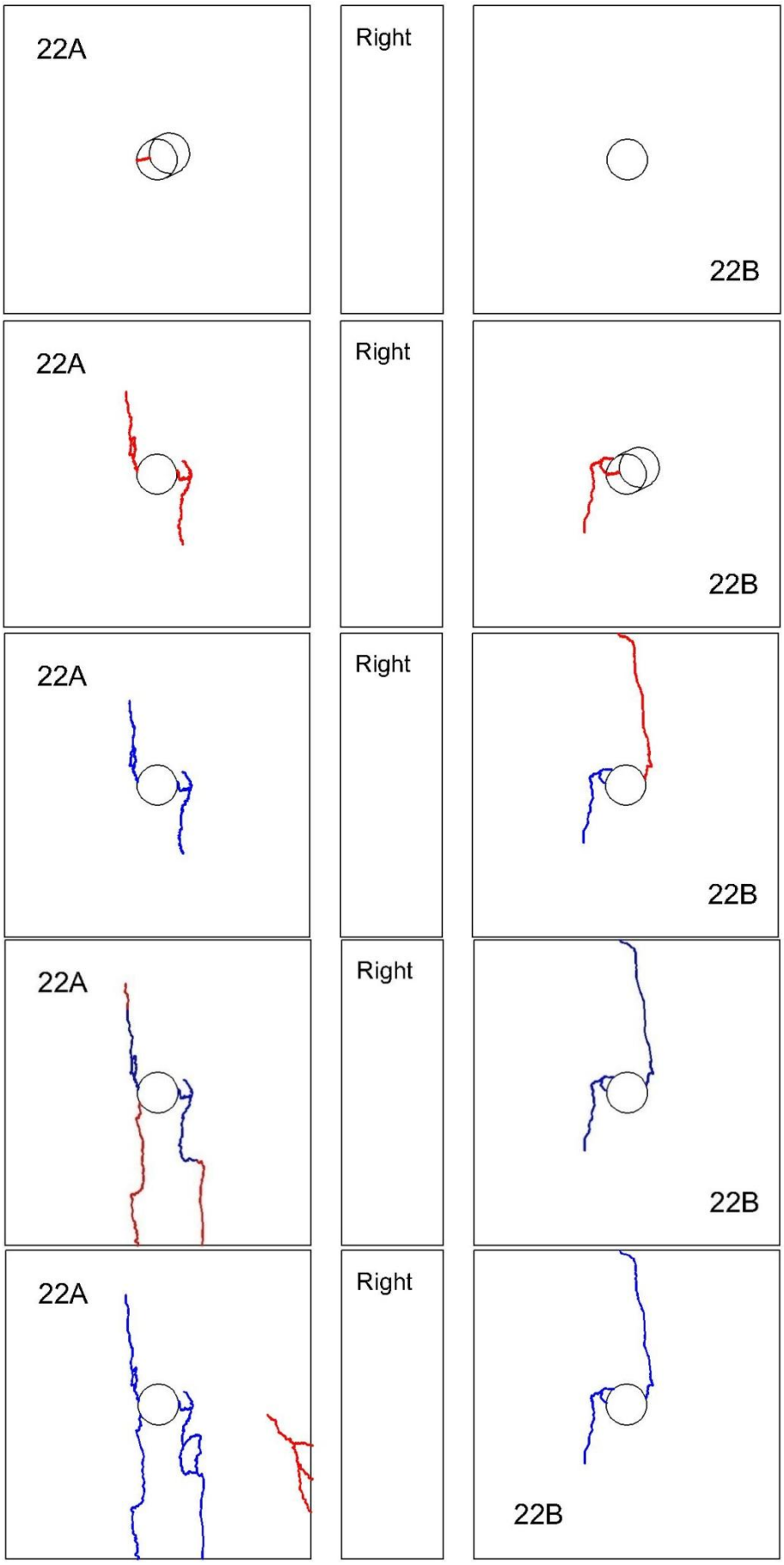

Fig. 5.47: Sketch of specimen 22 for points 1, 2, 3, 4 and 5 of the figure 5.38.

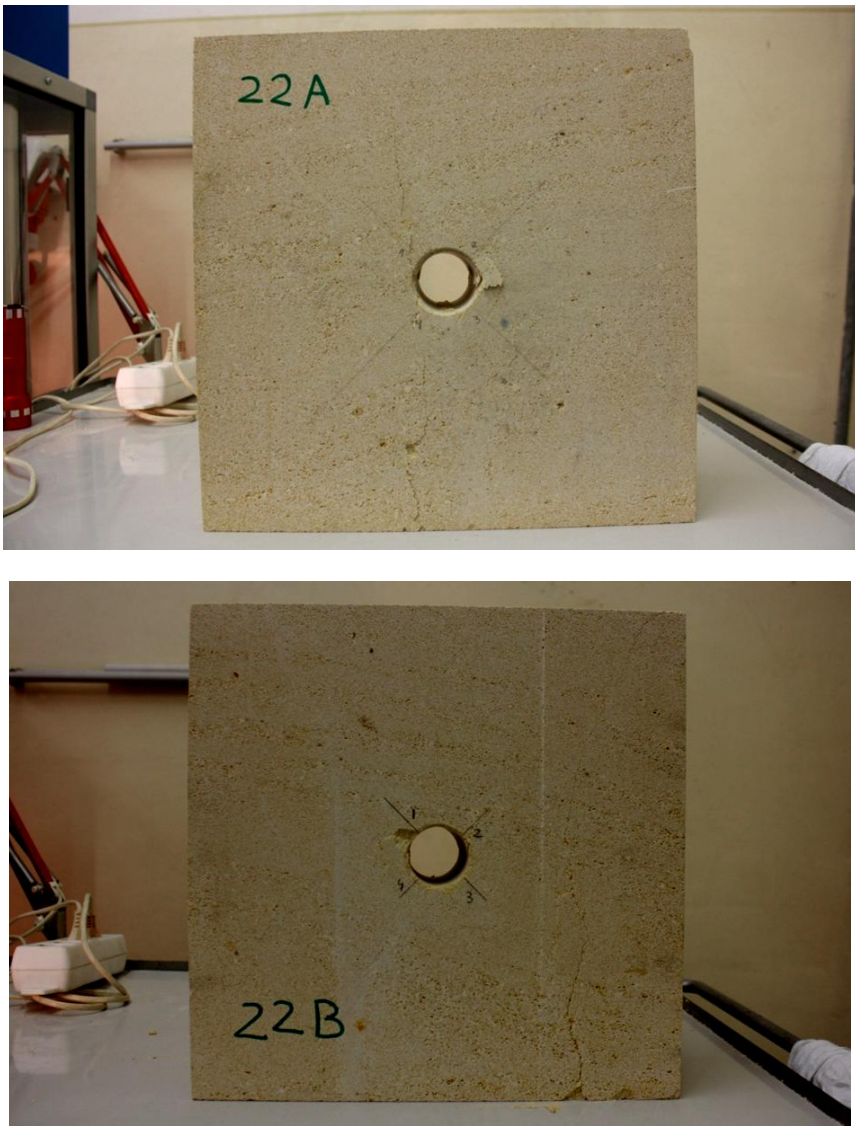

Fig. 5.48: Specimen 22 after testing. a) Side A. b) Side B. c) Drillhole of the specimen. The drillhole was photographed from side A.

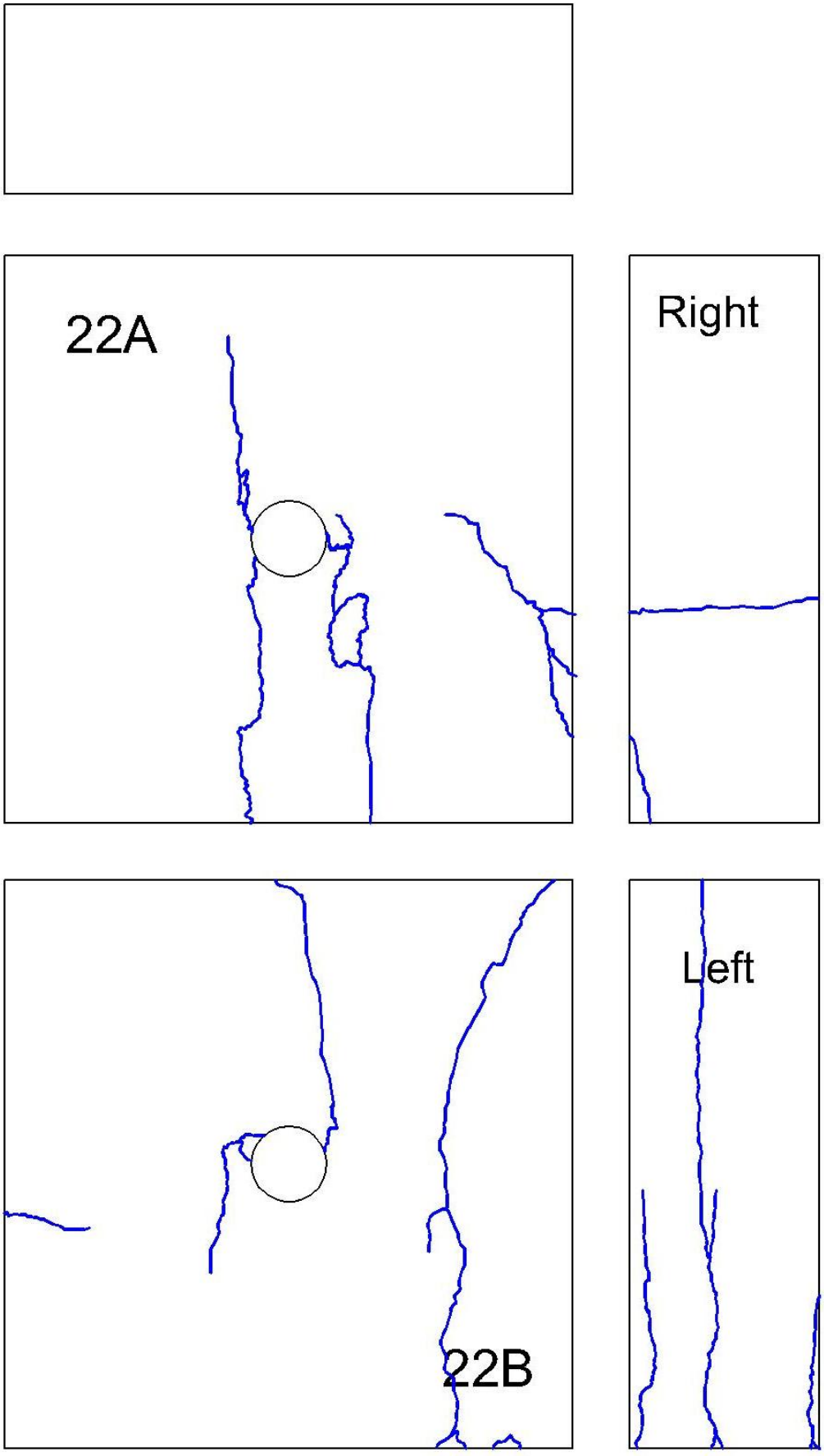

Fig. 5.49: Sketch of final state of specimen 22.

5.9. MAIN RESULTS COLLECTION

During the presentation of main results, the specimens with dimensions 200x200x50 mm and a circular drillhole of 25 mm diameter (test 1 to 19) will be designated as “small specimen” and the specimens with dimensions 300x300x100 mm and a circular drillhole of 36 mm of diameter (test 20 to 24) will be designated as “big specimens”.

Specimen that showed fracture patterns A, B and F were excluded for comparison of the results. The experiments that showed fracture pattern C (The rupture of the body and the drillhole occurs simultaneously), D (First the rupture in the body of the specimen occurs, on the right side, on the left side, on the back side or on the front side of the specimen. Afterwards the crack in the sidewalls of the drillhole became visible) and E (First the rupture on both sidewalls of the drillhole occurs. Later cracks on the body of the specimen became visible) were used to analyze the experiments.

Presentation of the main results can be found in table 5.8. In this table are represented the results of the tests; maximum force reached during the test, displacement and compressive strength of the test specimen appeared.

	Test	Body Nr.	Force max.	Way	Compressive Strength	Break type
	-	-	kN	mm	N/mm^2	-
Small sample	3	3	204.2	0.43	20.4	C
	4	4	202.3	0.92	20.2	C
	5	5	184.0	0.66	18.4	C
	10	10	163.7	0.44	16.4	D
	11	11	154.3	0.31	15.4	D
	12	12	200.7	0.47	20.1	D
	13	13	106.6	0.50	10.7	D
	14	14	138.0	0.45	13.8	D
	15+A	15	125.9	0.53	12.6	D
	16+A	16	123.0	0.47	12.3	D
	17+A	17	154.6	0.44	15.5	D
	18+A	18	103.1	0.33	10.3	D
	19+A	19	229.9	0.45	22.9	D
Big sample	20+A	20	1309.7	1.06	43.7	E
	21a+A	21	1128.5	0.89	37.6	E
	22+A	22	1353.2	0.89	45.1	E
	23+A	23	1101.1	0.96	36.7	E
	24+A	24	1332.5	0.97	44.4	E

Table 5.8: Summary of main results.

Small specimens showed two types of fracture, C and D. The displacement values varied between 0.31 mm and 0.92 mm, and the average was 0.49 mm. The compressive strength had values between 10.3 and 22.9 N/mm^2 and the mean strength was 16.7 N/mm^2.The tests lasted less than one hour from the shortest test to about 10 hours the longest test.

The big specimens showed the type of fracture D. The displacement values varied between 0.89 mm and 1.06 mm, the average was 0.95 mm. The compressive strength had values between 36.7 N/mm^2 and 45.1 N/mm^2, the mean strength was 41.5 N/mm^2. The duration of the tests were from an hour and a half in the shortest one until about nine hours the longest test.

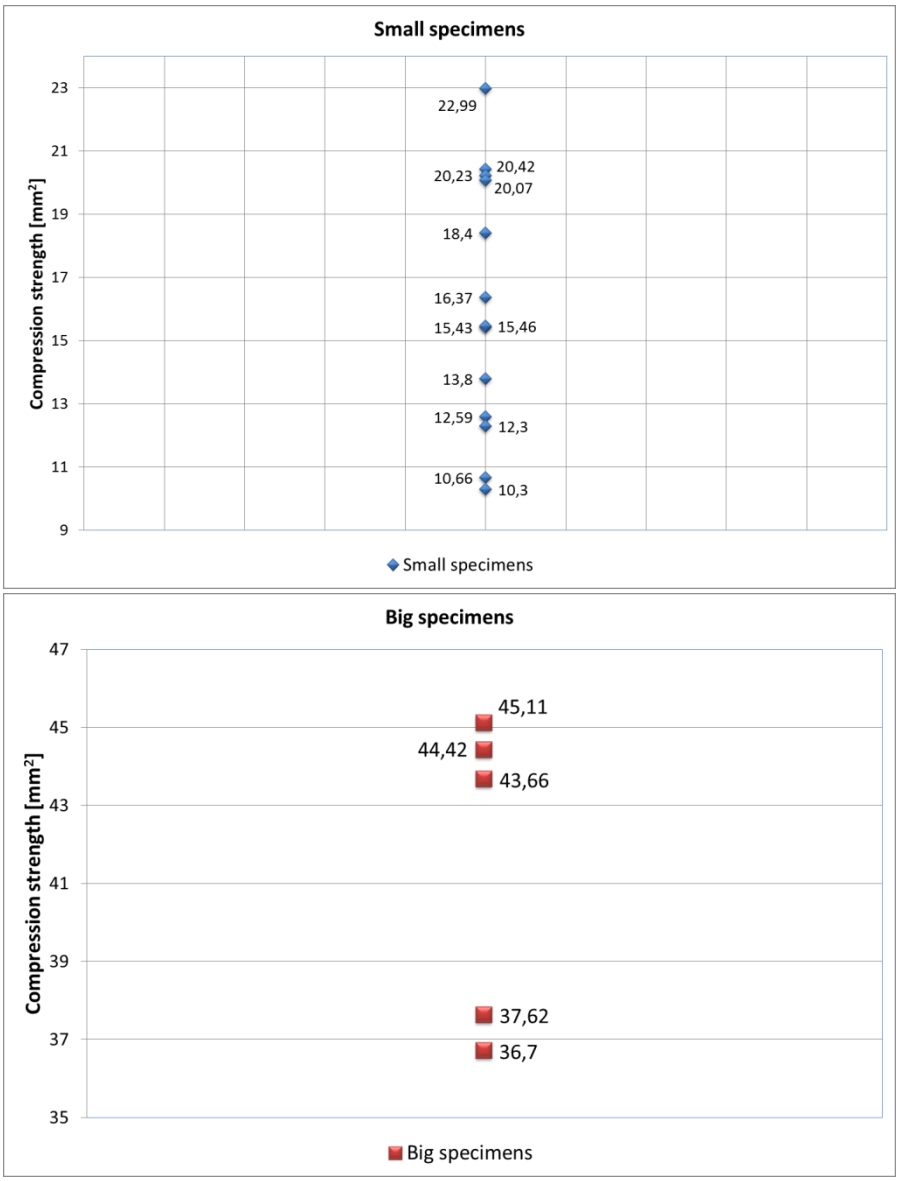

Fig. 5.50: Compressive strength vs. Specimen size. a) Results of small specimens. b) Results of big specimens.

The compressive strength values of the specimens are compared in figures 5.50 and 5.51 with the specimen size. Figure 5.51 shows that the big specimens had twice compressive strength than the small specimens.

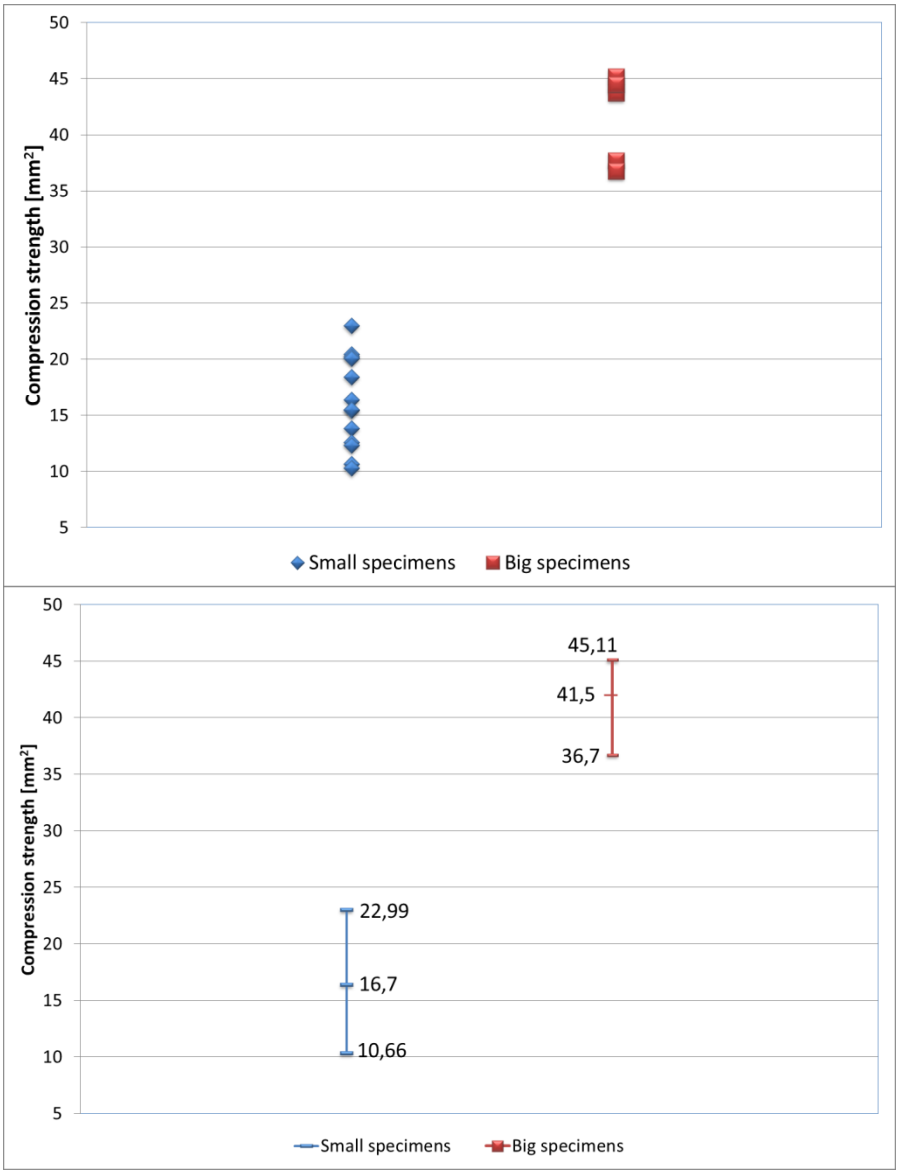

Fig. 5.51: Compressive strength vs. Specimen size. a) Results of all test. b) Maximum-minimum-average.

One observation throughout the experiment was the effect of size hole on fracture around circular underground openings. Big specimens were the only ones where first the rupture occurred in the cavity wall and later on the test specimen. Small specimens had two types of fractures, but the rupture of the body and the cavity occurs simultaneously or first the rupture in the specimen occurred and later in the cavity. Kaiser & Morgestern (1981) stated that the block be at least 4-6 tunnel diameters in width such that a uniform field stress state could be achieved. The

relationship between the cavity diameters and the size of the sample in these experiments is about 8, higher than the value stated by Kaiser & Morgestern.

During testing, friction forces develop at the interface between the loading platens and the test specimen as a result of the different lateral stiffness of the two different materials. In compression testing of a cylindrical sample the specimen tends to expand radially as it shortens longitudinally. Frictional constraint at the planes of contact between the cylinder and the loading machine tends to prevent expansion. Thus, the sample becomes slightly barrel-shaped and loading in specimens is nonunifmorm. The relative rigidity of the sample and the platens of the loading machine also is an important factor because the sample and the platens have different rigidities, the stress in the sample will be nonuniform. The most important aspect of the interface is to transfer the load uniformly into the specimen. A variety of inserts between the specimen and the loading platens were investigated, in order to find end-boundary condition that produced uniform loading in specimens.

The specimens were tested with and without interface between the loading platen and the end of a specimen. Figure 5.52 shows small specimens in direct contact with the loading platen and small specimens with an interface between specimen and loading platen. There isn´t a big difference in the compressive strength in both cases.

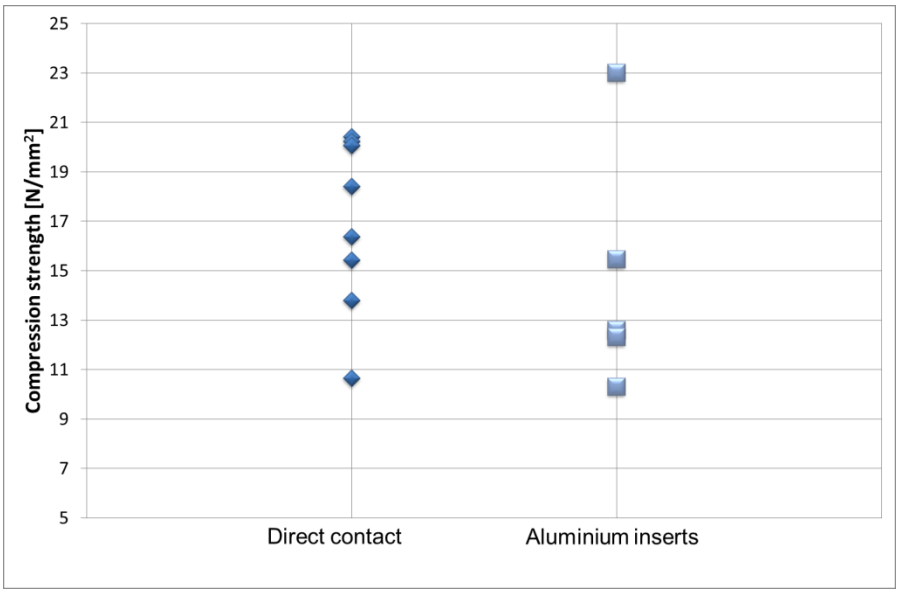

Fig. 5.52: Compressive strength vs. Interface.

For the interpretation of the test results, the effect of loading conditions must be to take into account. The optimal way to load the sample was obtained by “trial and error”. During tests, it was found that test velocity is

an important factor to obtain correct results. Display of the initiation and propagation of cracks was better when the test velocity was slower.

Samples with dimensions 200x200x50 with a circular cavity with 25 mm diameter showed two types of fracture patterns: type C, the rupture of the body and the cavity occur simultaneously and type D, First the rupture in the specimen occurs and later on in the cavity. The change from load increase velocity controlled tests to strain increase velocity controlled tests, caused a change in the type of break when the specimens had the same geometrical characteristics and they were under the same conditions (direct contact with the loading platen). Adding an interface between the sample and the loading platens did not cause a significant change in the compressive strength.

5.10. UNIAXIAL COMPRESSION TEST IN CYLINDRICAL SPECIMENS OF SANDSTONES

In the preceding section breakage processes in the surroundings of a drillhole within specimens of sandstone subjected to uniaxial loading was studied. In this section the compressive strength of sandstone by means of a test series will be studied. In this test series 29 specimens were tested under compressive loading. All the specimens for the test series were obtained in the quarry at St. Margarethen in Burgenland from one block with the dimensions 600X400X200 mm.

Fig. 5.53: Sandstone specimens.

The most common method for studying mechanical properties of rock is by axial compression of circular cylinders, with twice the diameter as length (Peng & Johnson, 1972). Specimens with different dimensions will be used. The dimensions of the specimens varied from the biggest specimen, XL, with 100 mm diameter and 200 mm length, to the smallest specimen, XS, with 19 mm diameter and 40 mm length. The other

specimens had 70 mm diameter and 140mm length (L), 50 mm diameter and 100 mm length (M) and 30mm diameter and 60 mm length (S). 5 specimens were tested from all sizes, except for the cylinder with 50 mm diameter for which 9 specimens were tested. All the specimen sizes from XL to XS are drawn in figure 5.53 and figure 5.54 shows the specimens.

Test parameters were calculated according to equation 5.1 so they fulfill it. This relation is constant for all sizes. A test rate of 0.005 mm/min was used for specimen size M (Φ=50 mm). The test rates, for the rest of the samples, were obtained using equation 5.1.

$$\frac{\Delta l/_{lo}}{\Delta t} = cte \qquad \frac{0.005\ mm/min}{30\ mm} = cte \qquad (5.1)$$

$$\frac{0.005\ mm/min}{30\ mm} = cte = \frac{X}{100\ mm} \qquad X = 0.017\ mm/\min \qquad \Phi = 100mm$$

$$\frac{0.005\ mm/min}{30\ mm} = cte = \frac{X}{70\ mm} \qquad X = 0.012\ mm/\min \qquad \Phi = 70mm$$

$$\frac{0.005\ mm/min}{30\ mm} = cte = \frac{X}{50\ mm} \qquad X = 0.008\ mm/min \qquad \Phi = 30mm$$

$$\frac{0.005\ mm/min}{30\ mm} = cte = \frac{X}{20\ mm} \qquad X = 0.003\ mm/min \qquad \Phi = 20mm$$

Specimen XS (Φ=19 mm) 0.003 mm/min was calculated, for specimen S (Φ=30 mm) 0.008 mm/min, for specimen L (Φ=70 mm) 0.012 mm/min and for specimens XL (Φ=100 mm) 0.017 mm/min.

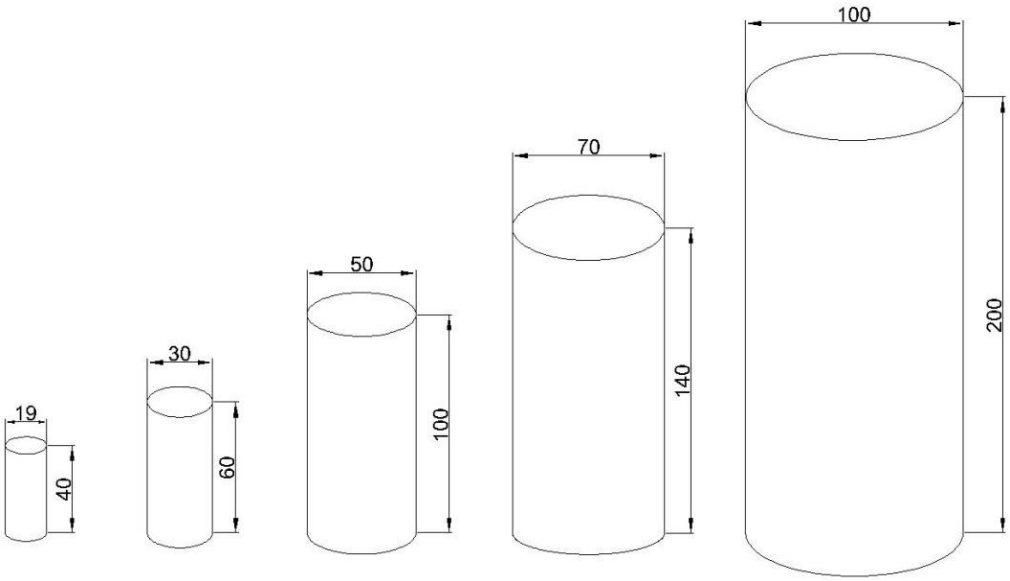

Fig. 5.54: Dimensions of the 5 sandstone specimen size.

In the preceding section the breaking processes were studied and an aluminium plate was used as interface between the loading platen and specimen loading face. In this test series the same interface was used because the conditions in the previous experiments were maintained. An aluminium plate with dimensions 300x100x50 mm was used with the biggest specimens and with samples number 6, 7 and 8 (with 70mm diameter). More aluminium platen were required, one with dimensions 100x100x20 mm, which was used for the samples number 9 and 10 (with a diameter of 70 mm) , and another one with dimensions 50x50x20 mm, which was used for the sample with 50 mm, 30 mm and 20 mm diameter.

Although the distance among the loading platens can be modified, the samples with 30 mm and 20 mm diameter were too small and it was necessary to add an extra plate. An extra plate with 45 mm thickness was added for the cylinder with 30 mm diameter and for the smallest samples two extra platens were used, one with 54 mm thickness and another one with 20 mm thickness. Two samples of the smallest specimens were tested with the new press but the last three samples were tested with the old press. Figures 5.55 and 5.56 show the samples during test.

Fig. 5.55: Cylinder during test a) Φ = 100 mm b) Φ = 70 mm c) Φ = 50 mm d) Φ = 30 mm.

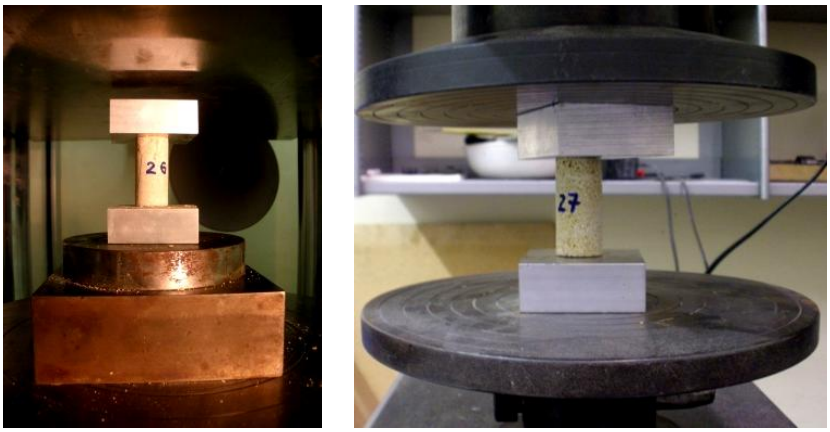

Fig. 5.56: Cylinder Φ = 20 mm during test a) New press b) Old press

Table 5.9 shows a summary of the results of this test series. The load displacement plots are represented for each specimen in figures 5.63 to 5.67 on pages 77 to 81.

The compressive strength values of the XL size varied between 25.1 N/mm^2 and 16.3 N/mm^2 and the mean strength was 20.7 N/mm^2. The mean strength of the L size was 12.6 N/mm^2 and the values of strength varied between 17.4 N/mm^2 and 6.1 N/mm^2. Reached strength values between 22.5 N/mm^2 and 10.1 N/mm^2 for the specimen M and the mean strength was 15.4 N/mm^2. The values of the compressive strength of the S size varied between 27.0 N/mm^2 and 12.7 N/mm^2 and the mean strength was 12.7 N/mm^2. The mean strength of the XS size was 15.3 N/mm^2 and the values of strength varied between 18.9 N/mm^2 and 11.8 N/mm^2.

Specimen	Dimensions	Nr.	Test	Force	Compressive Strength
	mm			N	N/mm^2
XL	Φ = 100 mm L = 200 mm	5	1	128.1	16.3
			2	174.3	22.2
			3	149.8	19.1
			4	196.8	25.1
			5	162.6	20.7
L	Φ = 70 mm L = 140 mm	5	6	47.1	12.2
			7	46.7	12.1
			8	23.4	6.1
			9	67.0	17.4
			10	57.4	14.9
M	Φ = 50 mm L = 100 mm	9	11	38.7	19.7
			12	21.4	10.9
			14	22.7	11.6
			15	21.7	11.1
			16	28.0	14.3
			17	44.2	22.5
			18	34.0	17.3
			19	30.5	15.5
S	Φ = 30 mm L = 60 mm	5	20	8.4	12.7
			21	17.9	27.0
			22	11.4	17.2
			23	10.1	15.4
			24	9.2	13.9
XS	Φ = 19 mm L = 40 mm	5	25	4.3	15.2
			26	5.1	18.0
			27	3.63	12.8
			28	3.34	11.8
			29	5.37	19.9

Table 5.9: Sandstone specimens used for test. Summary of the results.

The maximum, minimum and average values are represented in figure 5.58. The strength values of the specimens are compared in figure 5.57 versus specimen size. The results are displayed with linear of the axis. The mean strength is plotted versus specimen size in figure 5.59.

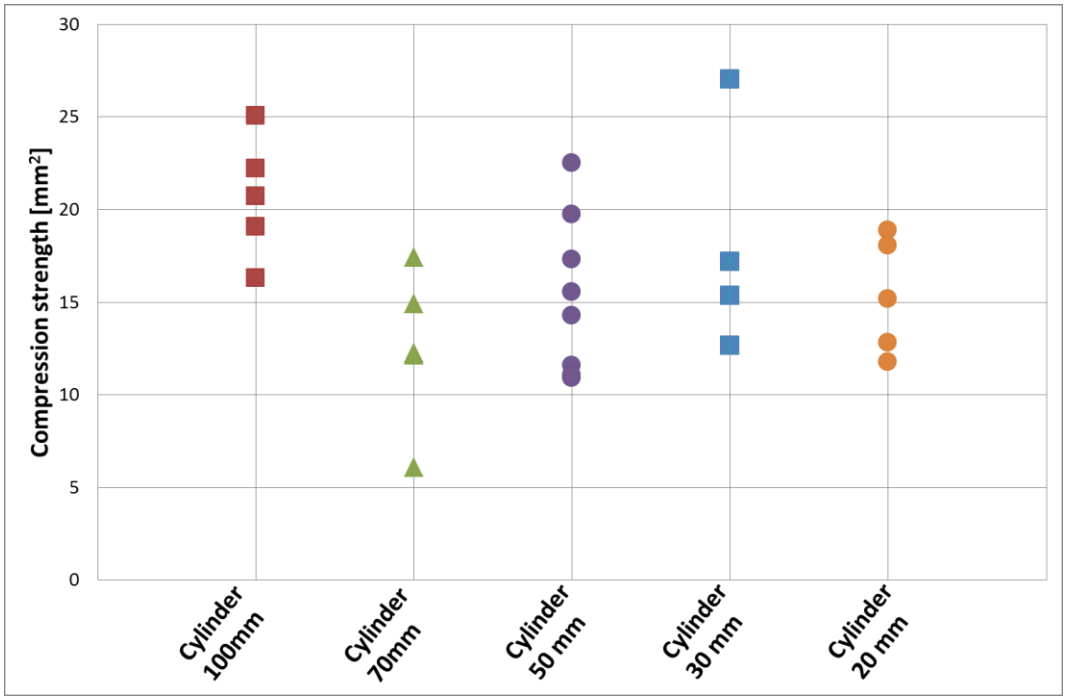

Fig 5.57: Compressive strength versus specimen size.

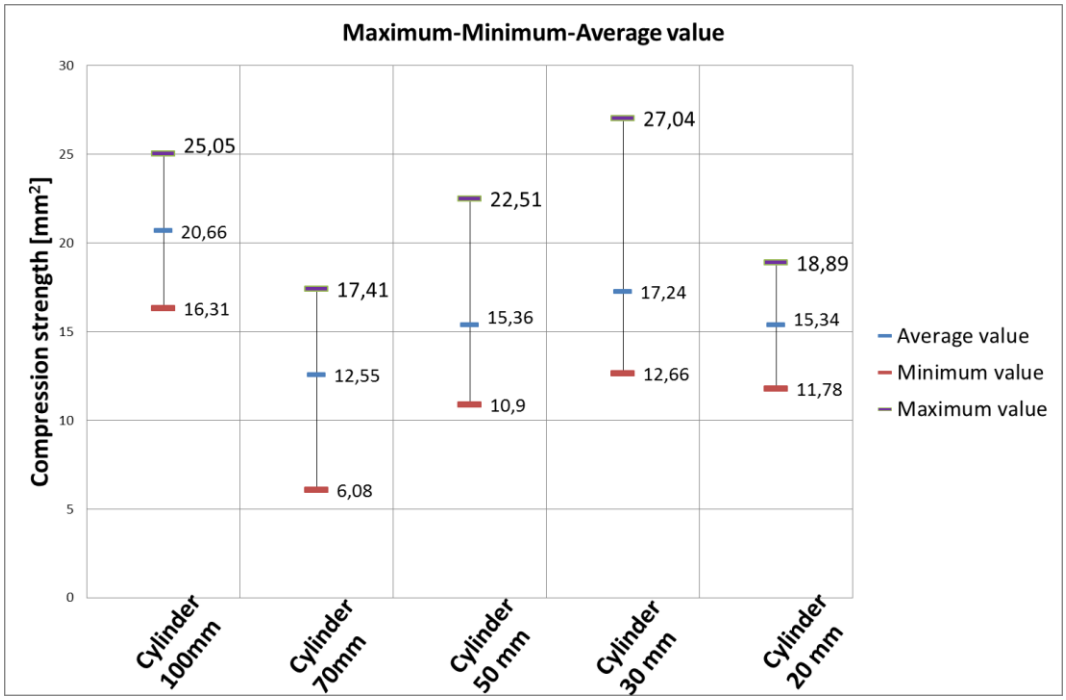

Fig 5.58: Compressive strength versus specimen size. Maximum, minimum and average.

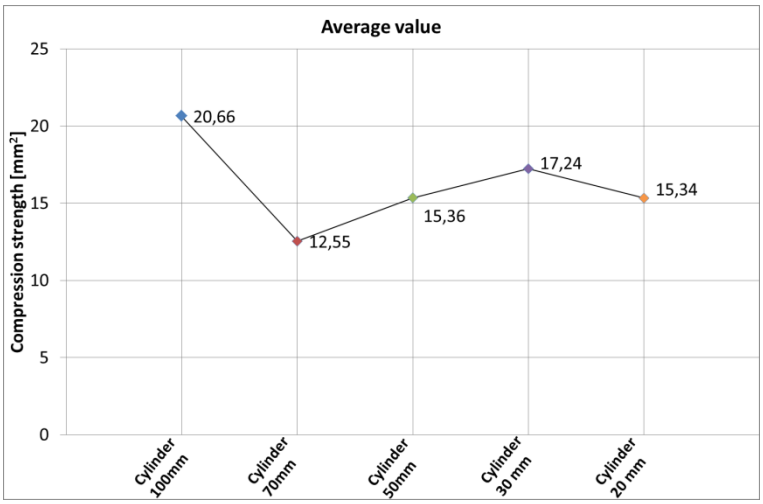

Fig. 5.59: Compressive strength versus specimen size. Average value.

Comparison of the results of this test series were made with the results of tests of the preceding section, specimens of sandstone with dimensions 300x300x100 mm and a circular drillhole with 36 mm diameter.

The compressive strength values of the cylindrical and rectangular specimens are compared in figure 5.60 versus specimen size. Some specimens were inclined, the planes are not totally parallel and they had lower compressive strength than straight specimens. The tilted specimens were excluded from the further data evaluation, specimens with number 8, 12, 13, 14, 15 and 16. In the diagram on the left size of figure 5.60 the results of all specimens are showed. In the diagram on the right size of figure 5.60 shows the results without crossed specimens

The maximum, minimum and average values are represented in figure 5.61 and as in the previous diagram, crossed specimens were excluded on the right diagram. The mean strength is plotted versus specimen size in figure 5.62.

Rectangular specimens have the greatest compressive strength, 41.7 N/mm^2. The mean strength decreases from rectangular specimens to cylindrical specimens (Φ = 100 mm) from 41.7 N/mm^2 to 20.7 N/mm^2. The mean strength of rectangular specimens was twice that the mean strength of cylindrical specimens.

Cylindrical specimens, Φ = 70 mm, have the smallest compressive strength. The mean strength increase from L (Φ=70 mm) to M (Φ=50 mm) and from M (Φ=50 mm) to S (Φ=30 mm), but from S (Φ=30 mm) to XS (Φ=20 mm) the mean strength decrease. Size effect was not present in the cylindrical specimens. If a size effect was present, strength should decrease as specimen size increases.

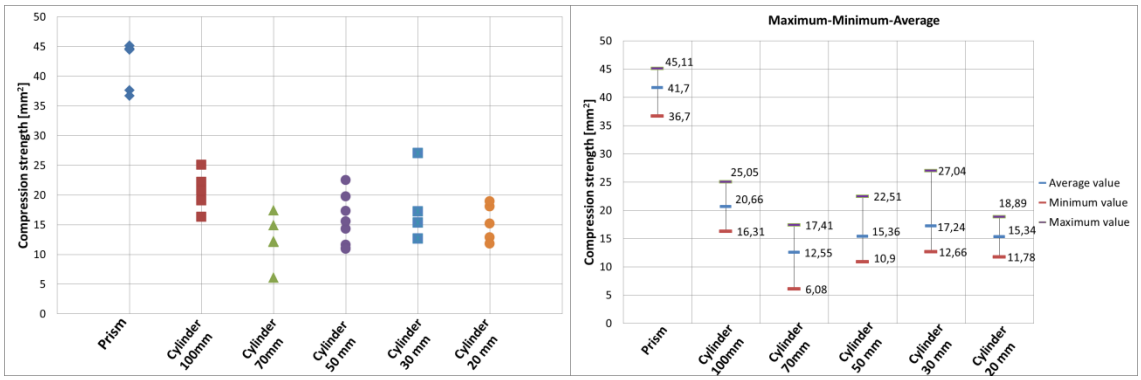

Fig. 5.60: Compressive strength versus specimen size. Cylindrical and rectangular specimens. (Left) For all specimens. (Right) Results without crossed specimens.

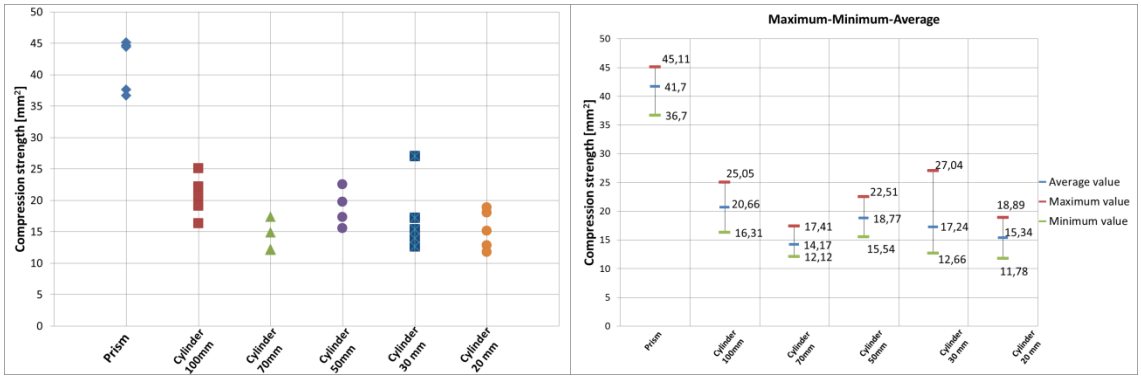

Fig. 5.61: Compressive strength versus specimen size. Maximum, minimum and average. Cylindrical and rectangular specimens. (Left) For all specimens. (Right) Results without crossed specimens.

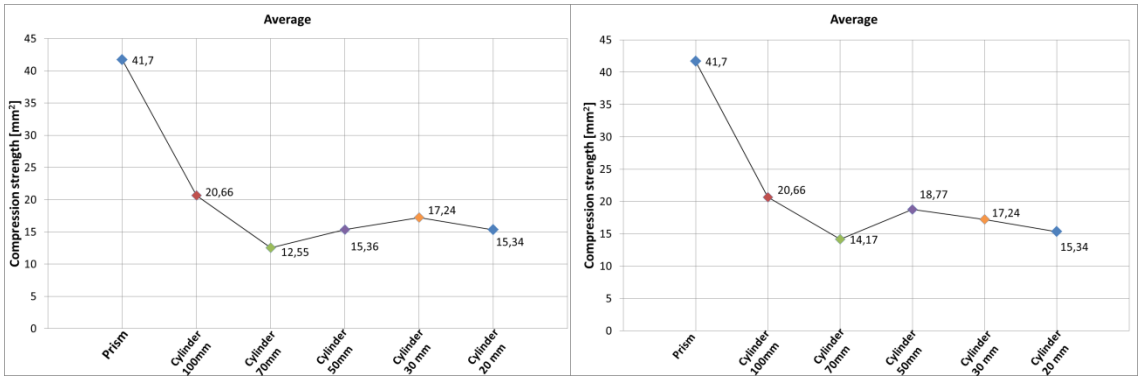

Fig. 5.62: Compressive strength versus specimen size. Average value for cylindrical and rectangular specimens. (Left) For all specimens. (Right) Results without crossed specimens.

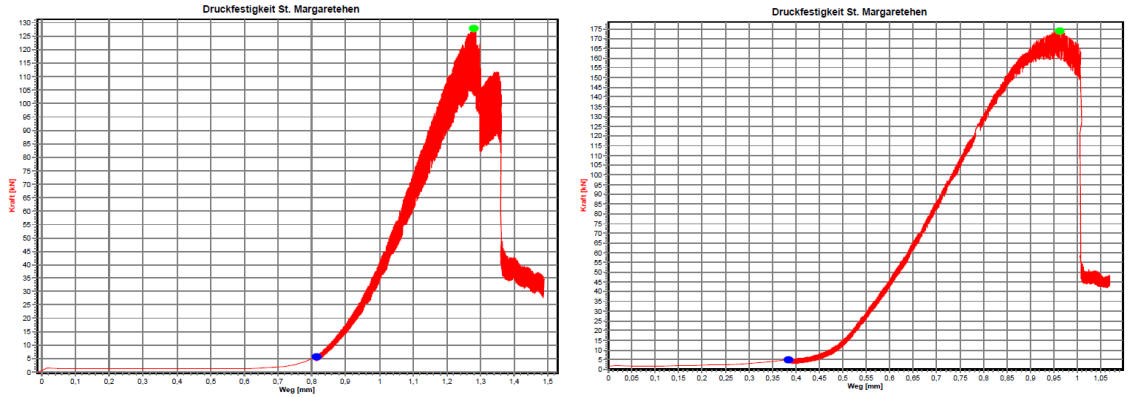

a) Sample 1. b) Sample 2.

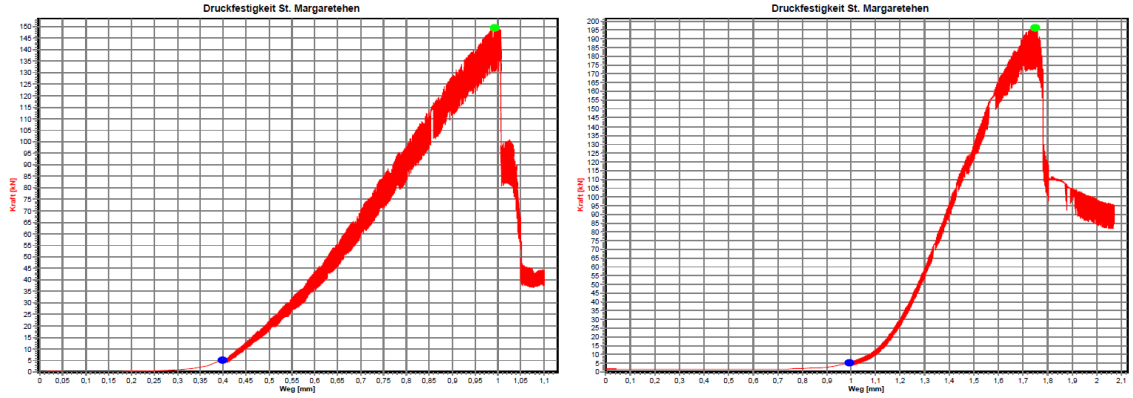

c) Sample 3. d) Sample 4.

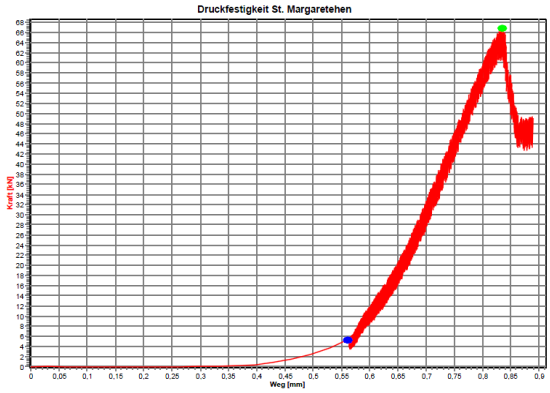

e) Sample 5.

Fig. 5.63: Load displacement curve for cylinder Φ = 100 mm. The blue dot represents the point where the displacement of the test starts and the green dot represents the maximum force and the point where the displacement of the test finishes.

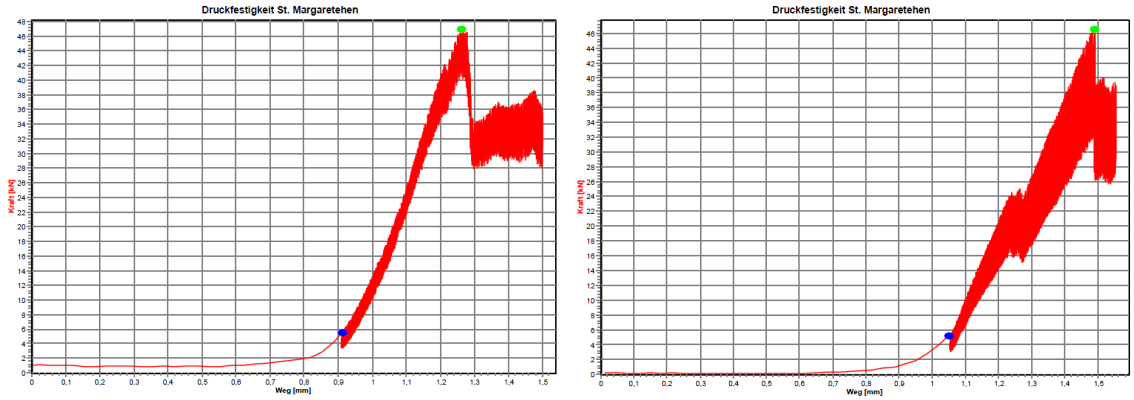

a) Sample 6. b) Sample 7.

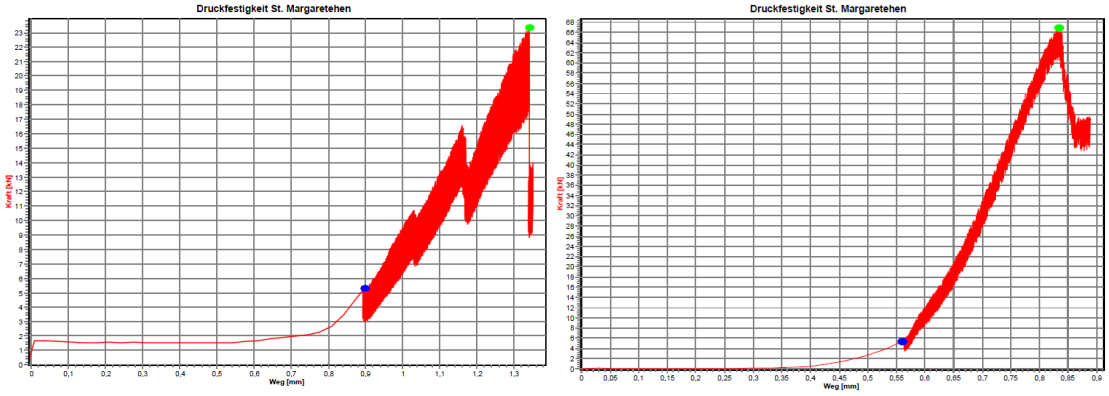

c) Sample 8. d) Sample 9.

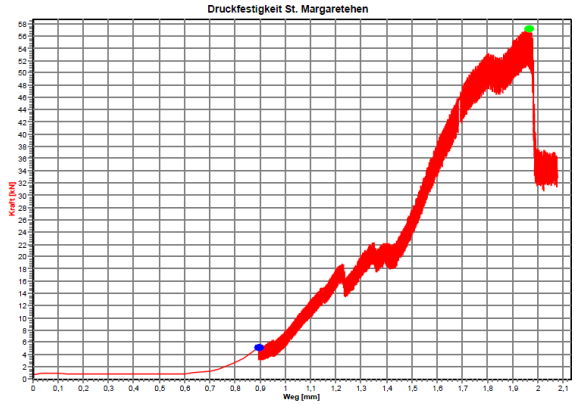

e) Sample 10.

Fig. 5.64: Load displacement curve for cylinder Φ = 70 mm. The blue dot represents the point where the displacement of the test starts and the green dot represents the maximum force and the point where the displacement of the test finishes.

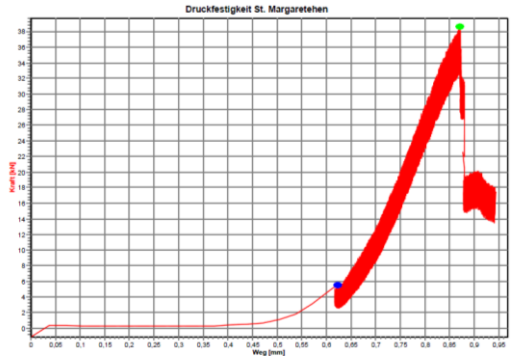

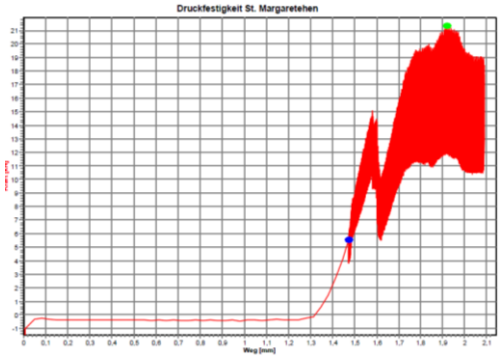

a) Sample 11. b) Sample 12.

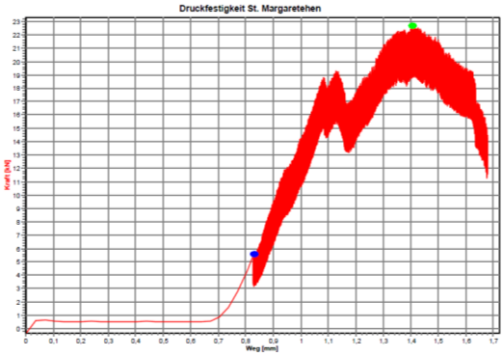

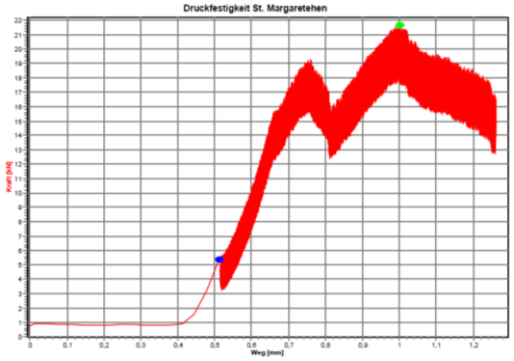

c) Sample 14. d) Sample 15.

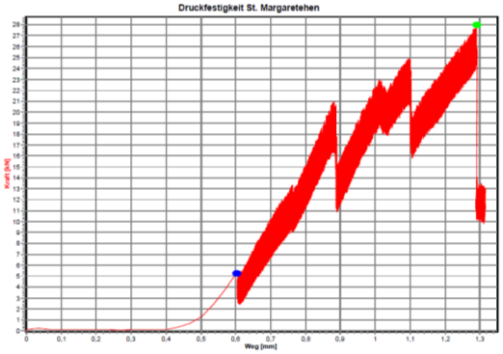

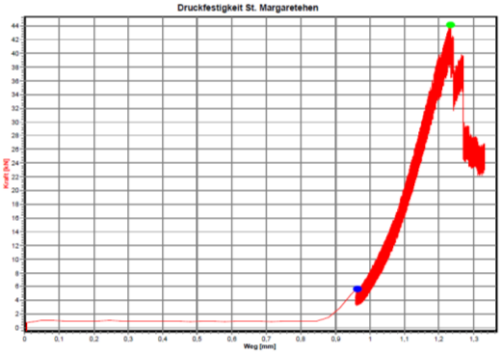

.e) Sample 16. f) Sample 17.

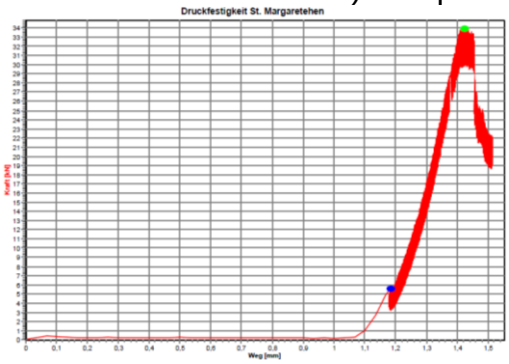

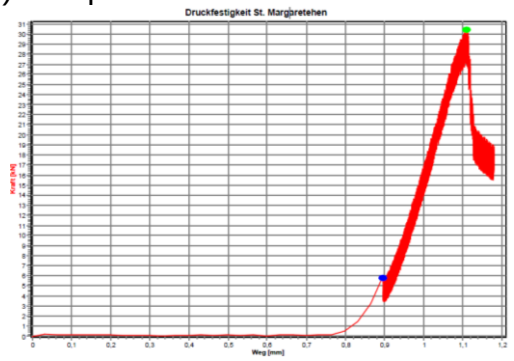

g) Sample 18. h) Sample 19.

Fig. 5.65: Load displacement curve for cylinder Φ = 50 mm. The blue dot represents the point where the displacement of the test starts and the green dot represents the maximum force and the point where the displacement of the test finishes.

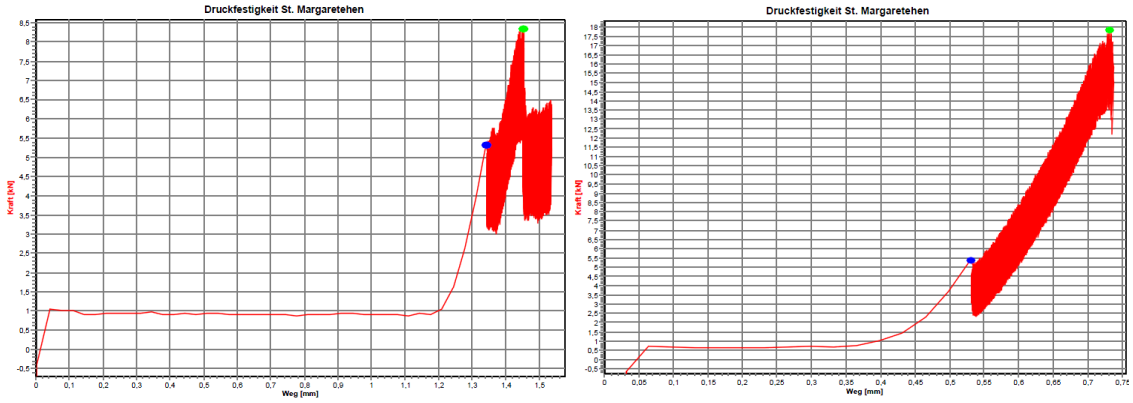

a) Sample 20. b) Sample 21.

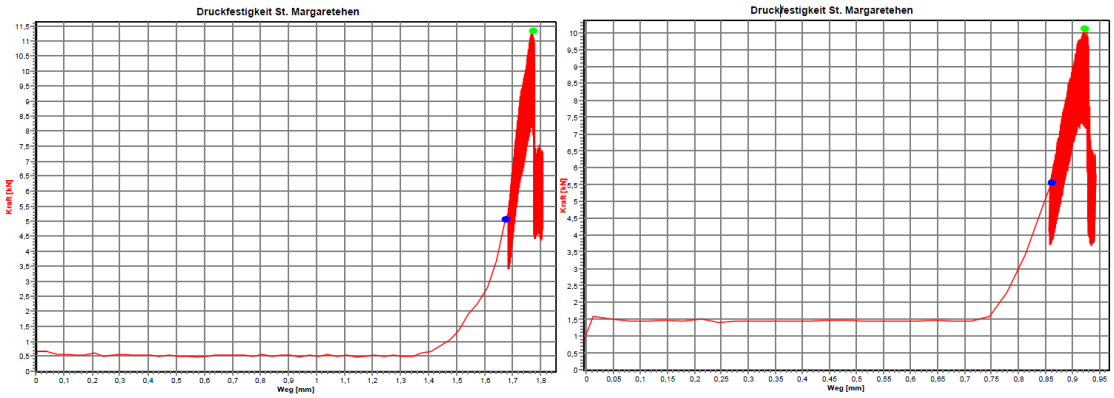

c) Sample 22. d) Sample 23.

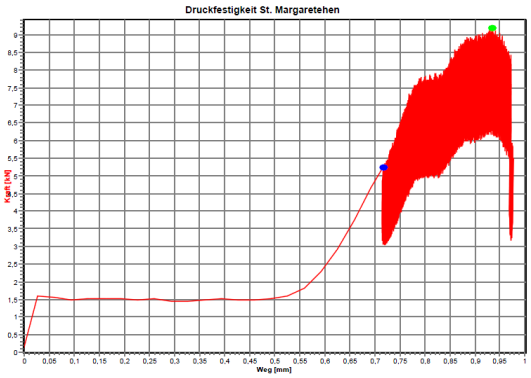

e) Sample 24.

Fig. 5.66: Load displacement curve for cylinder Φ = 30 mm. The blue dot represents the point where the displacement of the test starts and the green dot represents the maximum force and the point where the displacement of the test finishes.

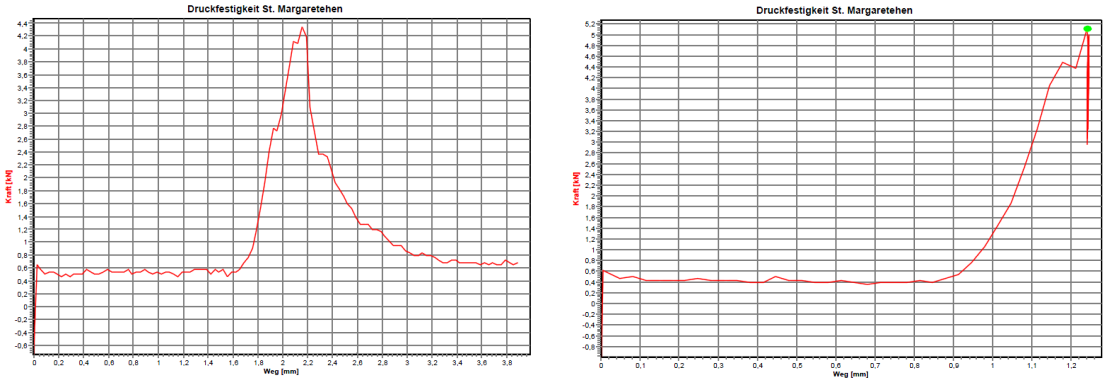

a) Sample 25. b) Sample 26.

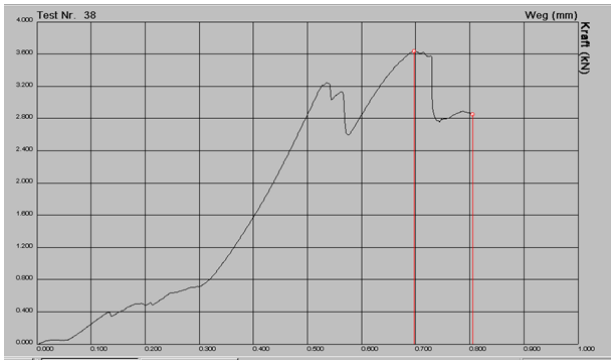

c) Sample 27.

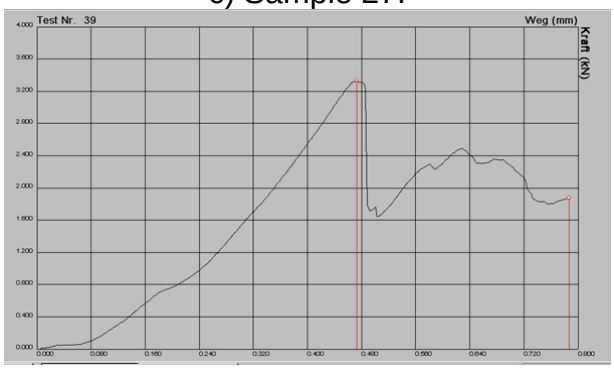

d) Sample 28.

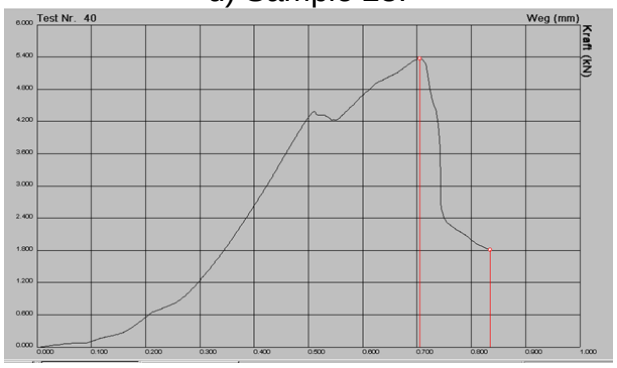

e) Sample 29.

Fig. 5.67: Load displacement curve for cylinder Φ = 20 mm. The blue dot represents the point where the displacement of the test starts and the green dot represents the maximum force and the point where the displacement of the test finishes. Red lines mark the maximum force and the end of the test.

6. INTERPRETATION

In theory, a prism with a circular cavity under uniaxial compression suffers, at the edge of the cavity, a stress three times higher than the uniaxial compression of the test. This means that the fracture phenomena around the cavity during the test (Kirsch, 1898) should occur once the loading has reached the value of 1/3 of the compressive strength (figure 6.1).

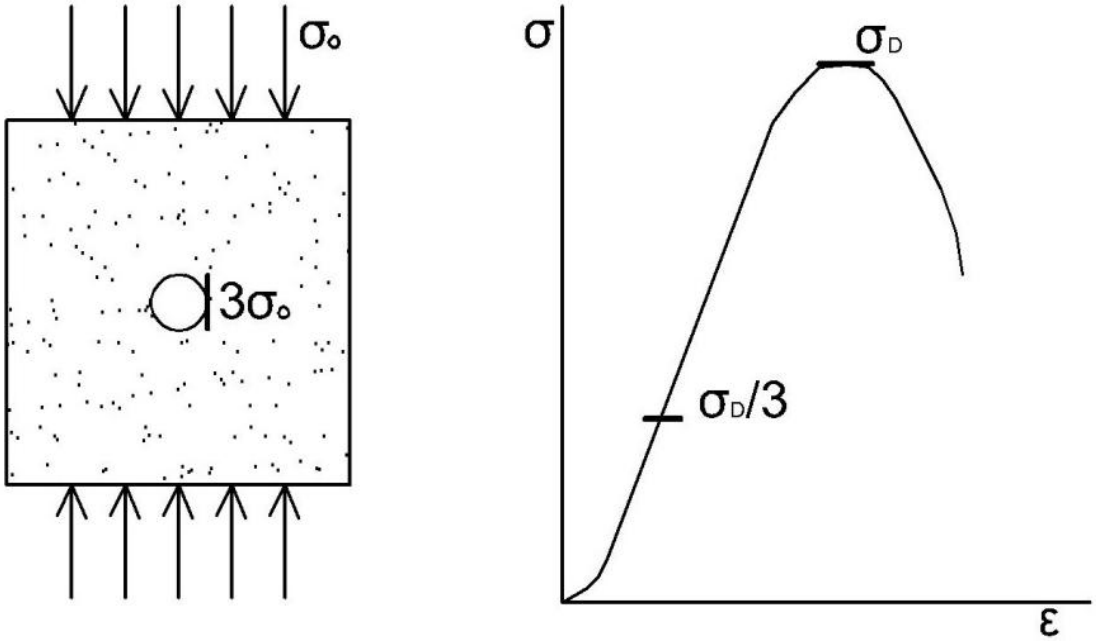

Fig. 6.1: Uniaxial compression tests on prisms with circular openings

Through the tests fracture phenomena at the edge of the hole occurred when stress achieved a value above $\sigma_D/3$. First visible damages in the cavity was observed at a point close far to the maximum force. Thus these results are contrary to the theory.

Figures 6.2 and 6.3 show the compressive strengths for the specimens and the loads when failure of the tunnel wall occurred. Visually detectable disruption of the tunnel wall in specimen 20, the first in this test series, was observed when loaded with 1217 kN (40.6 Mpa) and the maximum force was 1309.7 kN (43.7 Mpa). For specimen 21 the first crack in the cavity wall appeared at 1077 kN (35.9 Mpa) and the maximum force was 1128.5 kN (37.6 Mpa). The tunnel wall of specimen 22 was intact up to 1187 kN(39.6 Mpa) and the maximum force was 1353.2 kN (45.1 Mpa). In specimen 23 fracturing in the cavity wall was detected at 1002 kN (33.4 Mpa) and the maximum force was 1101.1 kN (36.7 Mpa). For the specimen 24 the force reached 1256 kN (41.9 Mpa) when damage in the tunnel wall was visible and the maximum force was 1332.5 kN (44.4 Mpa).

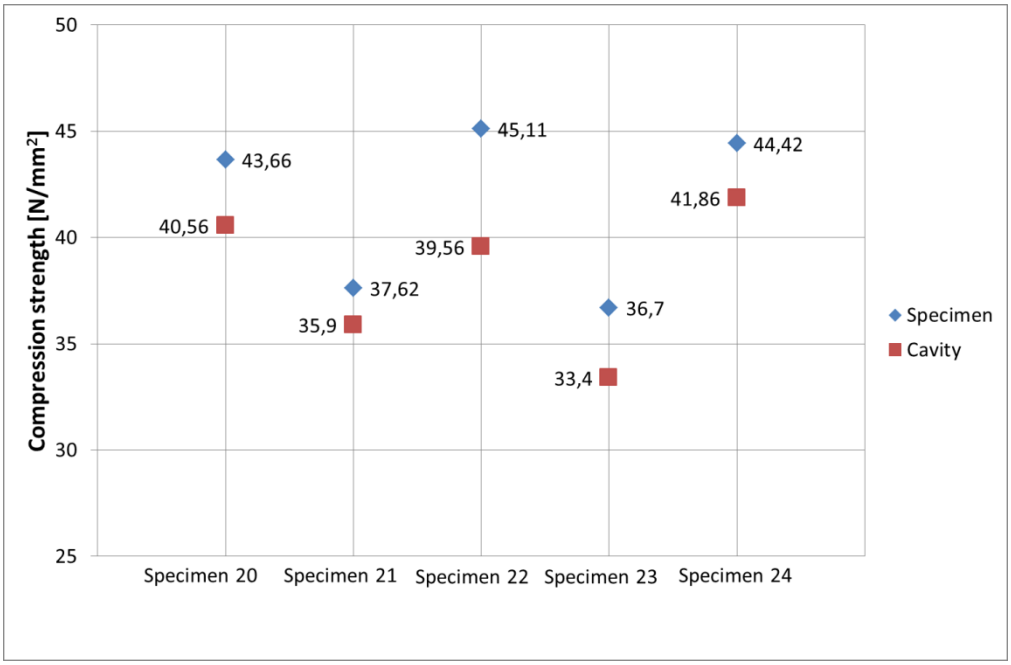

Fig. 6.2: Compressive strength for the specimen and for the tunnel wall.

This effect was also observed by Kaiser, Guenot & Morgenstern (1985). Accordingly, for a circular opening in an isotropic material and isotropic stress field, initiation of failure would be predicted for a stress level equal to one half of the unconfined compressive strength of the rock mass. No visually detectable disruption of the tunnel wall was observed until more than twice (2.2-3.3 times) the predicted stress level was reached.

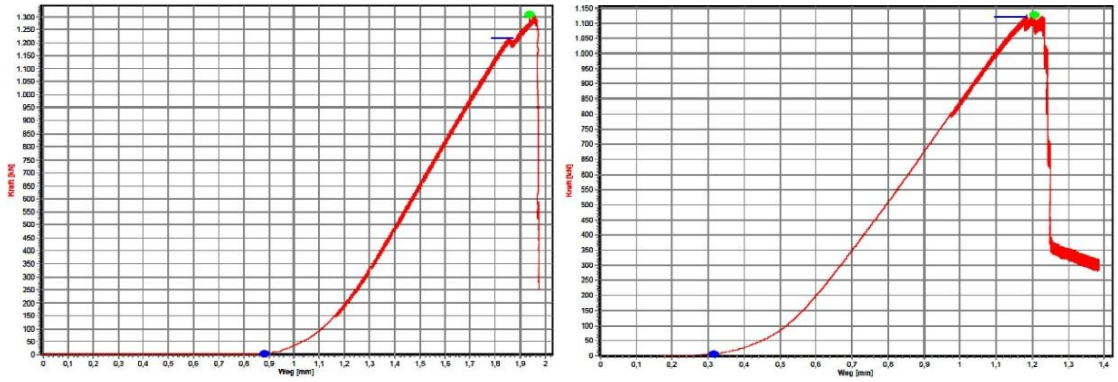

a) Specimen 20. b) Specimen 21.

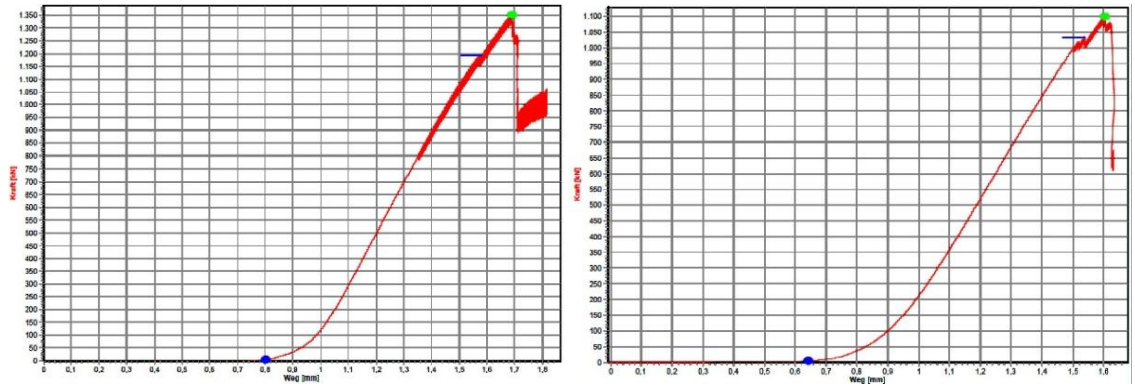

c) Specimen 22. d) Specimen 23.

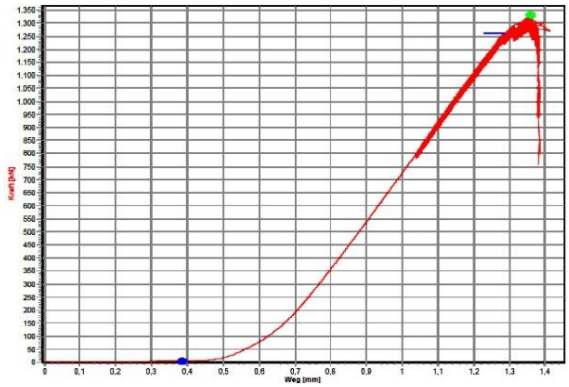

d) Specimen 24.

Fig. 6.3: Load displacement curve of specimens 20 to 24. Green dot represents the maximum force of the test and blue line represents the first visible damages in the cavity.

7. CONCLUSIONS

The discrepancy between failure stress in the tunnel wall according to theory and failure stress in the tunnel wall observed in compression tests can be explained as follows:

1. Kaiser, Guenot & Morgenstern (1985) observed a discrepancy between obtained results and expected results. The explanation of these results is connected to the initiation of yielding and rupture. During uniaxial and triaxial tests on a brittle material yield limit (σ_Y) and rupture limit (σ_r) are nearly equal, but initiation of yielding and rupture in a tunnel wall do not occur simultaneously (figure 7.1). For tunnels yielding and rupture must be considered as two separate phases of the failure process. Yielding starts if the tangential stress near the unsupported wall reaches the unconfined compressive strength of the rock. Rupture of the tunnel wall starts when the tangential stress is much higher.

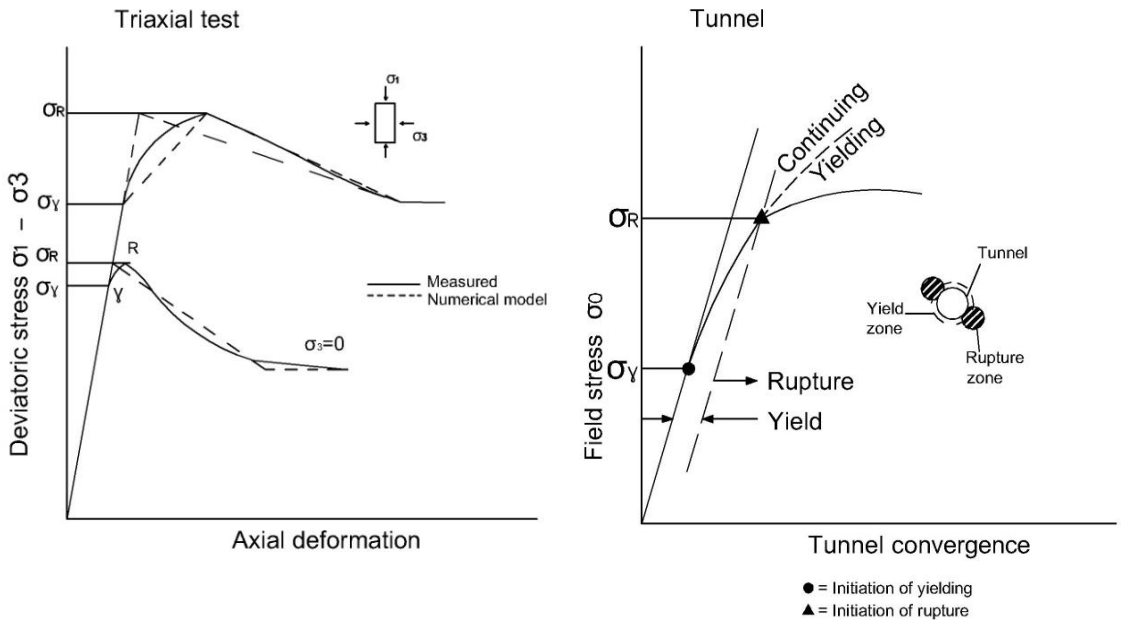

Fig 7.1: A) Stress-strain curve from triaxial test. b) Stress-convergence curve for externally loaded tunnel. From: Kaiser, Guenot & Morgenstern (1985).

2. Investigations of shear failures around a cavity using fracture mechanics were executed by Poisel et al. (1995). Fracture mechanics investigate three ways of applying a force to enable a crack to propagate. A crack tip is a singularity where the tangential stress is infinity. Thus the stress of the material near the crack tip is described by the stress intensity factor K while strength is described by the fracture toughness Kc. Fracture occurs when the stress intensity factor reaches the critical value of stress intensity, the fracture toughness. Figure 7.2 shows the factors of the

fracture mode II, sliding or in-plane shear mode, K_2 (stress intensity factor for the mode II) and K_{2c} (fracture toughness for the mode II) for a circular cavity under isotropic in situ stresses. When the tangential stress at the tunnel wall is equal to the uniaxial compressive strength, K_2 sinks under K_{2c} and the fracture stops, but when the tangential stress at the wall of the tunnel is about five times the uniaxial compressive strength, K_2 increases, a progressive extension of the shear failure occurs. Subsequent investigations by Poisel & Preh (2009) by means of continuum-mechanical and discontinuum-mechanical numerical models showed that, after the tangential stresses around the cavity reach many times the compressive strength, the deep-reaching overloading of the rock mass at the edge of the cavity under an anisotropic stress condition occurs in the form of shear failure bodies.

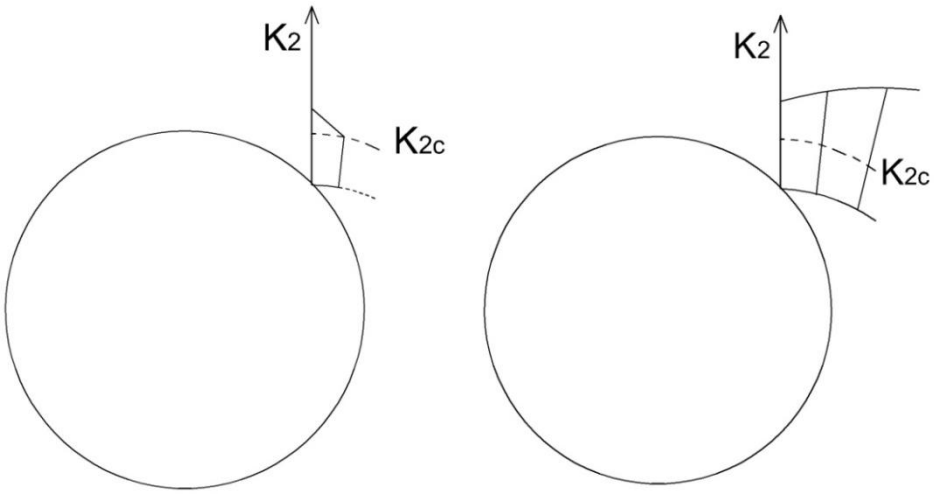

Fig. 7.2: Stress intensity factor and fracture toughness. Left: Tangential stress at tunnel boundary equals uniaxial compressive strength. Right: Tangential stress at tunnel boundary equals five times uniaxial compressive strength. From: Poisel et al. (1995).

3. Models of tunnels compare tangential stresses in the tunnel wall with the compressive strength of the rock determined in compression tests. However, the tangential stress in a tunnel wall is variable while the stress in a centrically loaded rock prism is constant over the width of the rock prism (Fig. 7.3).

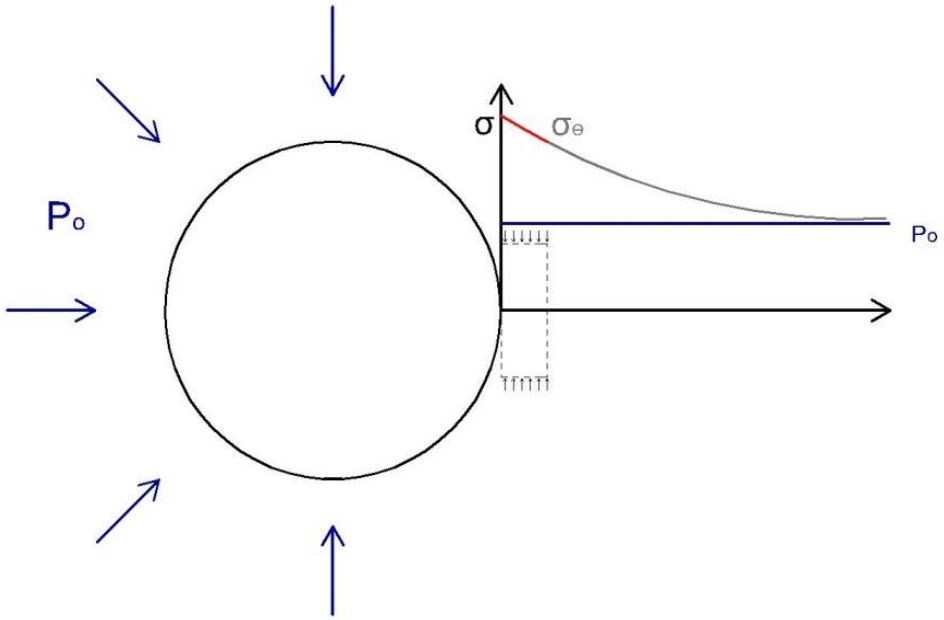

Fig. 7.3: Tangential stress around the cavity under isotropic stresses.

Tests on eccentrically loaded prisms simulate regions of rock under variable loading. Poisel (1979) compared the results of experiments carried out on cylindrical specimens and eccentrically loaded prims under uniaxial compression. The results showed that, despite the same material was used in all the experiments, the harder loaded side of the prisms with eccentric load reached a higher stress than the cylindrical specimens, figure 7.4. The fracture phenomena of the harder loaded side of the eccentrically loaded prisms were similar to the rock mass around a cavity.

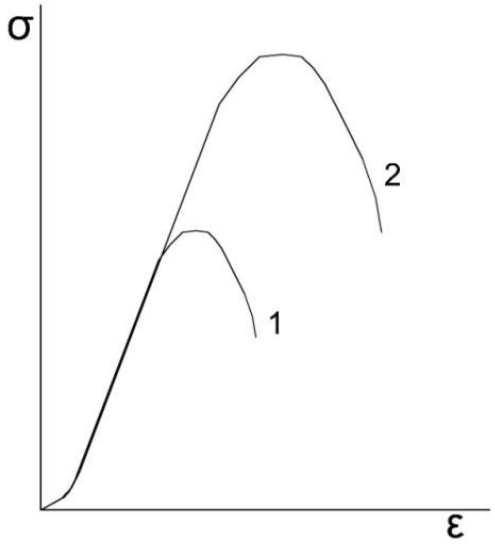

Fig. 7.4: Stress-strain curve of cylinder specimen (1) and prismatic specimen with eccentric load (2). From: Poisel (1979).

Results from laboratory tests revealed that experimental observations of the failure stress in the tunnel wall are not consistent with the theory: The formation of a shear failure in a tunnel wall is subjected to much higher cinematical constraints than a shear failure in uniaxial compression test. The understanding of the behaviour of rock around unsupported openings is quite important to solve underground engineering problems. Further study is still required to understand failure processes and design of tunnel support. Thus the material models as well as the calculation approches of tunnels should be reconsidered in order to establish models which correspond better with reality.

8. LIST OF REFERENCE

BOBET A. (2010): "*Numerical methods in geomechanics". School of Civil Engineering, Purdue University, West Lafayette, IN, USA.*

BURTSCHER S.L.,AUS DER SCHMITTEN H. , WATZL B. AND KOLLEGGER J. (2003): *"Experiments on the size effect of sandstone under Compression" Technical Report Number 4. Institute for Structural Concrete Vienna University of Technology*

CARRANZA-TORRES, C. (1998): "*Self-Similaity Analysis of the Elasto-Plastic Response of Underground Openings in Rock and Effects of Practical Variables". Ph. D. Thesis, University of Minnesota.*

DETOURNAY, E. (1983): "*Two-Dimensional Elastoplastic Analysis of a long, Cylindrical Cavity under Non-Hydrostatic Loading". Ph.D. Thesis, University of Minnesota.*

DOLI ELEKTRONIK GMBH (2009): "TEST&MOTION Anwenderhandbuch"

EWY, R. T. & COOK N.G.W. (1990): "Deformation and fracture around cylindrical openings in rock Part II. Initiation, Growth and Iteraction of fractures" Int. J. Rock Mech. Min. Sci & Geomech. Abstr. 27,No. 5, 409-427.

FAIRHURST, C. & CARRANZA-TORRES, C. (2002): "*Closing the Circle". Proc. 50th Annual Geotechnical Engineering Conference, Universitiy of Minnesota*.

GUSTAV HUMMEL GMBH & CO KG: "*www.hummel-stein.at"*

HOEK, E. (1983): "Strength of jointed rock masses" 23 Rankine Lecture. Géotechnique 33(3), 187-223.

HOFFMAN (2010): "*www.hoffmanonline.com"*

INGLIS, C.E. (1913): "*Stresses in a plate due to presence of cracks and sharp corners". Trans.Nav.Archit. 55, pp. 219-241.*

ISAACSON,E. (1958): *"Rock presure in mines". Mining Publications 212, 32-34 London.*

KAISER P.K. AND MORGENSTERN N.R. (1981): *"Time-dependent Deformation of small tunnels-I". Experimental Facilities. Int. J. Rock Mech. Min. Sci. & Geomech. Abstr. 18, 129-140.*

KAISER P.K. AND MORGENSTERN N.R. (1981): "Time-dependent Deformation of small tunnels-II. Typical Test Data". Experimental Facilities. Int. J. Rock Mech. Min. Sci. & Geomech. Abstr. 18, 141-152.

KAISER P.K. AND MORGENSTERN N.R. (1982): "Time-dependent Deformation of small tunnels-III. Pre-failure Behaviour". Int. J. Rock Mech. Min. Sci. & Geomech. Abstr. 19, 307-324.

KAISER P.K., GUENOT A., & MORGENSTERN N.R. (1985): *"Time-dependent Deformation of small tunnels-IV. Behaviour During Failure". Int. J. Rock Mech. Min. Sci. & Geomech. Abstr. 22, 141-152.*

KASTNER, H. (1962): *"Statik des Tunnel- und Stollenbuaes". Berlin: Springer.*

KIRSCH, G. (1898): Die Theorie der Elastizität und die Bedürfnisse der Festigkeitslehre. V.D.J. 42 (29).

LAME, G. (1852): *Lecons sur la theorie de l'elasticite. París: Gauthier-Villars.*

LEON, A. & WILLHEIM, F. (1910): "*Über die Zerstörung in tunnelartig gelochten Gesteinen". Österr. Wochenschrift für den öffentlichen Baudienst, Jg. 16, Heft 44, pp. 641-648.*

PENG, S. & JOHNSON, A. M. (1972) : "Crack growth and faulting in cylindrical specimens of Chelmsford Granite". Int. J. Rock Mech. Min. Sci. Geomech. Abstr. 9, 37-86.

POISEL, R. (1979): "Ein Betrag zur Mechanik des Gebirges um einen tiefliegenden Hohlraum im Post-Failure-Bereich" Rock Mech. 12 (1979), pp. 64-76.

POISEL. R., STEGER W. & ZETTLER A. (1995): *"Neue Ansätze für Standsicherheitsuntersuchungen von Tunneln*". Felsbau 13 Nr. 3, pp 146-152.

POISEL. R. & PREH. A. (2009): *"Notches formed by shear failures in tunnels (cherry pit mechanism) - advances in the progress of failure" Vol. 2, No. 5., pp. 544-552.*

WANG S.H., LEE C.I., RANJITH P.G. & TANG C.A. (2009); "*Modeling the Effects of Heterogeneity and Anisotropy on the Excavation Damaged/ Disturbed Zone (EDZ)". Springer-Verlag.*

9. ATTACHMENTS

9.1. Load displacement curve

The load displacement diagrams are plotted for each specimen in figures 9.1 to 9.4 on pages 92 to 95. Diagrams of specimen 8 and 9 are not included because of a problem with the software and the diagrams didn´t save. Test specimens 8 and 9 were used to find out the optimal way to load the sample by “trial and error”. Specimen 8 was loaded and unloaded 5 times and specimen 9 was loaded and unloaded 9 times.

Load and displacement of the tests are plotted on a graph, where load is plotted on the ordinate versus displacement on the abscissa. German software was used, so the load is named as Kraft and the displacement as Weg. The unit of measurement of load used is kilonewton and displacement is represented in millimeter. The load-displacement curve depends not only on the properties of the material but also on the size and shape of the sample tested.

The diagrams have two points, a blue dot and a green dot. The blue dot represents the point where the displacement of the test stars. The green dot represents the maximum force of the test and the end of the displacement. Test displacement is the distance between these two points.

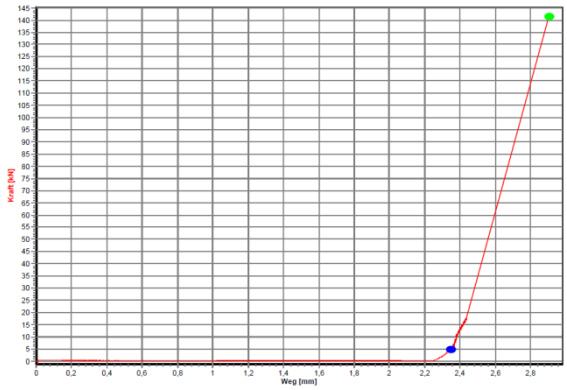

a) Specimen 1a

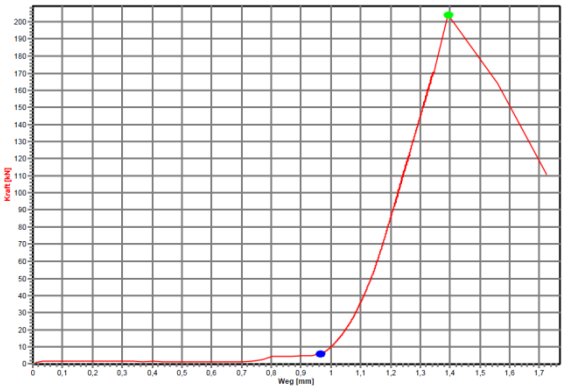

f) Specimen 3

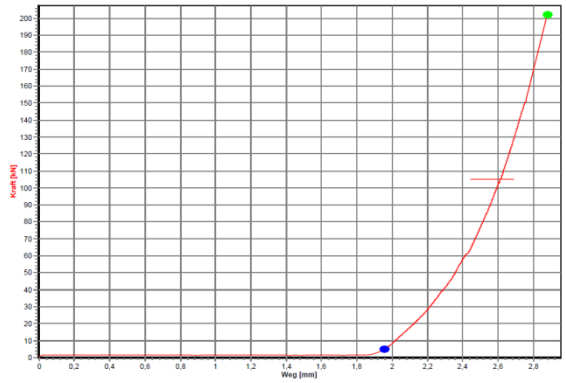

c) Specimen 4

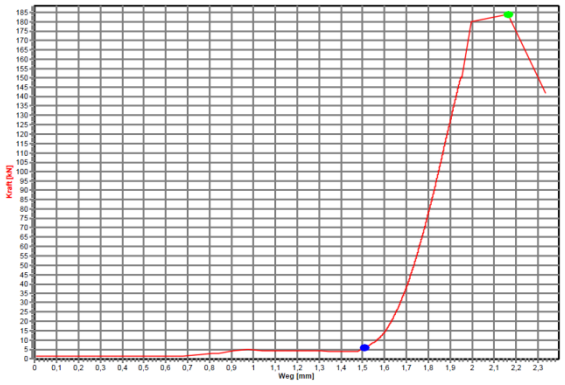

d) Specimen 5

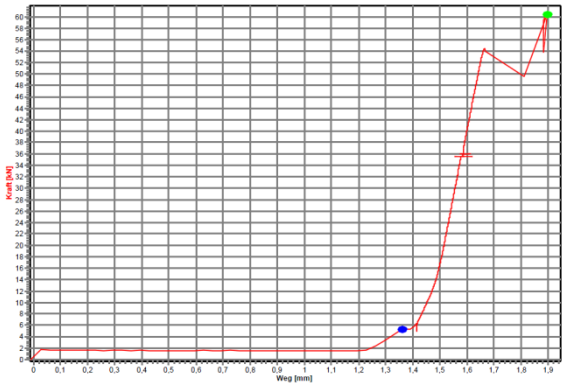

e) Specimen 6

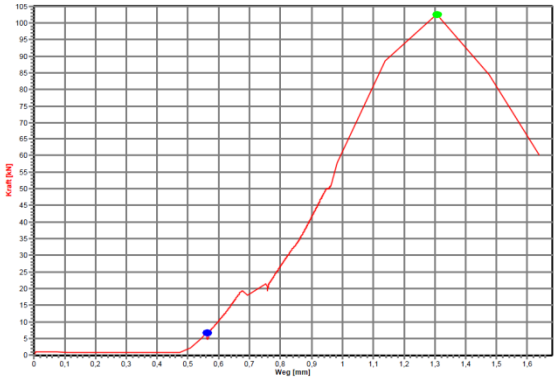

f) Specimen 7

Fig.9.1: Load displacement curve specimens from 1 to 9. The blue dot represents the point where the displacement of the test starts and the green dot represents the maximum force and the point where the displacement of the test finishes.

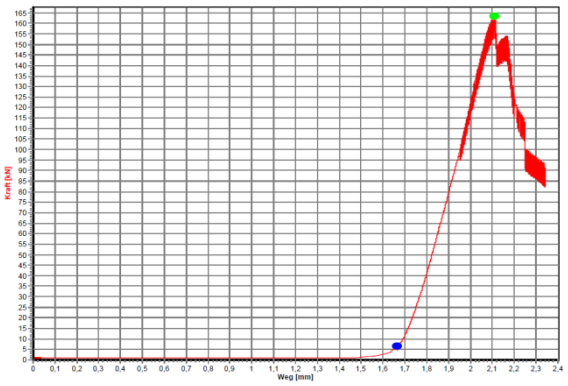

a) Specimen 10.

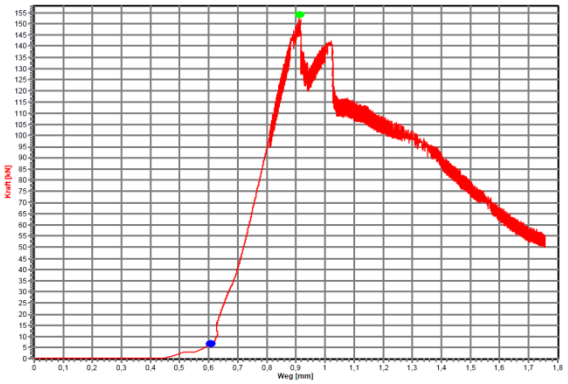

b) Specimen 11.

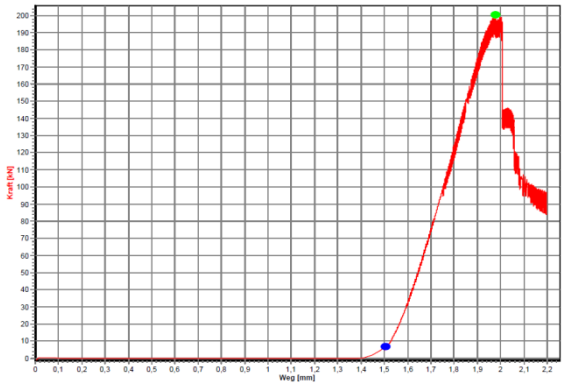

c) Specimen 12.

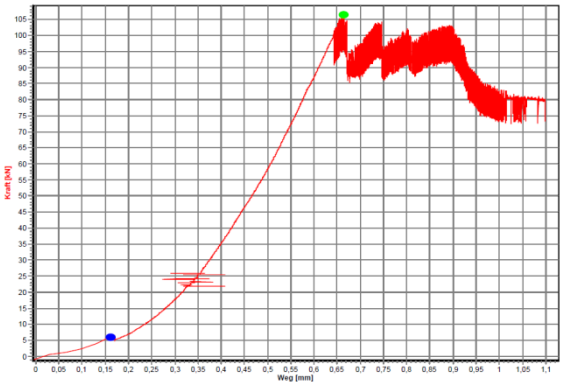

d) Specimen 13.

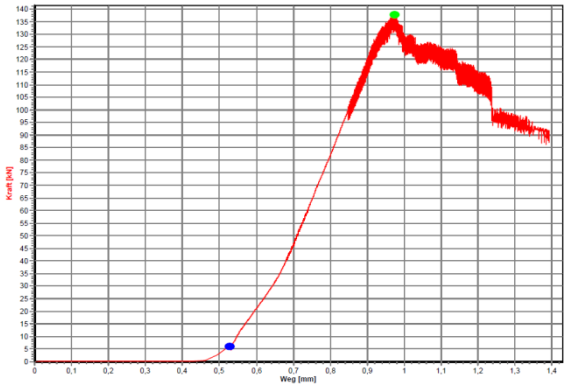

e) Specimen 14.

Fig.9.2: Load displacement curve for specimen 10 to 14. The blue dot represents the point where the displacement of the test starts and the green dot represents the maximum force and the point where the displacement of the test finishes.

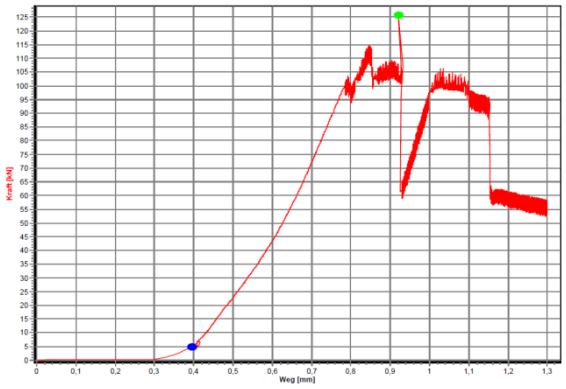

a) Specimen 15.

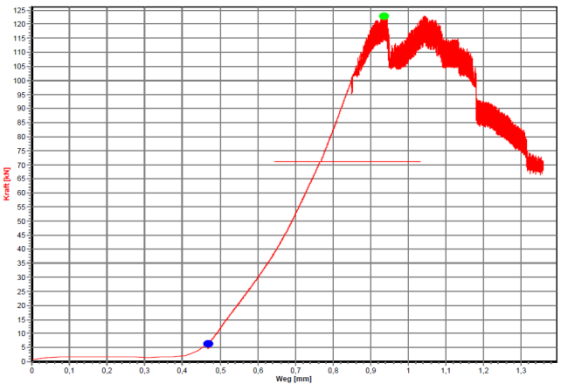

b) Specimen 16.

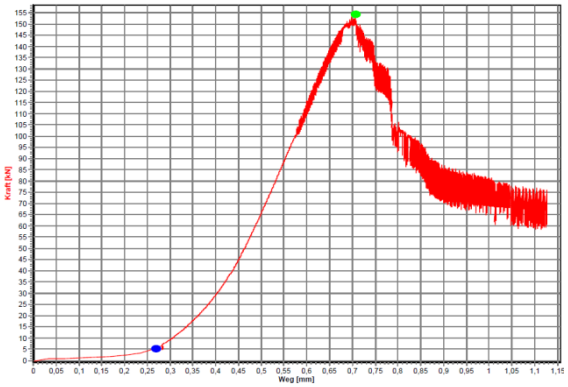

c) Specimen 17.

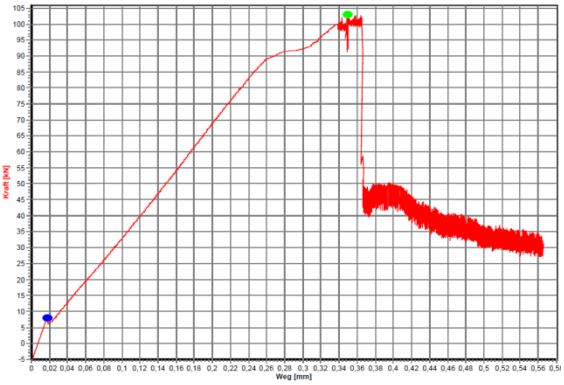

d) Specimen 18.

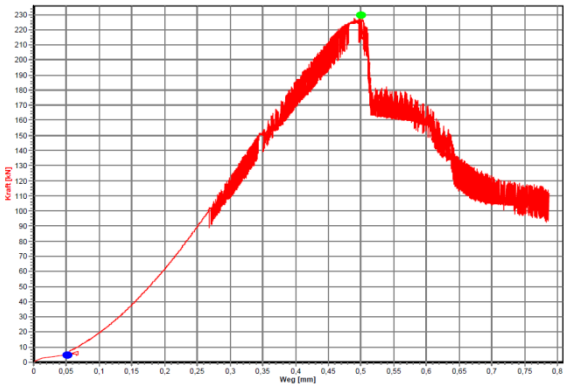

e) Specimen 19.

Fig. 9.3: Load displacement curve for specimen 15 to 19. The blue dot represents the point where the displacement of the test starts and the green dot represents the maximum force and the point where the displacement of the test finishes.

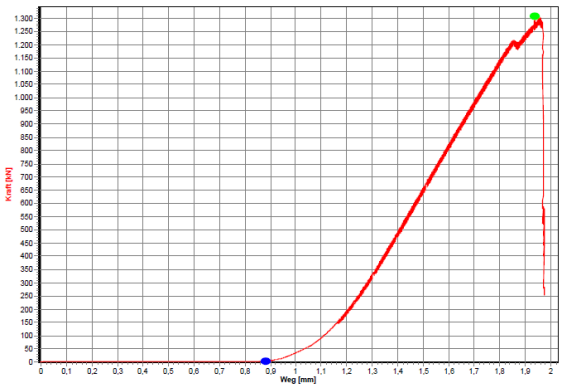

a) Specimen 20.

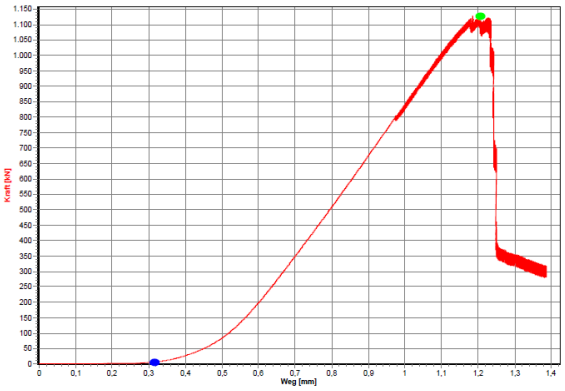

b) Specimen 21.

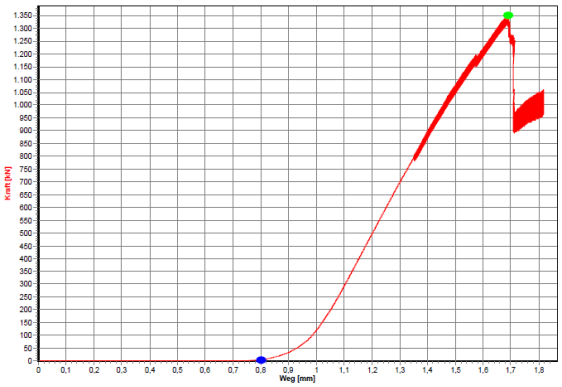

c) Specimen 22.

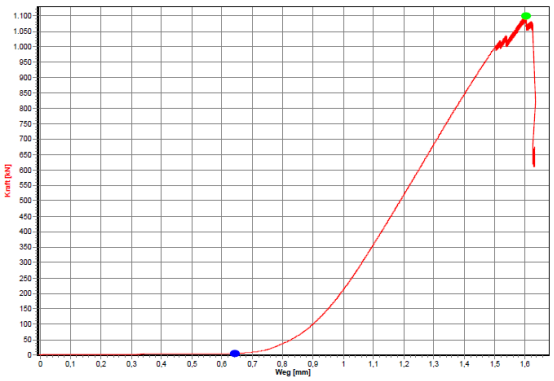

a) Specimen 23.

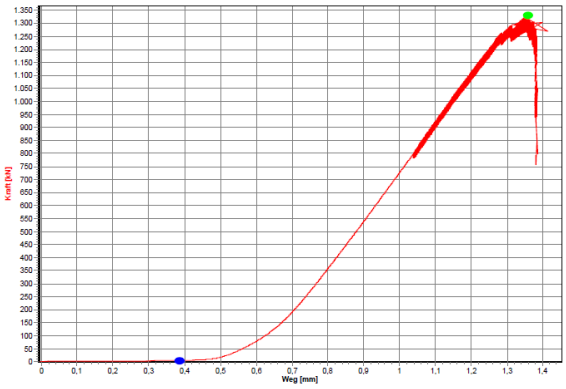

e) Specimen 24.

Fig. 9.4: Load displacement curve for specimen 20 to 24. The blue dot represents the point where the displacement of the test starts and the green dot represents the maximum force and the point where the displacement of the test finishes.

9.2. Photographs of specimens.

Photographs before, during and after tests were taken to document the experiments. A digital camera was also used to record crack initiation, propagation and failure of the specimens.

Figures 9.5 to 9.27, on pages 97 to 118, show the final states of the piece on the front side and on the back side of the specimen and rupture of the cavity sidewall after experiment. Photographs of the cavity were taken from the back side and from the front side. The best pictures were chosen and were used to see the rupture on both sidewall of the specimen.

Figures 9.5 to 9.23 show specimens with dimensions 200x200x50 mm and a circular cavity with a diameter of 25 mm. Photograph of the failure in specimen 3, 4 and 5 can be found in figures 9.6 to 9.8. In these specimens the rupture of the body and the drillhole occurs simultaneously.

Figures 9.9 and 9.10 show the test specimens 6 and 7. The fracture in the cavity is along the tunnel, on the roof and on the floor, and propagates away from the cavity parallel to the applied loading. Testing difficulties caused the destruction of the specimens 8 and 9, figures 9.11 and 9.12, so only one picture was used to show the final state of the specimen. These cases cannot be taken into account for the comparison of the results.

In specimens 10 to 19, first the rupture in the body of the specimen occurs, on the right side, on the left side, on the back side or on the front side of the specimen and later the crack in the sidewalls of the opening became visible, see figures 9.13 to 9.22.

Figures 9.23 to 9.27 show specimens with dimensions 300x300x100 mm and a circular cavity of 36 mm of diameter. In this case, first the rupture on both sidewalls of the circular cavity occurs and later, soon after reaching the point of maximum force, the first cracks on the body of the specimen became visible. The cracks start on the two opposite sides of the opening and grow in the parallel direction to the applied load. There are more cracks on the right side and on the left side of the specimen.

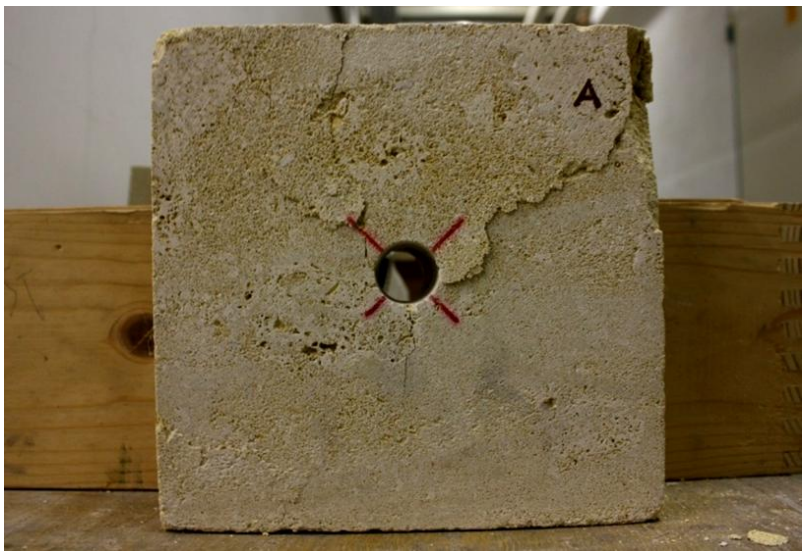

Fig. 9.5: Specimen 1 after testing 1a. a) Side A. b) Side B. c) Drillhole of the specimen. The drillhole was photographed from side A.

Fig.9.6: Specimen 2 after testing. a) Side A. b) Side B. c) Drillhole of the specimen. (Left) The drillhole was photographed from side A. (Right) The drillhole was photographed from side B.

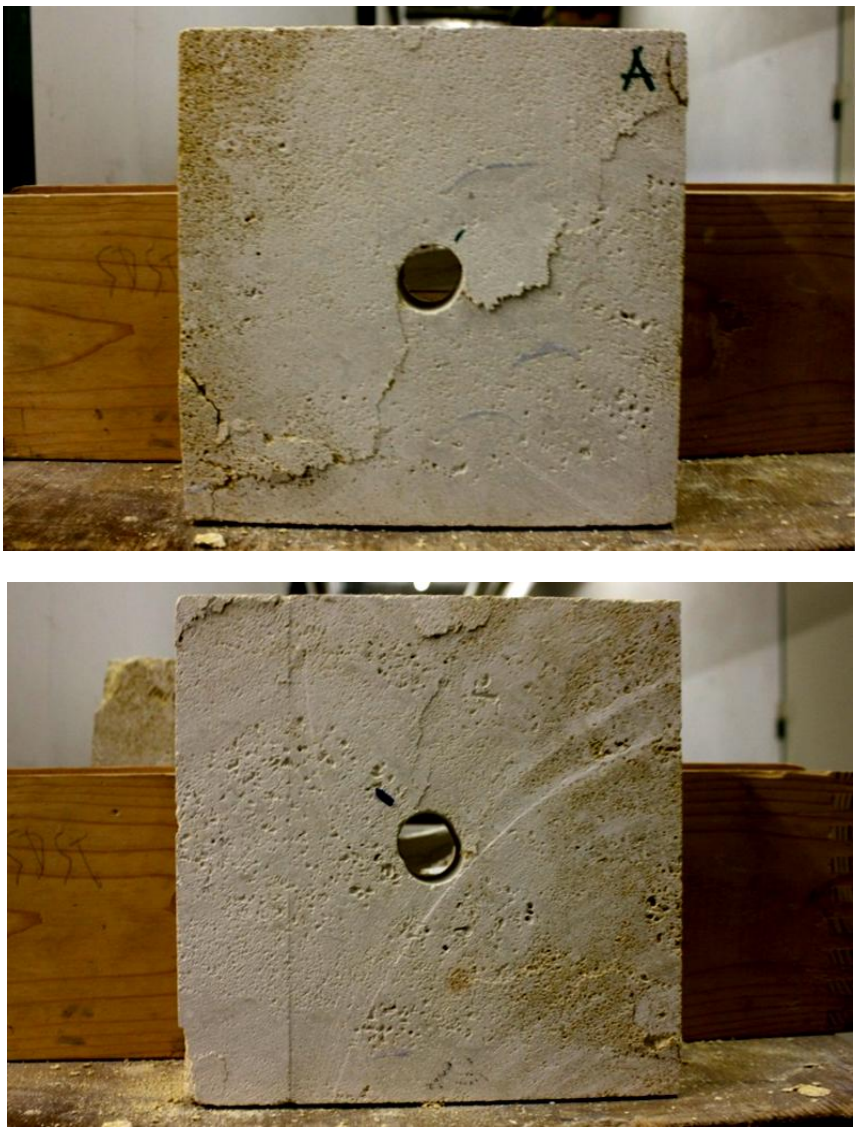

Fig. 9.7: Specimen 4 after testing. a) Side A. b) Side B. c) Drillhole of the specimen. The drillhole was photographed from side A.

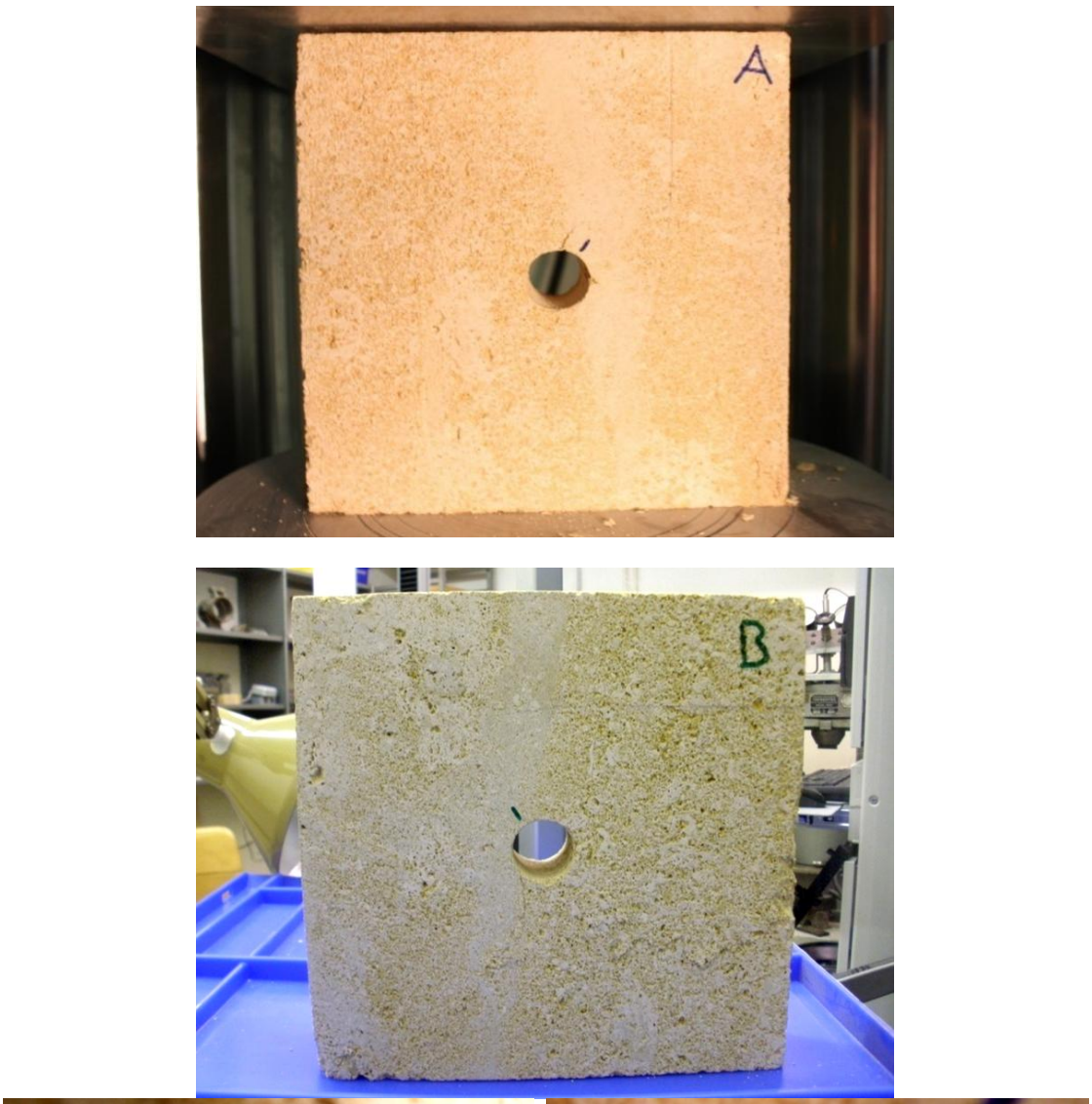

Fig. 9.8: Specimen 5 after testing. a) Side A. b) Side B. c) Drillhole of the specimen. The drillhole was photographed from side A.

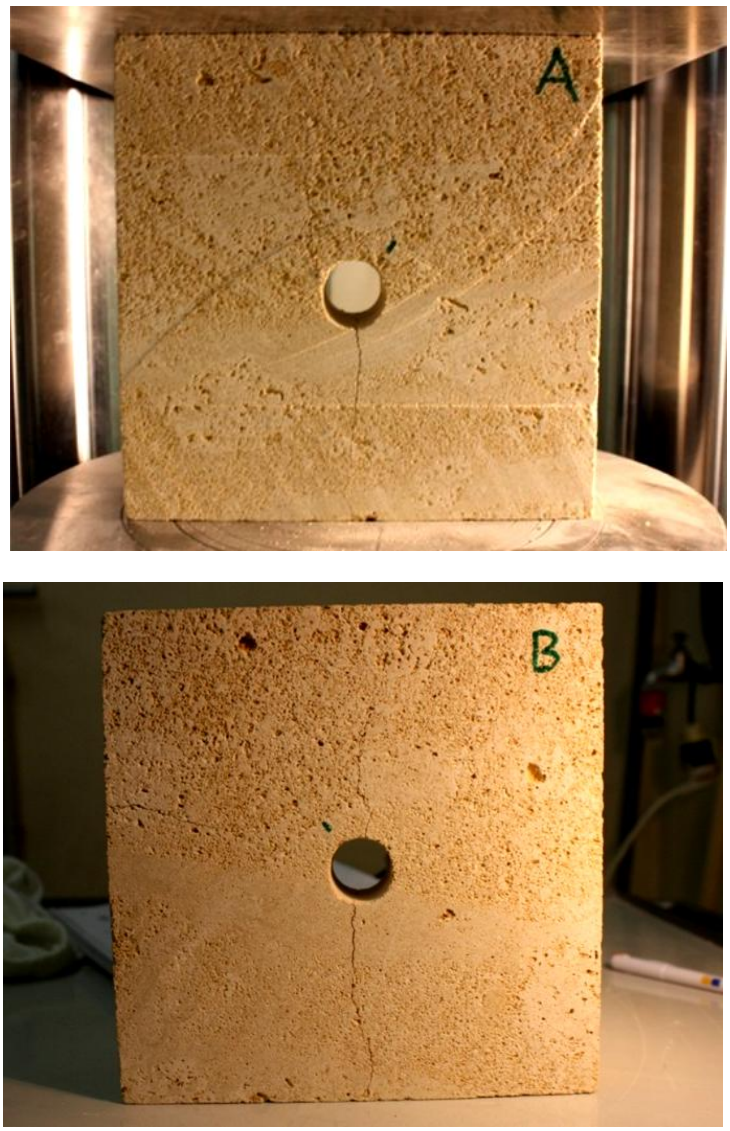

Fig. 9.9: Specimen 6 after testing. a) Side A. b) Side B. c) Drillhole of the specimen. (Left) The drillhole was photographed from side A. (Right). The drillhole was photographed from side B.

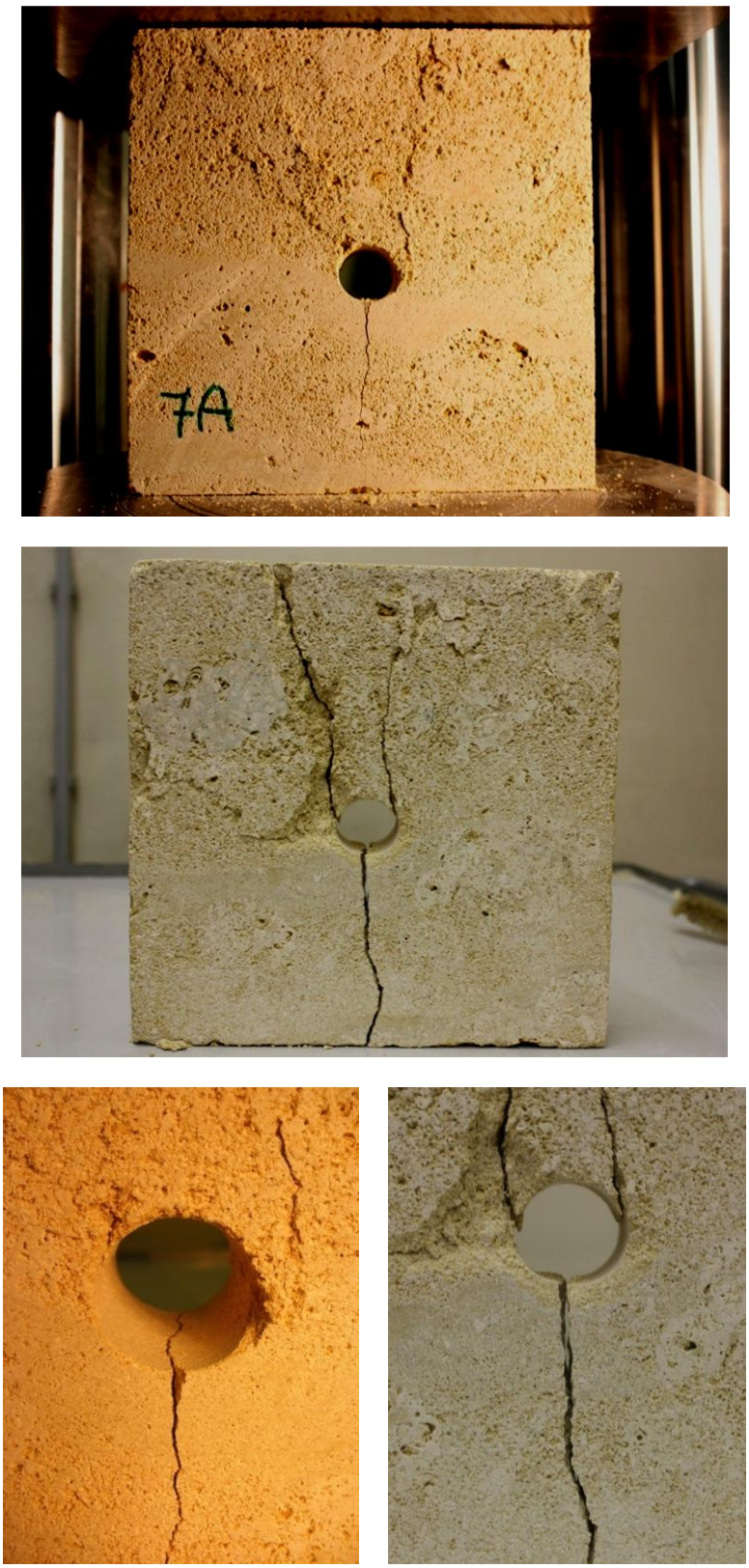

Fig.9.10: Specimen 7 after testing. a) Side A. b) Side B. c) Drillhole of the specimen. (Left) The drillhole was photographed from side A. (Right) .The drillhole was photographed from side B.

Fig.9.11: Specimen 8 after testing.

Fig.9.12: Specimen 9 after testing.

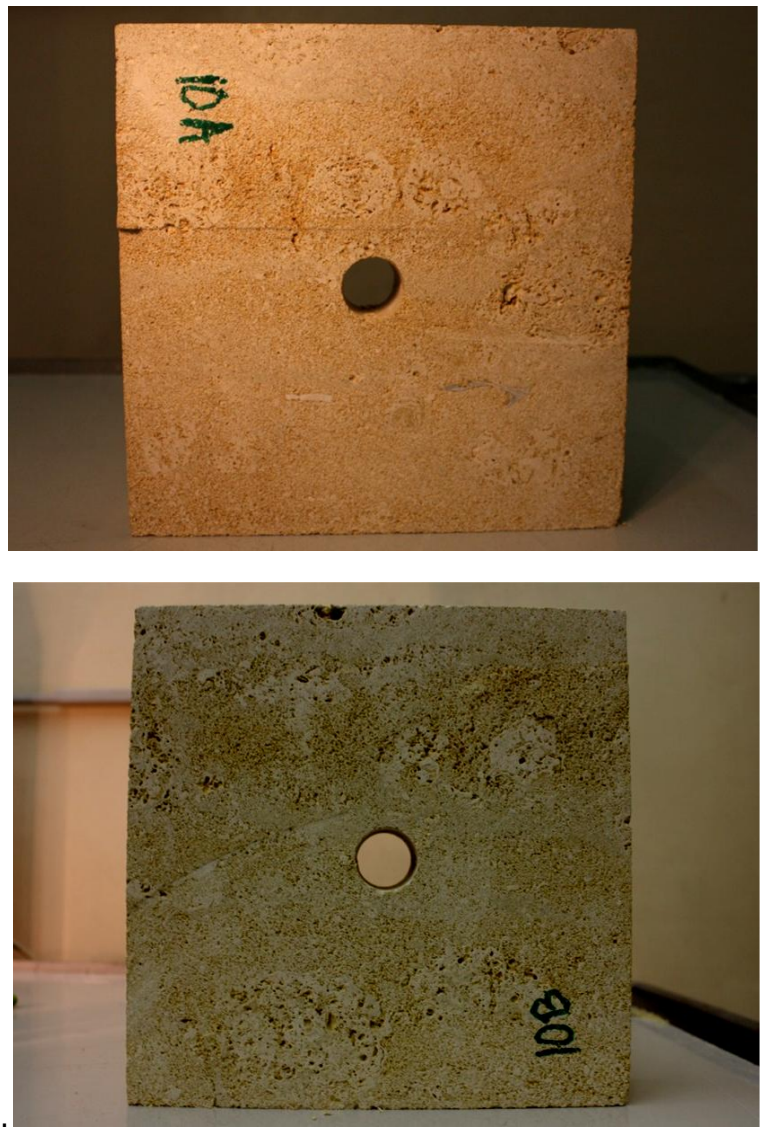

Fig. 9.13: Specimen 10 after testing. a) Side A. b) Side B. c) Drillhole of the specimen. The drillhole was photographed from side A.

Fig. 9.14: Specimen 11 after testing. a) Side A. b) Side B. c) Drillhole of the specimen 11 after testing. (Left)The drillhole were photographed from side A. (Right) The drillhole were photographed from side B.

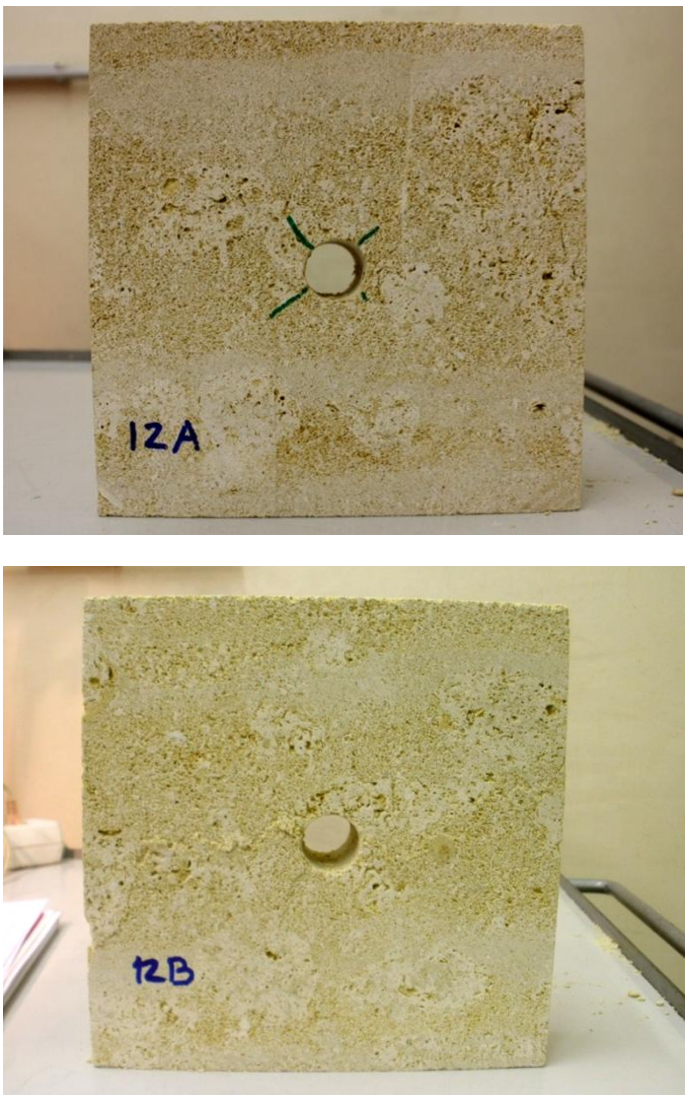

Fig.9.15: Specimen 12 after testing. a) Side A. b) Side B. c) Drillhole of the specimen. (Left) The drillhole was photographed from side A. (Right) The drillhole was photographed from side B.

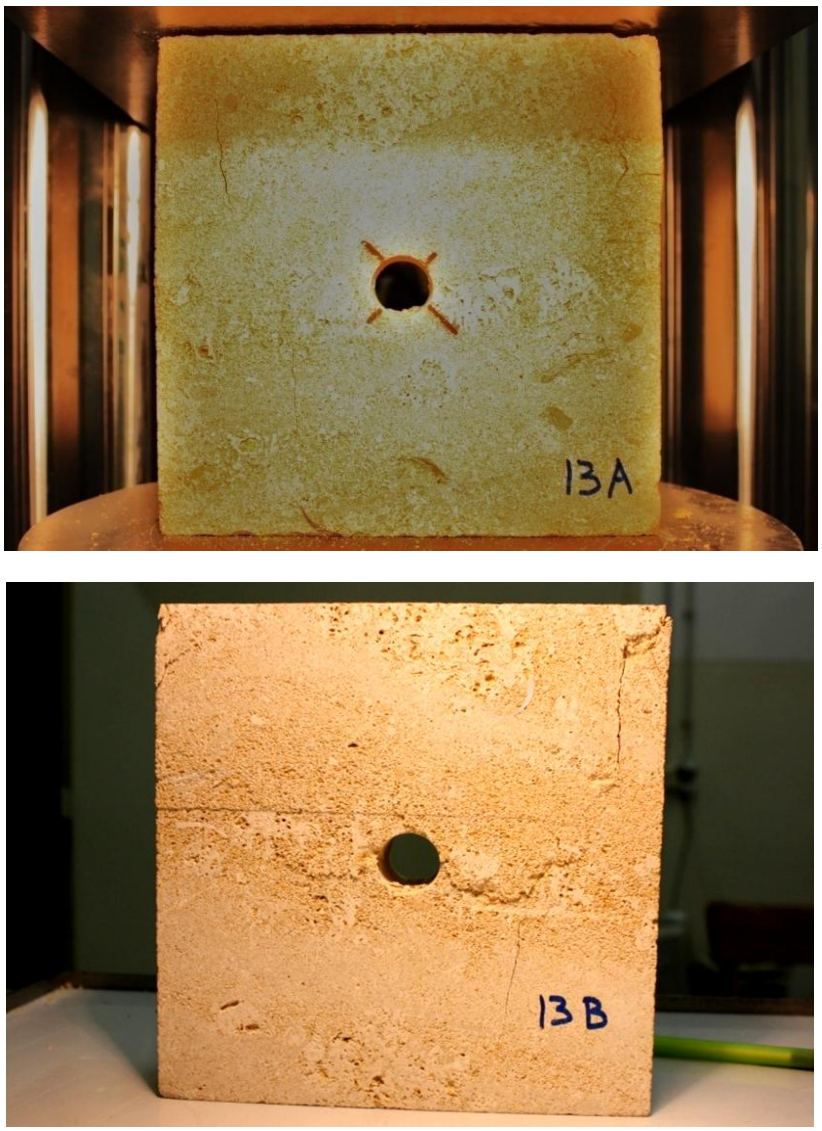

Fig.9.16: Specimen 13 after testing. a) Side A. b) Side B. c) Drillhole of the specimen. The drillhole was photographed from side B.

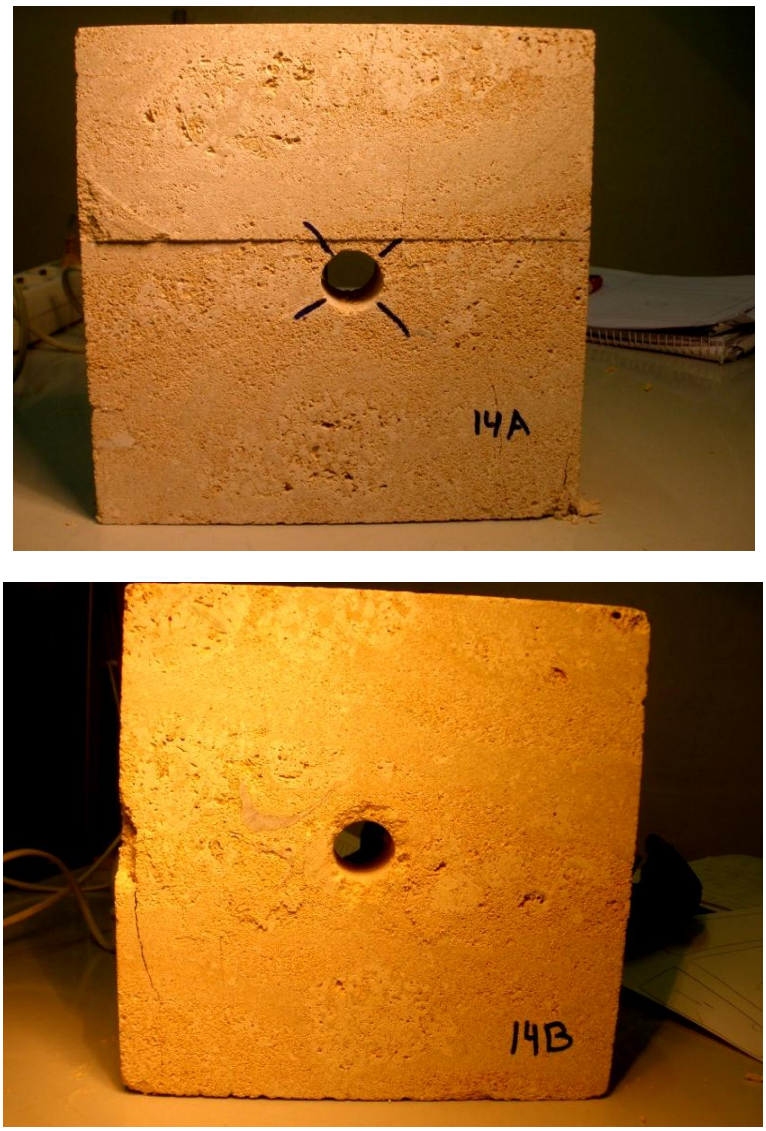

Fig. 9.17: Specimen 14 after testing. a) Side A. b) Side B. c) Drillhole of the specimen. The drillhole was photographed from side B.

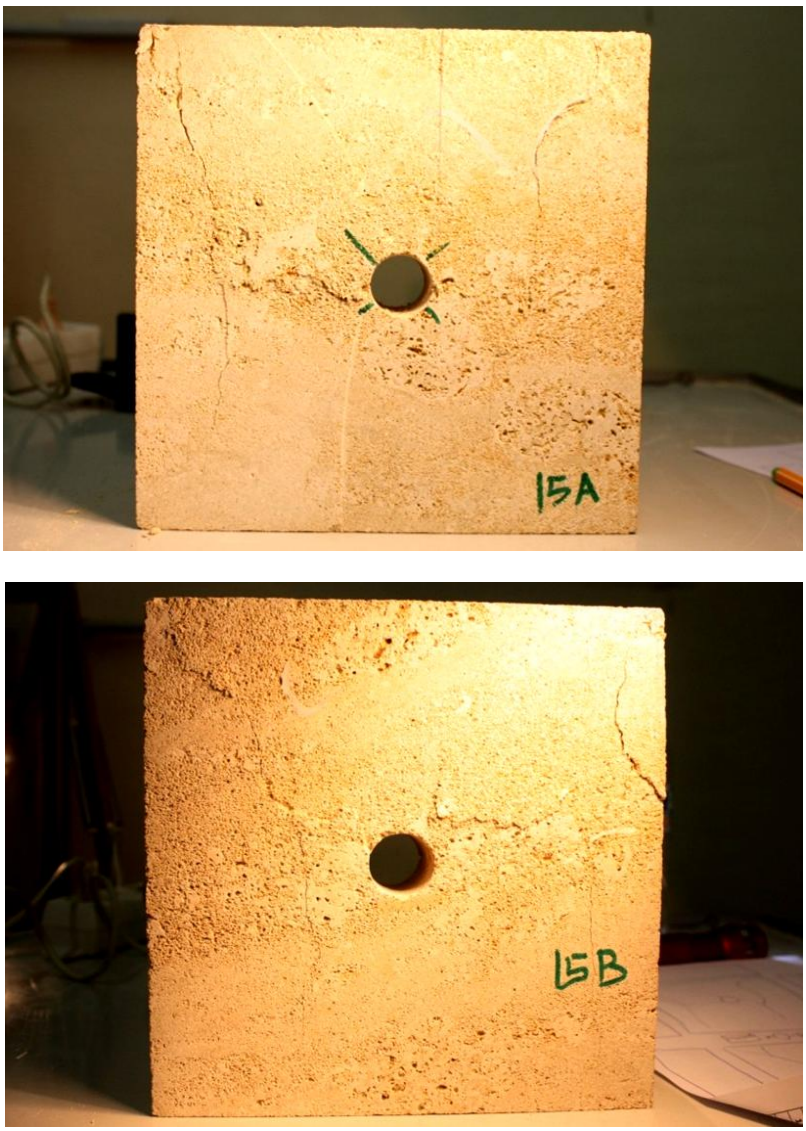

Fig.9.18: Specimen 15 after testing. a) Side A. b) Side B. c) Drillhole of the specimen. The drillhole was photographed from side B.

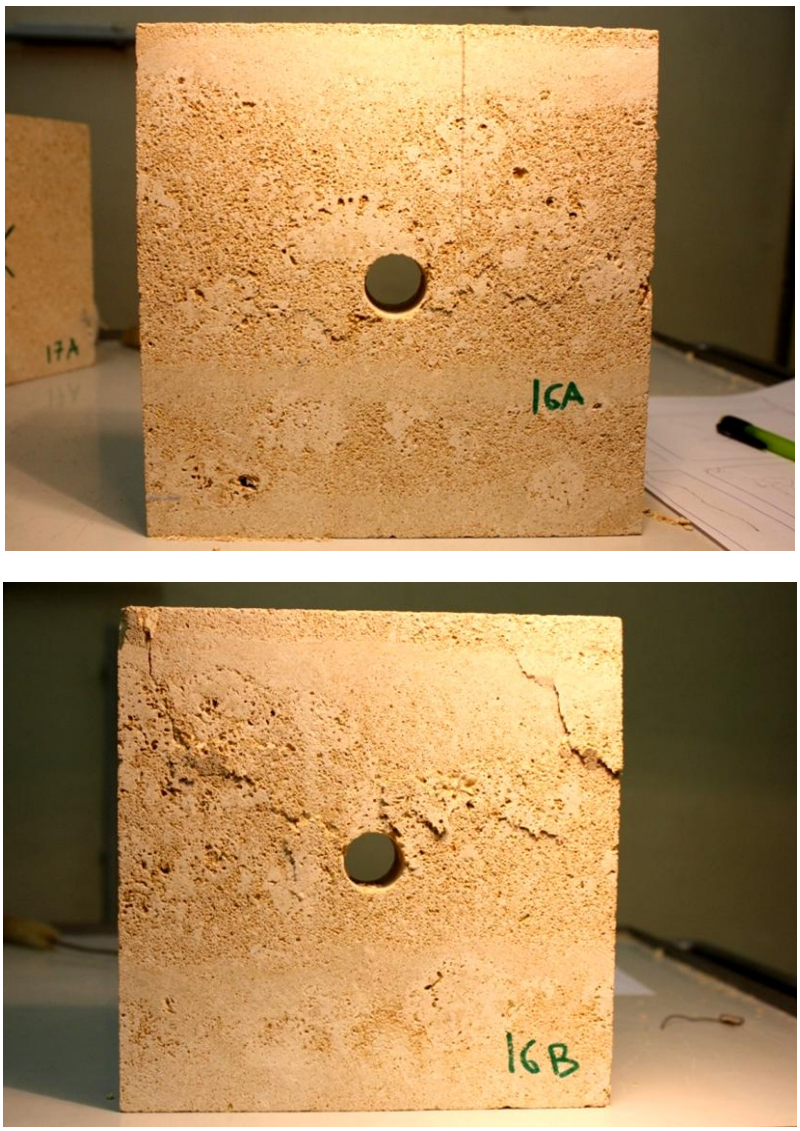

Fig. 9.19: Specimen 16 after testing. a) Side A. b) Side B. c) Drillhole of the specimen. The drillhole was photographed from side B.

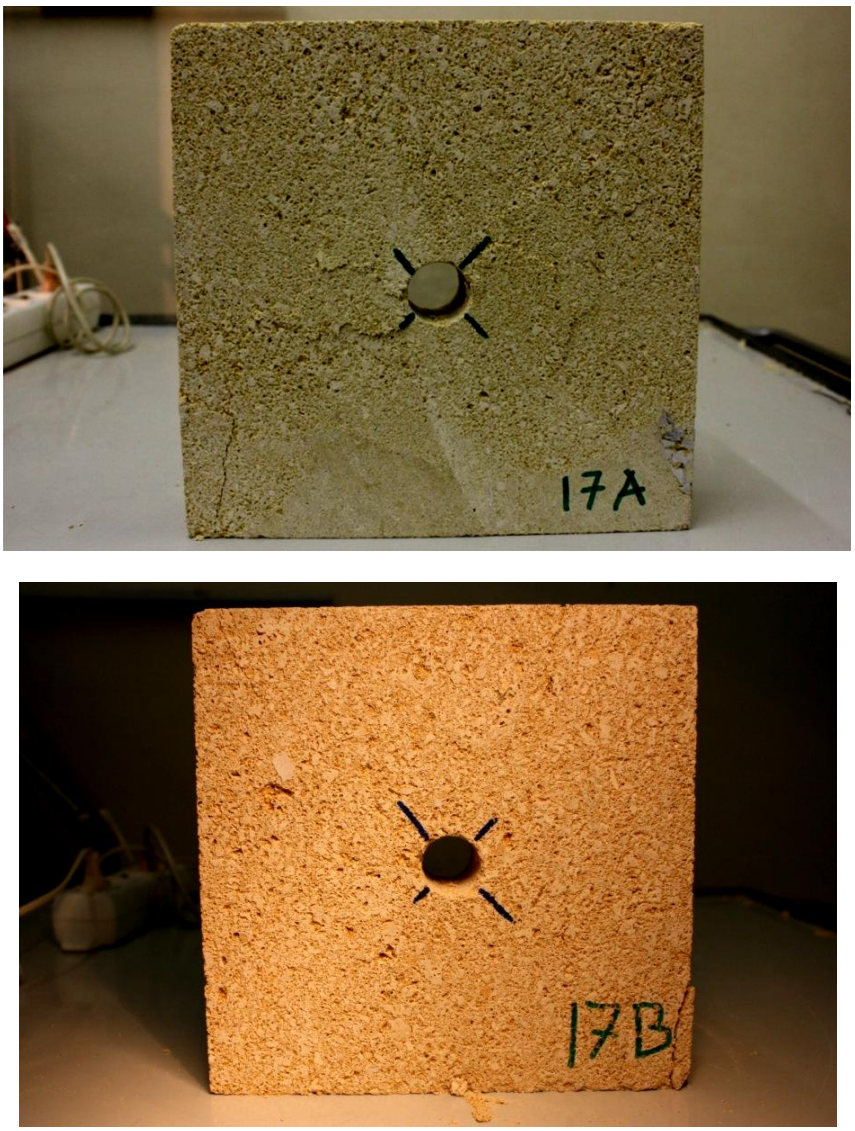

Fig. 9.20: Specimen 17 after testing. a) Side A. b) Side B. c) Drillhole of the specimen. (Left) The drillhole was photographed from side A. (Right) The drillhole was photographed from side B.

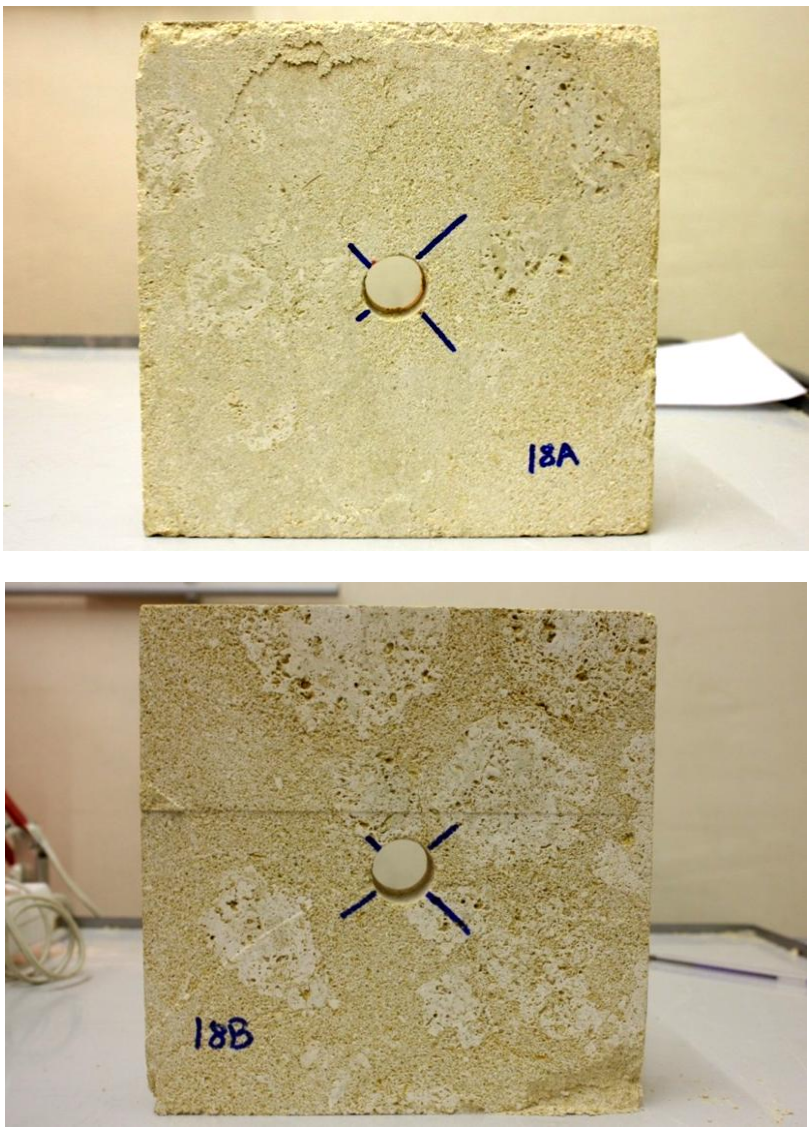

Fig. 9.21: Specimen 18 after testing. a) Side A. b) Side B. c) Drillhole of the specimen. The drillhole was photographed from side A.

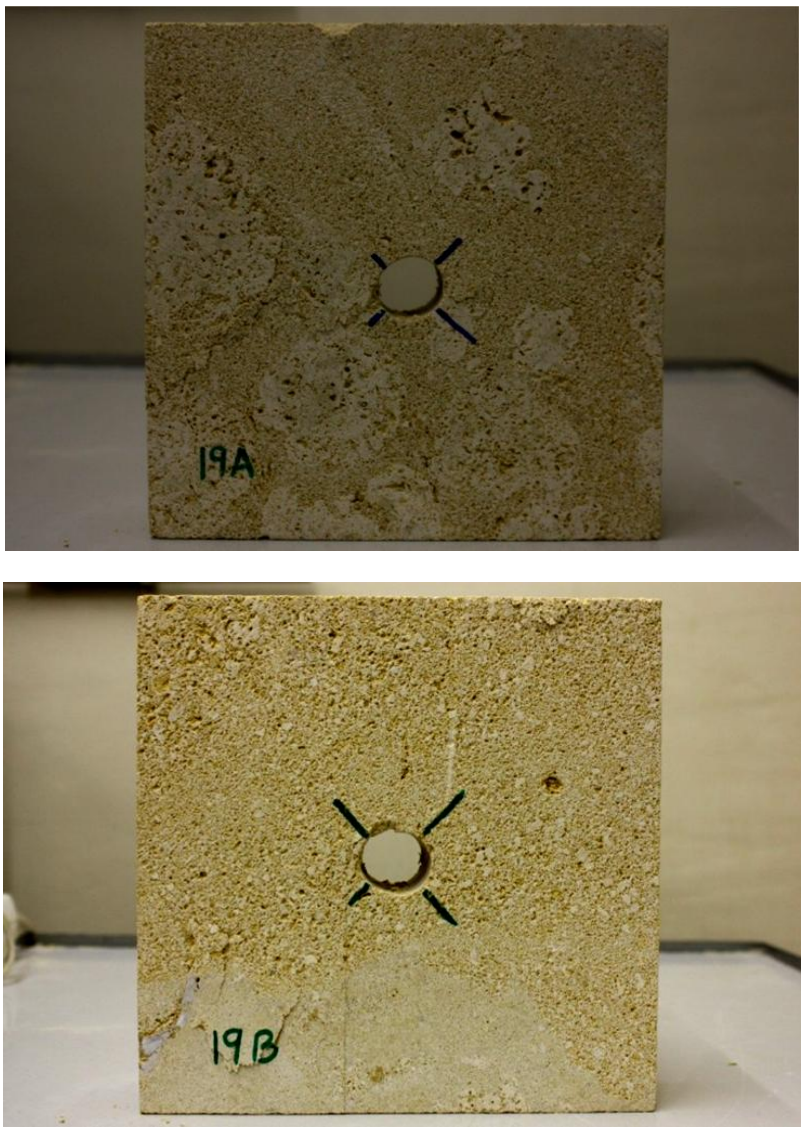

Fig. 9.22: Specimen 19 after testing. a) Side A. b) Side B. c) Drillhole of the specimen. (Left) The drillhole was photographed from side A. (Right) The drillhole was photographed from side B.

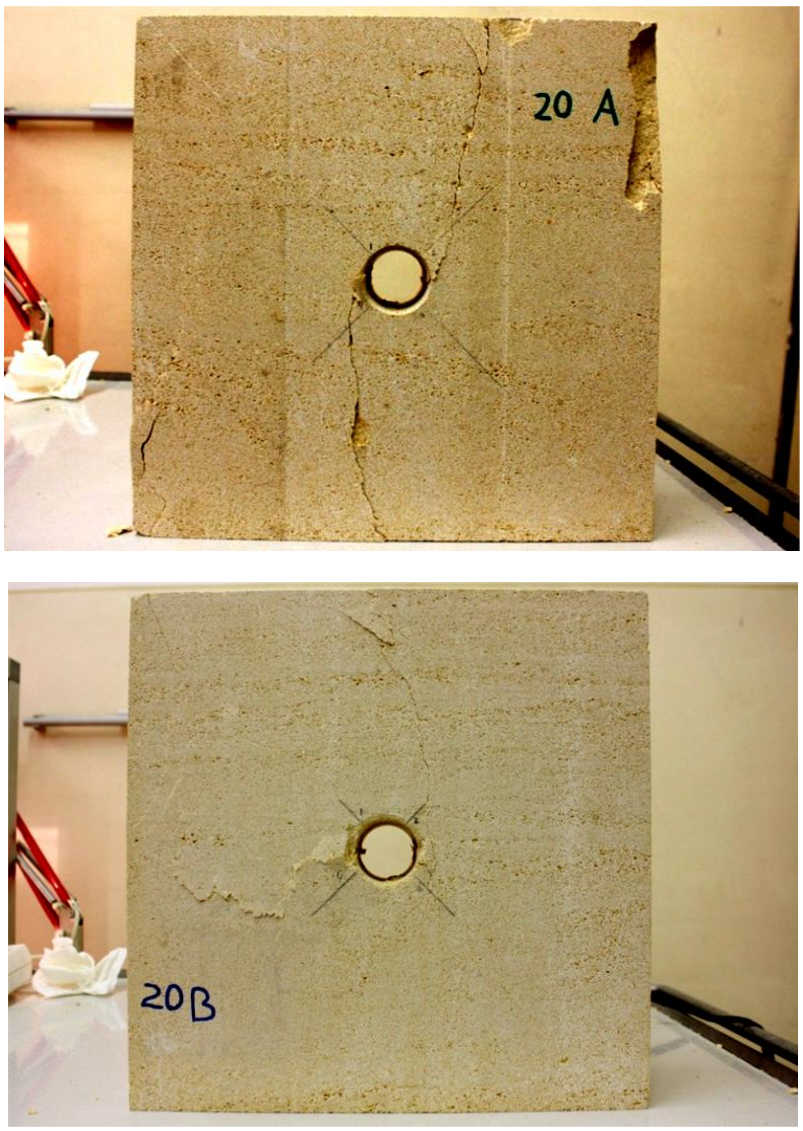

Fig. 9.23: Specimen 20 after testing. a) Side A. b) Side B. c) Drillhole of the specimen. The drillhole was photographed from side B.

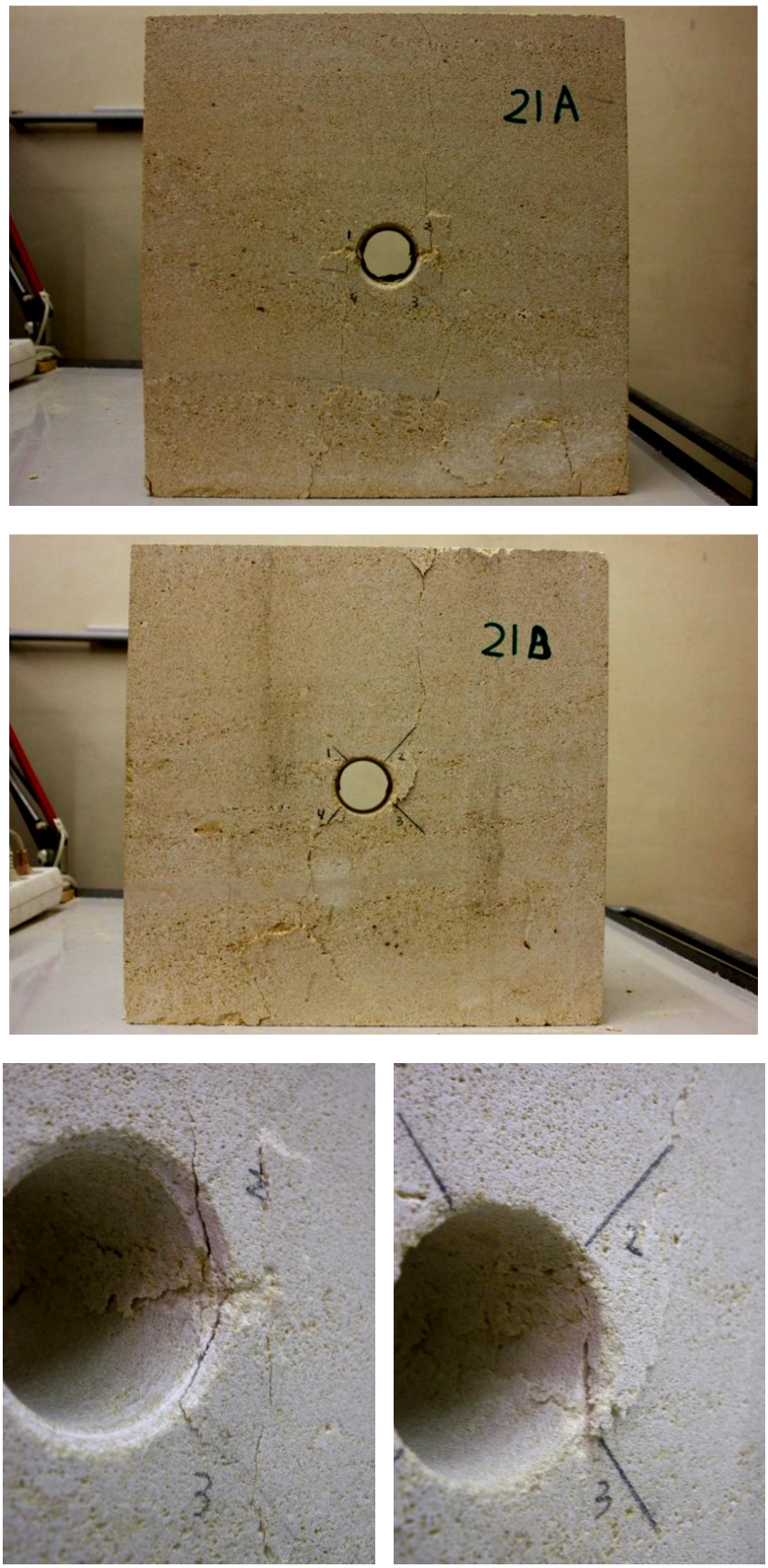

Fig. 9.24: Specimen 21 after testing. a) Side A. b) Side B. c) Drillhole of the specimen. (Left) The drillhole was photographed from side A. (Right) The drillhole was photographed from side B.

Fig. 9.25: Specimen 22 after testing. a) Side A. b) Side B. c) Drillhole of the specimen. The drillhole was photographed from side A.

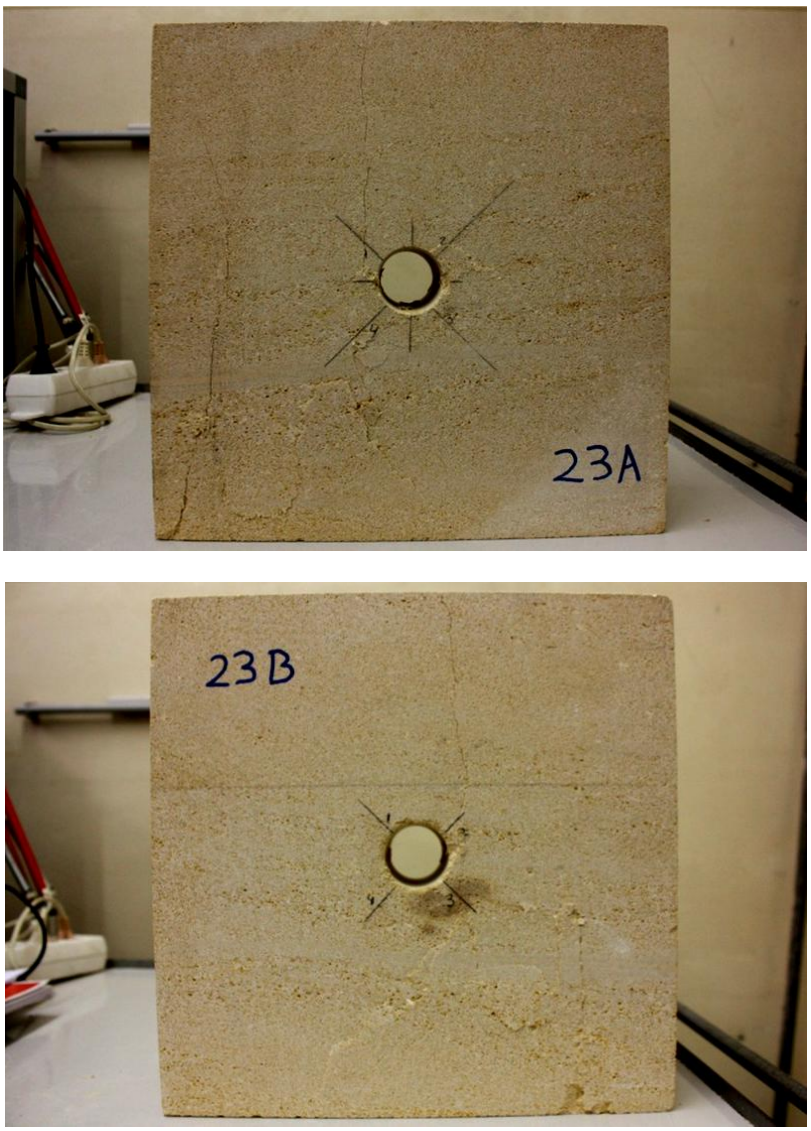

Fig. 9.26: Specimen 23 after testing. a) Side A. b) Side B. c) Drillhole of the specimen. The drillhole was photographed from side A.

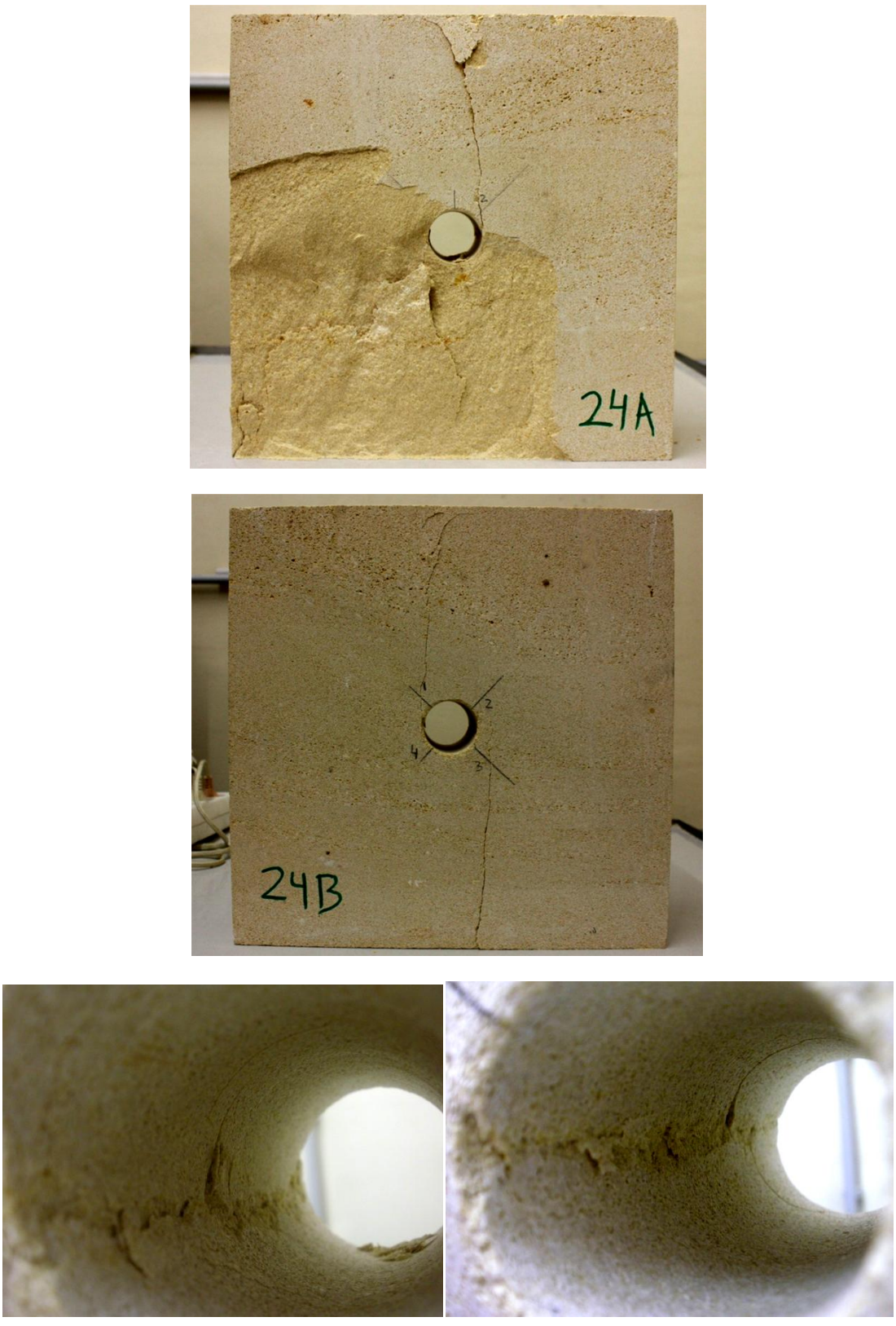

Fig. 9.27: Specimen 24 after testing. a) Side A. b) Side B. c) Drillhole of the specimen. (Left) The drillhole was photographed from side A. (Right) The drillhole was photographed from side B.

9.3. Testing facilities

9.3.1. Small machine, M500-100kN.

The compression tests, in order to obtain a first approach of compressive strength, were performed in the machine showed in figure 9.28. It is maximal force is 100 kN, so it could not be used for compression tests in prisms of rock with holes because 200 kN were needed for the smallest specimens and nearly 1.300 for the biggest specimens.

The compression machine is composed by two ground guide pillars and these pillars are covered with rubber gaiter closing. The front part and the left side of the machine is shown in figure 9.28.

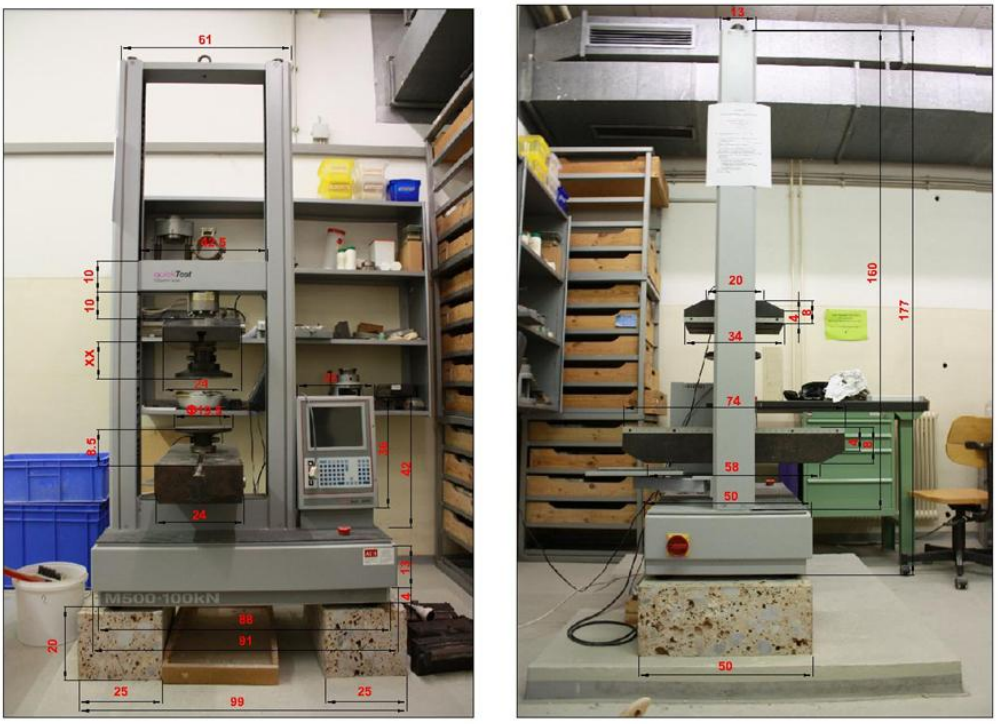

Fig. 9.28: Testing machine for compression test. Small machine.

The press also has a system for manual control located on the right side. Besides the manual control the press also can be controlled by a computer with special software. With this software you can increase or decrease the test velocity, monitor progress of the test and save the results of the test.

9.3.2. Big machine.

The tests have been executed in a compression testing machine with a capacity of 3000 kN. The basis of the compression machines is a structure with a weight of 2500 kg and the outer dimension of 72 x 146 x 66 mm. The machine is formed by four chromed columns with 6.34 mm diameter, a ground plate and a top with dimensions 66 x 66 x 17.5 cm and safety guards to polycarbonate and aluminum. The maximal capacity of the hydraulic pressure is 361.63 bar and the piston area is 829.6 cm^2. The distance among the loading platen can be modified, according to the height of the specimen to be tested. Pieces were added or removed to reduce or increase the vertical distance between the compression platens (figure 9.29).

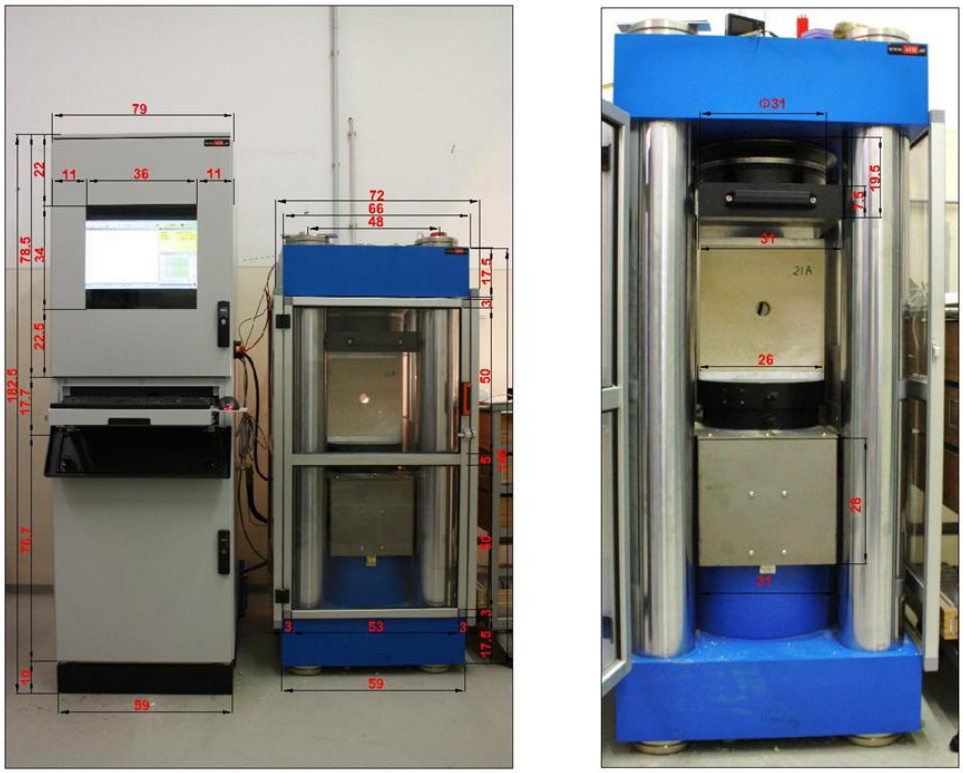

Fig.9.29: Testing machine for compression test. New machine.

An enclosure System is used to protect the computer system and the hydraulic equipment (Hoffman, 2010). The modular enclosure system was designed by Hoffman®. This company has a modular enclosure system called PROLINE®, which protect electrical and electronic equipment in industrial, local area networking and telecommunications applications from dirt, dust, moisture, oil and other contaminants. The company provides a wide variety of tops, bases, covers, sides and doors to configure a customized solution.

The software used in the compression testing machine is Test&Motion**,** a product of DOLI Elektronik GmbH. This software can be used in operating system Microsoft Windows 95/98/NT/2000/XP©/Windows7 (DOLI Elektronik Gmbh, 2009). It consists of the basic software containing a simple but adaptable tension/compression test and different modules for almost all kinds of testing applications. All sorts of signal sources can be displayed. Load, position and strain are standard, but other transducers or calculated results can be displayed, also. With the software you can data storage according to time or results, result can be chosen and displayed one by one and export as ASCII or Excel file.

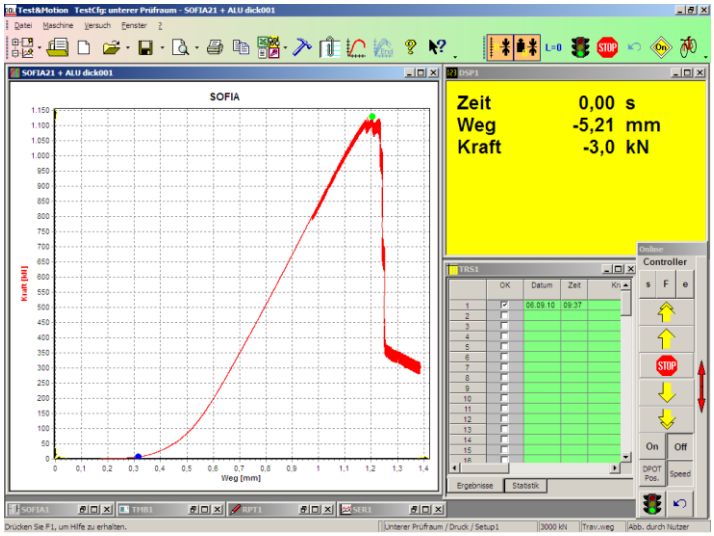

Fig.9.30 : Software Test & Motion.

The program is simple and intuitive. Figure 9.30 shows the program. There are many symbols, which show its function by means of a drawing. The toolbar is displayed horizontally above the main frame window.

	Open the file list		Adjustment test
	Opens an existing document		Comments
	save		Configuring diagram Axes
	constitute the active document as on screen		Help
	print		Tares the transverse position and the load
	Copies data in the active document to the clipboard		Starts a test
	Export as excel or ASCII		ends a test